GENETIC MODIFIERS THAT AFFECT THE ACCUMULATION OF THE MUTANT PROTEIN ALPHA-1 ANTITRYPSIN-Z

by
Olivia S. Long
B.A. Carlow University, 2005

Submitted to the Graduate Faculty of
University of Pittsburgh in partial fulfillment
of the requirements for the degree of
Doctor of Philosophy

University of Pittsburgh
2011

UNIVERSITY OF PITTSBURGH
School of Medicine

This dissertation was presented

by

Olivia S. Long

It was defended on

August 11, 2011

and approved by

Dr. Jeffrey Brodsky, Professor, Department of Biological Sciences, University of Pittsburgh

Dr. Alfred Fisher, Assistant Professor, Department of Molecular Genetics and Developmental Biology, University of Pittsburgh

Dr. David Perlmutter, Professor, Department of Cell Biology and Molecular Physiology, University of Pittsburgh

Dr. Michael Tsang, Associate Professor, Department of Molecular Genetics and Developmental Biology, University of Pittsburgh

Dr. Gary Silverman, Professor, Department of Cell Biology and Molecular Physiology, University of Pittsburgh

Copyright © by Olivia S. Long
2011

GENETIC MODIFIERS THAT AFFECT THE ACCUMULATION OF THE MUTANT PROTEIN ALPHA-1 ANTITRYPSIN-Z

Olivia S. Long

University of Pittsburgh, 2011

Alpha 1-antitrypsin deficiency (ATD) is an autosomal recessive disorder characterized by mutations in *SERPINA1*. Since α1-antitrypsin (α1-AT) is the predominant serine peptidase inhibitor in extracellular fluids, decreased α1-AT secretion results in a loss-of-function phenotype manifested by peptidase-inhibitor imbalance, connective tissue matrix destruction, and susceptibility to chronic obstructive lung disease. In contrast, the accumulation of aggregation-prone alpha-1 antitrypsin-Z (ATZ) variant in liver cells leads to a toxic gain-of-function phenotype characterized by liver failure and carcinogenesis. Curiously, only ~10% of all ATZ homozygous individuals develop severe liver disease. This observation suggests that additional genetic disease modifiers and/or environmental conditions make an important contribution to disease severity and outcome. Our current understanding of these factors is incomplete and effective therapeutic options are very limited.

I report here the development of a *C. elegans* model of ATZ deficiency that recapitulates the ER transport defect associated with ATD. Furthermore, we identified key components of the disposal mechanism of ATZ in *C. elegans,* which parallels those in mammalian systems. Lastly, I developed a semi-automated high content genome-wide RNAi screen technology and used this method to identify <100 genes that modify the accumulation of ATZ. Many of these genes implicated in playing a role in the disposal of ATZ are novel and provide a source of potential ATZ genetic modifiers for future study.

Table of Contents

PREFACE

This dissertation represents a culmination of work and learning over the past six years. It has been an honor to work with my thesis advisor Dr. Gary A. Silverman. I would like to thank him for his unwavering support, motivation, and guidance. His dedication to both medicine and scientific research has been my inspiration to put in the countless hours of work. From all of the different lessons I have learned over the past 6 years, the one that will always remain is the importance of experimental design and controls.

I would also like to thank all of the hard-working members of the Silverman lab, both past and present. First, without the help of Dr. Stephen Pak, Anne Vetica, and Sager Gosai the α-1 antitrypsin project would not have been possible. These individuals have devoted their time and effort to the successful development of this project. Additionally, they have been key to my success in the laboratory. Furthermore, I would like to thank Dr. Cliff Luke and Dr. Mark Miedle, both of which have assisted and supported my research and my sanity. Lastly, to all other people that I have had the honor to work with over the years, you have contributed to molding me into the person I am today.

I would like to thank my thesis committee Dr. Jeff Brodsky, Dr. Alfred Fisher, Dr. David Perlmutter, and Dr. Michael Tsang. You have provided excellent support, advice,

motivation, and critiques all of which has helped improve both my thesis project, and myself as a scientist.

Furthermore, I would like to thank my family and friends. I can honestly say, that without their loving support, I would never have completed this journey. I would especially like to thank my parents, even though they laughed about my love of worms. Your work ethic and values are what taught me to endure. Your confidence in me has inspired me to succeed. Lastly, your love has encouraged me to continue through the arduous and daunting times. I would not be where I am today without you, so thank you.

Lastly, I would like to thank my loving husband. Mark you have supported me through all the long hours, weekends, and missed dinners. You convinced me that all my time, effort, and energy would not go unnoticed or unappreciated. I would especially like to thank you for writing such eloquent wedding vows. You stated that the key to our marriage would require “the 3 P’s” patience, persistence, and perseverance. I have found that patience, persistence, and perseverance are also the key to a successful life, so thank you for giving me the words.

LIST OF FIGURES

LIST OF TABLES

LIST OF ABBREVIATIONS

19S	Regulatory cap of 26S proteasome
20S	Core particle of 26S proteasome
26S	Proteasome
α-syn	Alpha-synuclein
α1-AT	α1-antitrypsin
AT	α1-antitrypsin
ATD	α1-Antitrypsin Deficiency
ATM	α1-antitrypsin wild type M allele
ATZ	α1-antitrypsin Z allele
COPD	Chronic obstructive pulmonary disease
EDEM	ER degradation enhancing alpha-mannosidade-like
ER	Endoplasmic reticulum
ERAD	Endoplasmic reticulum-associated degradation
ERAD-C	Endoplasmic reticulum-associated degradation cytosolic lesion
ERAD-L	Endoplasmic reticulum-associated degradation lumina lesion
ERAD-M	Endoplasmic reticulum-associated degradation membrane lesion
ES	Embryonic stem
FENIB	Familial encephalopathy with neuroserpin inclusion bodies
GT	Glucosyl transferase
HCS	High content screen
HD	Huntington's disease
IIS	Insulin/ insulin like signaling
IPTG	Isopropyl β-D-1 thiogalactopyranoside
L4	Larvel Stage - 4

NF-kB	Nuclear factor kappa-light-chain enhancer of activated B cells
NGM	Nematode growth media
NHK	AT null mutant Null Hong Kong
NS	Neuroserpin
OD	Optical Denisty
PAS	Periodic acid Schiff
PBS	Phosphate Buffer Solution
PD	Parkinson's disease
PiZ	α1-antitrypsin Z transgenic mice
polyQ	Polyglutamine
PPM2	Cathepsin L mutation (W28A, Y31A)
RCL	Reactive center loop
RISC	RNAi silencing complex
RNAi	RNA interference
RSL	Reactive site loop
Saar	AT Null mutant Saar
Serpin	Serine protease inhibitor
SRP	Signal recognition particle
TBG	Thyroxine-binding globulin
Tet	Tetracycline
TGN	*Trans*-Golgi network
TRE	Tet response element
Ub	Ubiquitin
UFD	Ubiquitin fusion degradation
UPR	Unfolded protein response
UPS	Ubiquitin proteasome system
YA	Young adult

1.0 INTRODUCTION

1.1 OVERVIEW

α1-antitrypsin deficiency (ATD) is an autosomal recessive disorder characterized by mutations in *SERPINA1* [1]. Phenotyopically, ATD can present with pulmonary dysfunction caused by the loss of the protective mechanisms of α1- antitrypsin (α1-AT) in the lungs [2] and/or hepatic dysfunction due to protein accumulation in the endoplasmic reticulum (ER) of hepatocytes [3]. The prevalence of ATD is estimated to be 1 to 3% of the Caucasian population [4]. However, current data suggest that less than 10% of people living with ATD in the United States have been diagnosed, suggesting that a portion of individuals has few or no symptoms of the disease [5]. This disparity suggests that additional genetic disease modifiers and/or environmental conditions make an important contribution to disease severity and outcome. In patients presenting with ATD associated liver disease, the primary cellular phenotype is the presence of accumulated α1-AT in the ER of hepatocytes [6]. The mechanism underlying the accumulation of α1-AT in the ER is largely unexplained. Therefore, the primary objective of this dissertation is to determine the underlying mechanisms that result in α1-AT accumulation. To accomplish this objective, I used a *C. elegans* model system to identify genes involved in the accumulation of the Z mutant of α1- antitrypsin (ATZ), through the use of phenotypic analysis and RNAi screening approaches.

This chapter provides an introduction to the work presented in this dissertation. It includes an overview of 1) the general features of serpins and serpin associated diseases, 2) characterization of ATD, 3) description of current models of ATD, 4) molecular mechanisms of protein folding and degradation and 5) transgenic *C. elegans* models of human diseases.

1.2 SERPINS

Serpins (serine protease inhibitors) are the largest family of protease inhibitors [7]. Serpins are unique among the protease inhibitors as they employ a suicide substrate-like mechanism to covalently bond to their targets. In their native inhibitory form, serpins posses an exposed reactive-center loop (RCL) which acts as bait resembling the substrates of proteases, through the identity of the P_1 and P_1' residues (met^{358} and ser^{359}, respectively) [8, 9]. When proteases attempt to cleave the RCL it becomes trapped in a covalent complex that is subsequently removed from the system [10]. Serpins are comprised of 330 - 500 amino acids [7]. Serpins have been identified in all multicellular eukaryotes; 36 have been identified in humans (29 inhibitory and 7 non-inhibitory), 32 have been identified in *Drosophila*, and *C. elegans* have 9 (of which 5 appear functional) [11, 12]. The function and specific targets of many of these serpins are unknown. In the following sections, I will summarize the functions, biochemistry, structures, and diseases associated with serpins.

1.2.1 Serpin Function

The primary function of serpins is to regulate the proteolytic activity of serine proteases, which are involved in biological processes such as coagulation, fibrinolysis, complement activation, inflammation, tumor metastasis, and extracellular matrix remodeling [11]. In addition to inhibiting serine proteases, serpins can inhibit caspases, and papain-like cysteine proteases [13-15]. Alternatively, a subset of serpins have lost inhibitory activity and serve as hormone transporters or molecular chaperones [11, 16]. In humans, serpins are classified into 16 different serpin clades encoding both inhibitory and non-inhibitory serpins. Furthermore serpins can be divided based upon cellular location; extracellular and intracellular. The following sections discuss the function of extracellular and intracellular serpins in humans.

1.2.1.1 Extracellular serpins

The majority of human serpins are extracellular and perform a wide variety of inhibitory functions. For example, antithrombin plays a key role in controlling a proteolytic cascade essential for blood coagulation [17]. Specifically, antithrombin is the principle inhibitor of thrombin and coagulation factor X [18, 19]. Additional inhibitory functions of extracellular serpins include: antitrypsin (neutrophil eleastase inhibitor), antichymotrypsin (cathepsin G inhibitor), and C1 inhibitor (C1 esterase inhibitor) [3, 20-23]. In addition to inhibiting proteases, several extracellular serpins also perform non-inhibitory roles. For example, thyroxine-binding globulin (TBG) serves as a transporter for thyroxine [7, 24].

1.2.1.2 Intracellular serpins

Studies have identified serpins that are not secreted and instead perform roles within the cell [25]. Determining the protease targets of intracellular inhibitory serpins has been difficult, possibly because many of these proteins appear to have overlapping protein expression and proteolytic inhibitory profiles [11]. However, several lines of evidence suggest that some of the inhibitory intercellular serpins have cytoprotective roles, whereby they prevent cells from undergoing protease-induced cell death [26]. For example, SERPINB9 has been shown to inhibit the cytotoxic granule protease granzyme B, therefore preventing the activation of cell death pathways [27]. As with the extracellular serpins, the intracellular subfamily contains non-inhibitory members as well. For example, the serpin maspin (SERPINB5) is an intracellular non-inhibitory serpin. While the protein pathways in which maspin plays a role are not know, maspin seems to be important for preventing metastasis in prostate and breast cancers [28-33].

1.2.2 Serpin Structure

All serpins share a common tertiary structure (Figure 1.1). Serpins fold into a metastable structure that consists of three β sheets (A, B and C), eight - nine α helices and a RCL [34]. The RCL extends outward from the serpin scaffold and presents itself as a pseudosubstrate for target proteases. Once a proteases binds to the RCL, and cleaves between the P_1 and P_1' residues (α1-AT contains met^{358} and ser^{359} respectively), the serpin undergoes an extensive conformational change [7]. The amino-

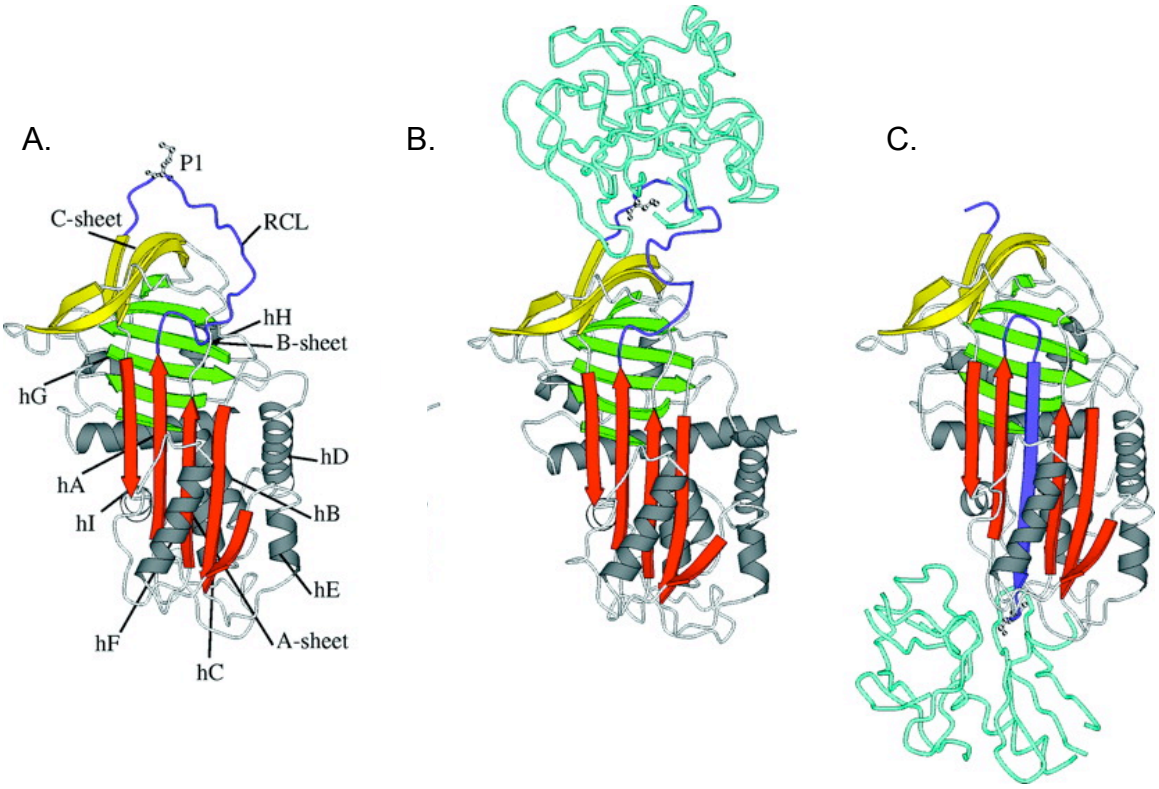

Figure 1.1 Serpin Structure

Serpin structure consists of three β sheets (A= red, B= green, C= yellow), nine α-helices (gray) and the RCL (blue). A. Native serpin structure. B. Initial binding event between serpin and target peptidase (turquoise). C. Diagram of conformational rearrangement of serpin structure to trap target peptidase (blue strand highlights insertion of RCL into β-sheet A. Image obtained from Silverman et al. (2001) [11].

terminal portion of the RCL irreversibly inserts into the center of β-sheet A, forming an additional strand in β- sheet A (Figure 1.1). This conformational change results in the transition from a stressed to a relaxed conformational state [35]. Additionally, the protease active site is distorted preventing the release of the protease (Figure 1.1). Since both the serpin and the protease are now inactive, the serpin-protease complex is rapidly degraded. The exact mechanisms that degrade serpin-protease complexes are unclear, however, studies have shown that lipoprotein-related protein (LRP) specifically binds to and promotes the internalization of some extracellular serpin complexes (SERPINA1, SERPINC1, and SERPINI1) [36, 37], whereas intracellular serpins seem to be degraded at least in part by the proteasome [38][Luke & Silverman, unpublished data].

1.2.3 Inhibitory Function

Metastability of the native state and the ability of serpins to undergo controlled conformational changes upon cleavage of RCL is central to the inhibitory activity of serpins. As such, slight mutations in the serpin framework can lead to protein misfolding and dysfunctional serpins [39]. Human diseases that are associated with mutations that affect the structure/function of serpins are termed serpinopathies [40-42].

The serpinopathies are a group of conformational diseases in which mutations facilitate serpin protein misfolding, polymerization, and/or aggregation [43]. Examples include; ATD (cirrhosis, emphysema), α1-antichymotrypsin (cirrhosis, emphysema), antithrombin (thrombosis), C1 esterase inhibitor (angioedema) and heparin-cofactor II (thrombosis), all of which lead to protein misfolding, intracellular aggregation, cellular

injury and distinct disease phenotypes [41-44]. Another example is familial encephalopathy with neuroserpin (NS) inclusion bodies (FENIB), which is due to missense mutations in the NS gene. These mutations cause an autosomal dominant neurological disorder characterized by progressive deterioration of cognition, memory and visuospatial skills [45, 46]. At least 5 different missense NS mutations have been identified, and based on their location within the serpin scaffold, they confer different degrees of instability relative to the native fold [47]. The more destabilizing mutations (G392R > G392E > H338R >S52R > S49P) are associated with a greater number and more pervasive distribution of inclusions, and an earlier onset and more severe progression of dementia and progressive myoclonus epilepsy [47, 48]. Transient transfection of the mutant genes into cell lines also shows that the more destabilizing mutations result in the formation of longer polymers and a greater degree of ER retention [49, 50].

1.3 α1- ANTITRYPSIN DEFICIENCY

α1-AT is an inhibitory serpin produced primarily in hepatocytes and secreted into the blood stream, where it functions to protect the lungs from degradation by neutrophil elastase. ATD, like FENIB, results from a missense mutation in the α1-AT gene resulting in polymers and/or aggregates formation. ATD can present with pulmonary dysfunction caused by the loss of the protective mechanisms of α1-AT in the lungs [2] and/or hepatic dysfunction due to protein accumulation in the ER of hepatocytes (Figure 1.2) [3]. As the archetypical member of the serpin family, α1-AT has been well

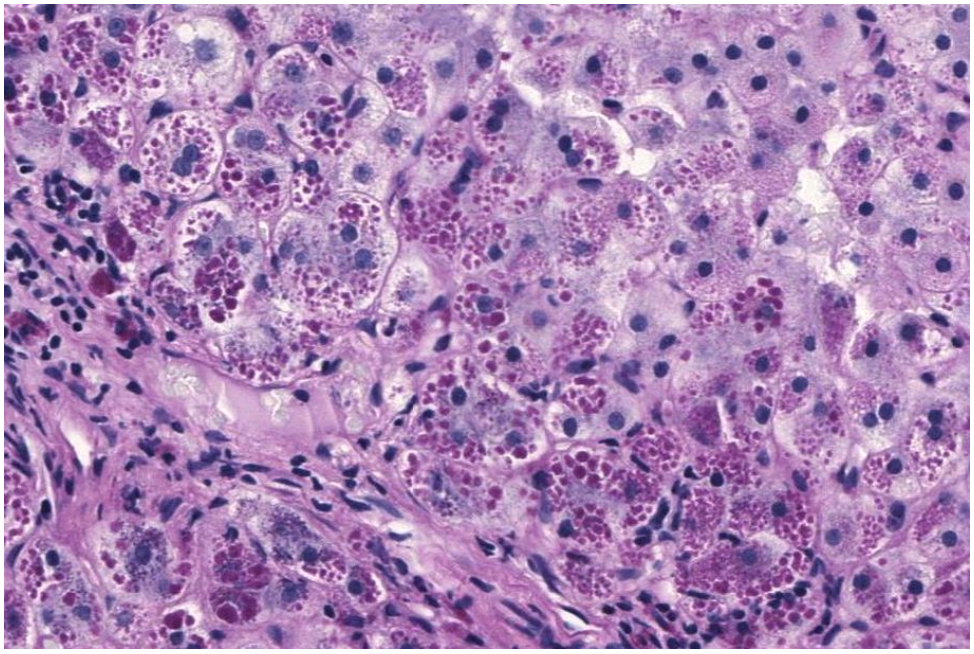

Figure 1.2 α1- Antitrypsin Expression in Liver Cells

Photomicrograph of hepatocytes obtained from a patient with ATZ. PAS (periodic acid Schiff stain used to identify AT glycoprotein) positive inclusions (purple) caused by ATZ accumulation in the ER of hepatocytes. Image obtained from: http://en.wikipedia.org/wiki/File:Alpha-1_antitrypsin_deficiency.PAS_Diastase.jpg#file Imaged by Jerad M Gardner, MD., Accessed June 18, 2011.

characterized. Therefore, in the following sections I will review the genetics, epidemiology, clinical manifestations, and protein characteristics of α1-AT.

1.3.1 Genetics of α1-AT

The α1-AT gene (SERPINA1) is located on the protease inhibitor cluster locus at 14q31-32.3 [51]. The gene spans 12.2 Kb in length and contains seven exons and six introns [52]. Studies have identified over 120 different alleles, each producing a different phenotypic variant [51]. Originally, α1-AT isolates were named based upon mobility during electrofocusing [53]. Normal wild type α1-AT was termed M, as it had a medium rate of mobility and all other variants were named A-L and N-Z based on whether they ran more proximal or distal to the M band [53].

α1-AT isolates can be broadly classified into three categories (Table 1.1). The first category is characterized by normal plasma levels, of which the M variants are the most common (approximately 95% frequency in the United States) [54, 55]. The second category is characterized by reduced plasma levels of circulating α1-AT. In this category, the two most common deficient alleles are Z and S. The Z allele is caused by a single point mutation (Glu342Lys) and is the most common deficiency mutant (ATZ) [55]. Similar to the Z allele, the S allele is also caused by a single point mutation (Glu264Val) but is associated with higher levels of circulating α1-AT as compared to ATZ [56]. The third category, null mutant is characterized by no detectable levels of circulating plasma α1-AT, and is commonly associated with an increased risk of developing emphysema (Table 1.1) [57].

Table 1.1 AT Variants and Mutants

Category	Allele	Mutation site (exon)	Sequence compared to base allele
Normal Variants	M1(Ala^{213})	V	
	M1(Val^{213})	III	Ala^{213} -> Val
	M2	II	Arg^{101} -> His
	M3	V	Glu^{376} -> Asp
	$M4^{11}$	II	Arg^{101} -> His
Deficiency Mutants	Z	V	Glu^{342} -> Lys
	S	III	Glu^{264} -> Val
	M_{malton}	II	Phe^{52} -> Delete
	S_{iiyama}	II	Ser^{53} -> Phe
Null Mutants	$Null_{HongKong}$	M2	Leu^{318} -> delete -> 5' shift -> $stop^{334}$
	$Null_{Saar}$	V	Glu^{376} -> stop codon-> truncation from carboxyl terminus

1.3.2 Epidemiology of α1- AT

Although AT variants have been described in every major racial group, an accurate account of frequency of ATD is difficult due to the large phenotypic variations amongst ATD individuals [51]. To try to determine the prevalence of ATD a number of population screenings have occurred. For example, in the 1970's a large nationwide α1-AT deficiency screen of newborns was carried out by Laurell and Sveger in Sweden [58]. Of the 200,000 individuals studied, 127 were identified as being homozygous for the Z allele and were followed for signs of disease progression. In this study, only 8%-10% of ZZ homozygotes developed clinically significant liver disease [58].

Since 1960's, when Laurel and Eriksson originally described ATD, gene frequency for ZZ homozygotes has been reported for different populations. The highest prevalence of ATD is reported in northern and western European countries [57, 59]. In the United States, it is estimated than ATD affects 1 in 2000 live births [1]. By utilizing computer modeling, it has been estimated that there are over one million people with severe ATD. If these estimates are accurate then ATD is one of the most common hereditary disorders [57].

1.3.3 Clinical Manifestations of & Treatments For α1-AT

ATD is associated with higher incidence of emphysema and cirrhosis. Patients with clinical manifestations of lung disease usually present with symptoms of shortness of breath, coughing, wheezing, and fatigue. Most ZZ homozygote patients are commonly

diagnosed as adults while in their 30's or 40's. Because ATD has many of the same symptoms as other common lung disease, such as COPD or asthma, it is often initially misdiagnosed. One study has shown that there was a seven year lapse between the onset of symptoms and the diagnosis of ATD [5].

Patients with ATD can also present with liver disease such as inflammation and cirrhosis [60]. ATD resulting in liver disease occurs in two age groupings; infants and adults. Approximately 10% of infants with ATD develop severe liver disease and accounts for a high portion of liver transplants in children [61]. As adults, only a small population of ATD patients develop liver disease. Specifically, liver disease is associated with the ER retention of ATZ in the hepatocyte cells, resulting in damage and cirrhosis (Figure 1.3). Currently, no patients expressing the null alleles (such as Null Hong Kong or Saar) have presented with liver disease [60]. These findings suggest that individuals with only certain mutations in α1-AT are prone to the development of liver disease [60].

Currently, the treatment options for α1-AT deficiency are very limited. In patients with cirrhosis or liver failure, ATD can be treated by organ transplantation [5]. The only approved treatment for ATZ related lung disease is intravenous α1-AT augmentation therapy, which boosts circulating levels of α1-AT [51]. Additionally, long-acting bronchodilators and inhaled corticosteroids can relieve the symptoms associated with COPD [62].

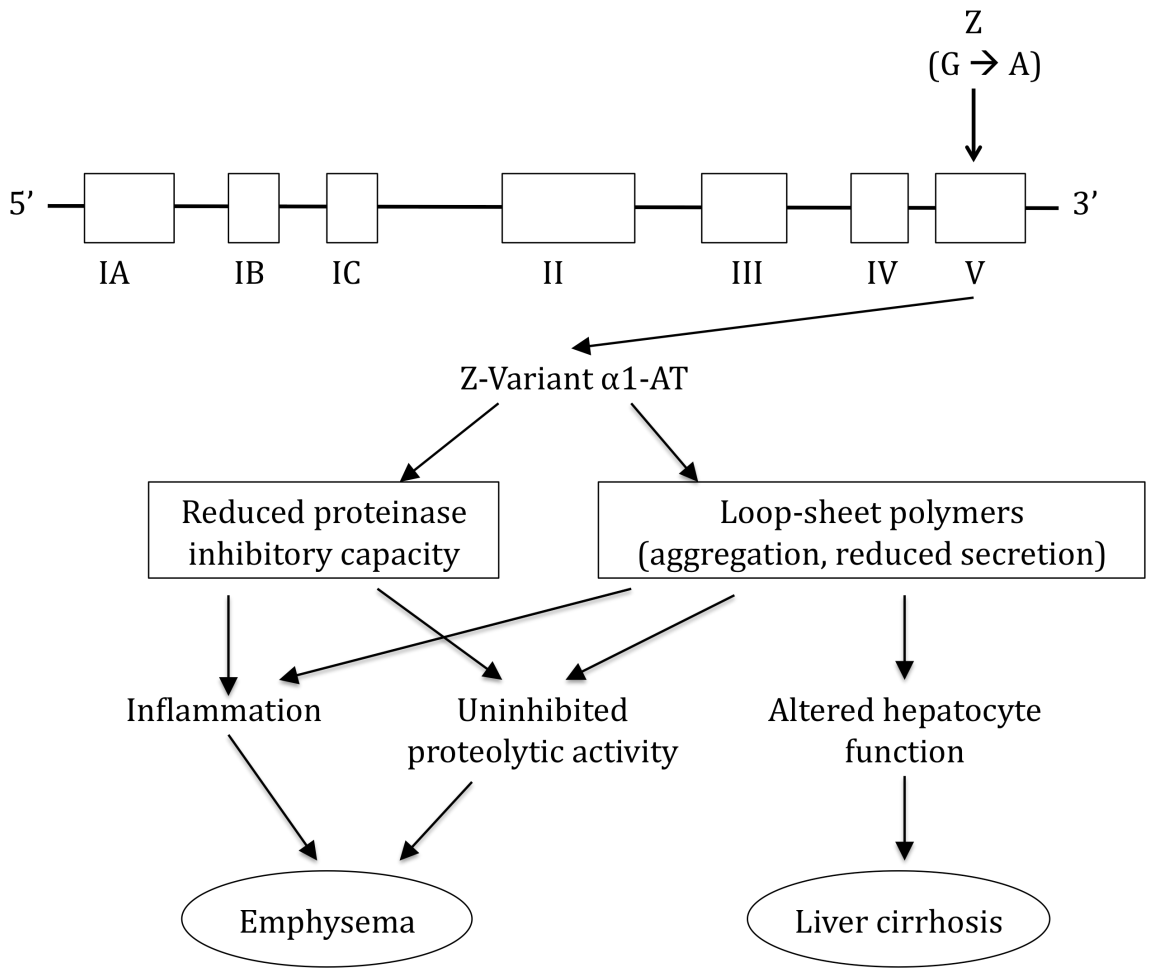

Figure 1.3 Common Manifestations of ATZ

ATZ is caused by a single point mutation in exon 5 of the AT gene. The Z allele results in polymerization and decreased serum concentrations, which can ultimately result in liver cirrhosis and/or emphysema. Image adapted from Fregonese and Stolk (2008) [63].

1.3.4 Protein Characterization of α1-AT

α1-AT is a 52-kDa glycoprotein produced primarily in hepatocytes, but also expressed in mononuclear phagocytes and neutrophils [52]. It inhibits a variety of serine peptidases, but its primary target is neutrophil elastase. As such, it has its greatest affect in the lungs, where it acts as an acute phase protein to protect against proteolytic damage caused by neutrophil elastase. Normal α1-AT plasma levels range from 20-53 μM [60]. Individuals with deficient alleles (Z or S) are associated with plasma levels that are (ZZ) 10-15% or (SS) 50-60%, compared to wild type levels, while null alleles (NHK or Saar) are associate with no circulating α1-AT [60].

The classical form of ATD is caused by a single point mutation, Z (Glu342Lys), in the α1-AT protein [55]. The substitution of a negatively charged glutamic acid with a positively charged lysine causes a destabilization of the serpin conformation by eliminating a crucial salt bridge that helps maintain the integrity of β-sheet A. This mutation distorts the relationship between the RCL and β-sheet A. This change in conformation results in the formation of higher ordered polymers causing the formation of complex aggregates in the ER of liver cells (Figure 1.4) [64].

The pathogenesis effect of the Z mutation is twofold. First, α1-AT is the major inhibitor of peptidase neutrophil elastase, which during an inflammatory response can destroy normal lung tissue [65, 66]. Thus, α1-AT protects the lungs by neutralizing misdirected neutrophil elastase through utilization of the irreversible serpin-protease complex, which is then targeted for degradation [67]. Therefore, retention of ATZ in liver

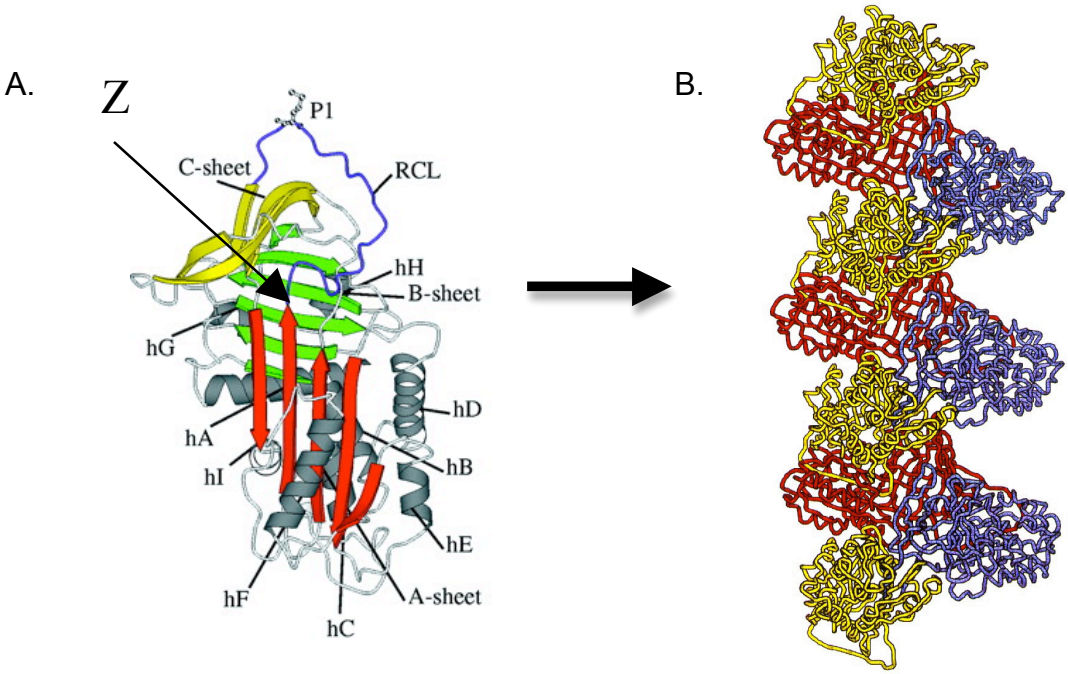

Figure 1.4 α1- Antitrypsin Z Variant Results in Polymerization

A. Z variant of α1- antitrypsin eliminates a crucial salt bridge that helps maintain the integrity of β-sheet A (red) resulting in a destabilization of the serpin structure. B. β-sheet A can then accept the loop of another ATZ molecule to form a dimer, which extends into a polymer (red, yellow, and blue each represent an individual molecule of ATZ). Reproduced from Lomas and Mahadeva, (1998) [40] and Silverman et al., (2001) [11].

cells significantly reduces the amount of α1-AT available to act as elastase inhibitors, causing a loss-of-function phenotype [65]. This reduction in serum levels of α1-AT results in premature development of emphysema, asthma, chronic bronchitis and bronchiectasis (Figure 1.3) [59]. Additionally, the retention and subsequent polymerization of α1-AT in the hepatocytes appears to be toxic, causing a gain-of-function phenotype resulting in liver disease (Figure 1.3 and 1.4).

1.4 CURRENT MODELS OF α1- ANTITRYPSIN DEFICIENCY

The expression of liver disease among homozygous ATZ patients is highly variable with clinical manifestations ranging from asymptomatic to fatal [4, 5]. This heterogenity suggests that additional genetic and/or environmental factors play an important role in development of liver disease. Currently, studies in yeast, mammalian cell lines, and transgenic mouse models have been employed to elucidate the molecular mechanisms of ATZ-induced liver disease. The following sections will highlight these model systems and how they have advanced out understanding of ATD.

1.4.1 Cell Culture Models

Mammalian cell lines indicate that the proteasomal and autophagic pathways may be limited in ATZ patients, thereby causing increased severity of the disease [68]. Studies by Wu and colleagues utilized skin fibroblast cell lines isolated from ATZ homozygous

patients that presented with or without liver disease [69]. Pulse chase experiments on fibroblasts transduced with ATZ showed that the cell lines cultured from patients exhibiting liver disease exhibit a decrease in the degradation of ATZ. This study suggested that differences exist in quality control recognition and/or disposal mechanisms in patients presenting with liver disease compared to those that do not present with liver disease. This study also suggested that improved ATZ clearance may help prevent liver disease [69].

Furthermore, studies completed by Kamimoto et al., utilized embryonic stem (ES) cells that were deficient for the *Atg5* gene (necessary for initiation of autophagy) to examine the effect autophagy has on ATZ accumulation [70]. Specifically, pulse-chase analysis of *Atg5* -/- ES cells transfected with ATZ showed significant reduction in the degradation of ATZ [70]. Additionally, in the absence of autophagy, aggregation of ATZ increased to the extent that large aggregates were found both in the ER and also in the cytoplasm of the cells. These data suggested that the degradation of ATZ, through autophagy, is likely to be fundamentally important in preventing liver damage caused by ATZ [70].

ATZ is also eliminated through the ubiquitin proteasome system [71]. Qu et al. showed a role of the proteasomal degradation pathway in the elimination of ATZ in a cell culture model [72]. Human fibroblasts transfected with ATZ showed inhibition of ATZ degradation when cell lines were exposed to proteasome inhibitors [72]. The reduced clearance of ATZ provided evidence that the proteasome plays a role in ATZ degradation. Overall, cell lines have indicated that the proteasomal and autophagic

pathways might be limited in ATZ patients causing increased severity of the disease [68].

1.4.2 Yeast Models

Yeast are simple single-celled organisms they share many of the same biological properties of mammals. Importantly, they have been shown to have similar aspects of protein synthesis, signaling, trafficking, and degradation. Yeast have been utilized to help elucidate the mechanism of liver disease associated with ATZ. For example Werner and colleagues showed that a portion of ATZ is eliminated by the ubiquitin proteasome system [71]. An AT yeast expression system was utilized to monitor degradation of ATZ during pulse-chase analysis. Wild-type yeast strains degraded the majority (~94%) of ATZ, while a yeast proteasome mutant (*pre1-1 pre2-2)* strain cleared less than half (~39%). The reduced clearance of ATZ provided parallel evidence that the proteasome plays a role in ATZ degradation.

Research utilizing the ATZ yeast expression model is notable for establishing ATZ as an ERAD substrate and identifying BiP, a molecular chaperone, as important for ATZ turnover [71, 73-75]. Furthermore, screens of yeast mutants for defects in the ER degradation of human ATZ have been completed. In one screen, *atg6*, was identified as a key player in ATZ disposition [76, 77]. Specifically, *atg6* is required for initiation of formation of autophagosomes in autophagy [77]. Additionally, *atg16*, another autophagy gene, is important for degradation of aggregated ATZ that accumulates at high levels after protein expression. Furthermore, yeast overexpressing ATZ distributed the

accumulated protein to the autophagic pathway [77]. These results confirmed the importance of autophagy, in addition to the proteasome, in the disposal of ATZ.

1.4.3 Mouse Models

A number of different ATZ transgenic mouse model have been developed [78-80]. ATZ transgenic mice (PiZ) exhibit the hallmarks of the human deficiency including; development of PAS-positive intracellular globules of ATZ aggregates, liver disease and hepatocellular carcinoma [78-81]. Studies completed by the Perlmutter laboratory utilized PiZ transgenic mice to examine hepatocytes for damage caused by expression of ATZ [82]. Results indicated two types of hepatocytes within the PiZ mouse, those with PAS-positive accumulations and those without accumulations. ATZ globule containing cells showed activation of caspases, NF-κB (nuclear factor kappa-light-chain-enhancer of activated B cells), and autophagy, but a block in proliferation. ATZ globule-devoid hepatocytes showed an increase in proliferation, suggesting that the globule-deficient cells are younger (possibly before globule formation) or are better able to eliminate the accumulated protein through the activation of autophagy [82].

Transgenic mice with liver-specific inducible expression of ATZ were also developed [83]. This system is advantageous because it allows for characterization of early cellular responses to ATZ. Furthermore, constitutively active systems may adapt to the expression of ATZ over time, and therefore the inducible system removes this bias [83]. The inducible system utilizes a tetracycline (Tet) controlled expression system, in which the ATZ transgene was downstream of a Tet response element (TRE) [84]. In

this Tet-off system the tetracycline is removed, which allows binding of the TRE to occur, resulting in the transactivation of the ATZ gene. Studies showed that inducing ATZ expression activated caspases, NF-κB , and Bap31 (endoplasmic reticulum associated degradation (ERAD) protein) but not the unfolded protein response (UPR) [83].

Mouse studies were also important for establishing autophagy as an important mechanism for ATZ degradation. The ATZ inducible transgenic mice were mated to GFP-LC3 mice. *LC3* is a cytosolic protein that is processed and inserted into the phagophore. During enhanced autophagy, the distribution of GFP-LC3 changes from diffuse to punctate. This feature is used to monitor increases in autophagy. Under starved conditions the GFP-LC3 mouse generates GFP positive puncta. Studies utilizing the transgenic mouse with inducible expression of ATZ mated with GFP-LC3 resulted in accumulation of GFP positive puncta spots [70]. These results indicated that autophagy is activated by aggregated ATZ and the changes it specifically imposes on the cell. Overall, the mouse studies suggested that the accumulation of ATZ is toxic, which is due, in part, to the limited capacity of protein quality control systems to eliminate the misfolded protein

In summary, studies in yeast, mammalian cell lines, and transgenic mice have started to elucidate the molecular mechanisms of ATZ-induced liver disease. Importantly, this research has shown that misfolded ATZ accumulates in hepatocytes and that multiple degradation pathways are required for its elimination. In mammals, studies indicate that aggregated or insoluble proteins are degraded via the autophagic pathway [64, 77]; whereas, the soluble misfolded oligomers are degraded via the proteasomal pathway [70, 76, 85-88]. The next section of this dissertation will examine

general protein folding, how proteins transverse the secretory pathway, and cellular mechanisms for degradation of abnormal proteins.

1.5 PROTEIN FOLDING AND SECRETORY PATHWAY

Protein folding is the process by which a polypeptide folds into its functional three-dimensional structure (Figure 1.5). Proteins destined for secretion begin in the rough endoplasmic reticulum, which they enter as newly synthesized polypeptide. The polypeptides enter the ER as a result of the interaction between their emerging signal peptide and the signal recognition particle (SRP) complex. In eukaryotes, the SRP complex is a multimeric protein, which is comprised of 6 distinct polypeptides and a RNA molecule. The interaction of the SRP with the receptor is required for cotranslational protein targeting [89]. The requirements for this event and even the targeting of the ribosome to an ER translocation pore are still being investigated. Following the delivery of the nascent protein into the ER lumen, proteins must fold and assemble. Therefore, one of the main functions of the ER is to initiate protein folding, which is accomplished through a complex network of protein chaperones, enzymes, and co-factors [90-92]. These components are expressed within the ER lumen and help catalyze the folding and maturation of proteins that traverse the secretory pathway.

Proteins with destinations beyond the ER are sorted and packaged into transport vesicles. ER vesicles are formed by the binding of COPII to the external side of the membrane, selection of cargo, and then budding from the ER membrane (Figure 1.5)

[93]. At this time it is still being investigated as to how the COPII vesicles are able to selectively recognize and sort the variety of proteins transported as cargo [94]. The vesicles are then directed towards the Golgi complex, uncoated, and fused to the *cis*-Golgi membrane to deliver cargo to the Golgi complex. During transport from the ER to the Golgi complex the cell ensures that vesicles dock correctly through the use of targeting molecules termed SNAREs, which can be present on both vesicles (vSNAREs) and target membranes (tSNAREs). Proteins that are required in the ER and recycled vesicle components are retrograde transported back to the ER from the Golgi via COPI coated vesicles [95].

Proteins remaining in the Golgi then undergo cisternal migration in which they move from the *cis*-Golgi stack to the *trans*-Golgi (Figure 1.5). During this progression post-translational modification such as glycosylation and phosphorylation occurs. Additionally, sugars may be added to the proteins to help direct the protein to its final destination. Proteins then undergo another round of sorting in the *trans*-Golgi network (TGN). Proteins are trafficked into more specialized compartments and shipped to their intended destinations by their placement into one of at least three different types of vesicles: exocytotic, secretory, and lysosomal.

Exocytotic vesicles contain proteins destined for extracellular release. After packaging the vesicles bud off and move immediately towards the plasma membrane where they fuse and release their contents into the extracellular space. Secretory vesicles contain proteins destined for extracellular release. However, after the vesicles bud off they are stored in the cell until a signal is given for their release. When the

Figure 1.5 Protein Synthesis and Secretory Pathway

Ribosomes synthesizing proteins bearing an ER signal sequence become bound to the rough ER. As translation is completed on the ER, the polypeptide chains are inserted into the ER membrane or cross it into the lumen. Some proteins remain resident in the ER, the remainder move into transport vesicles that fuse together to form new *cis*-Golgi vesicles. Each *cis*-Golgi cisterna, with its protein content, physically moves from the *cis* to the *trans* face of the Golgi stack (red arrows). As this cisternal progression occurs, many luminal and membrane proteins undergo modifications, primarily to attached oligosaccharide chains. Some proteins remain in the *trans*-Golgi cisternae, while others move via small vesicles to the cell surface or to lysosomes. Certain proteins move to the cell surface in transport vesicles and are secreted continuously (constitutive secretion). Retrograde movement via small transport vesicles retrieves ER proteins that migrate to the *cis*-Golgi and returns them to the ER. Similarly, *cis*- or *medial*-Golgi proteins that migrate to a later compartment are retrieved by small retrograde transport vesicles. Adapted from Glick and Malhotra (1988) [96] .

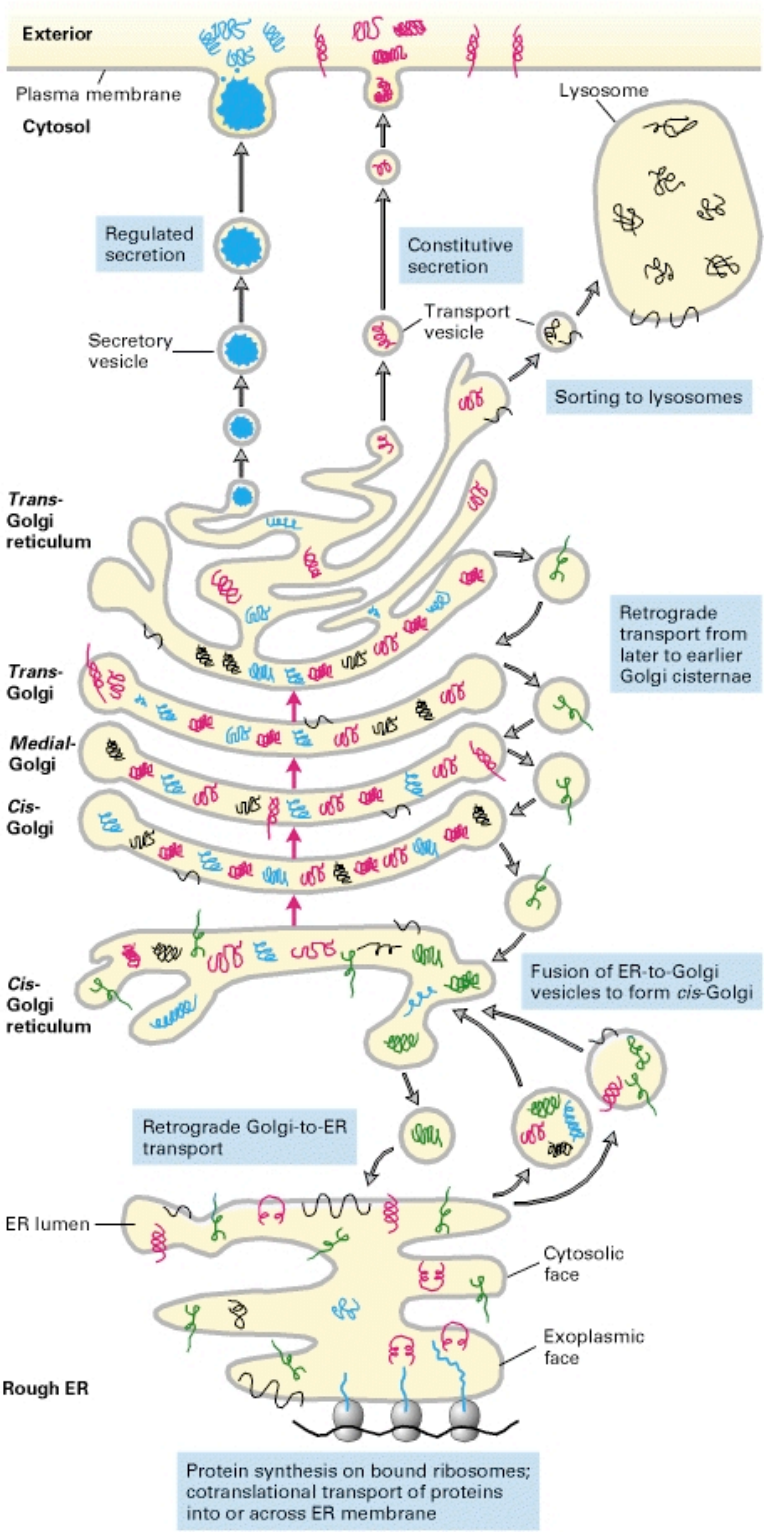

Figure 1.5 Protein Synthesis and Secretory Pathway

appropriate signal is received the vesicles move towards the plasma membrane and fuse to release their contents. Lysosomal vesicles contain proteins destined for the lysosome. When this vesicle fuses with the late endosomes it becomes a mature lysosome.

The secretory pathway is a highly regulated process, and as a result, proteins are delivered and function in their correct environment. Examples of this specificity are that the ER retains chaperones, the Golgi maintains a concentration of oligosaccharide trimming enzymes, lysosomes receive digestive enzymes such as proteases, and receptors accumulates at the cell surface, all as a result of the secretory pathway. Furthermore, if a protein fails to fold correctly the cell is able to recognize the misfolded protein and activates different cellular responses (described below).

1.6 ENDOPLASMIC RETICULUM QUALITY CONTROL

The endoplasmic reticulum has a quality control system that is capable of recognizing misfolded proteins and targeting abnormal proteins for destruction. Proteins that enter the secretory pathway start by translocating into the ER, which contains molecular chaperones that assist in protein folding and enzymes that catalyze post-translational modifications. These proteins are essential in the quality control system, because proteins must obtain a correct state in order to be processed through the secretory pathway [97]. This quality control process involves the glycosylation of nascent proteins including *N*-linked glycosylation within the lumen of the ER and *O*-linked glycosylation

within the Golgi complex. In eukaryotes, most *N*-linked glycosylation begin with addition of a 14-sugar core (3 glucose, 9 mannose, and 2 N-acetylglucosamine molecules) to an asparagine in the polypeptide chain of the target protein. After transfer of the core oligosaccharide two glucoses are removed by glucosidases I and II, which generates a monoglucosylated protein that interacts with molecular chaperones calnexin and calreticulin. Cleavage of the remaining glucose by glucosidase II terminates the interaction with calnexin and calreticulin allowing correctly folded proteins to exit the ER.

Although the exact mechanisms are still being defined, it is known that glucosyl transferase (GT), senses the folding status of newly synthesized proteins and specifically tags the oligosaccharide moieties of incompletely folded proteins by adding glucose residues to their *N*-linked glycans. This addition of glucose residues prevents incompletely folded proteins from exiting the ER while allowing them to re-enter the calnexin/calreticulin cycle [98]. Proteins persistently misfolded are retrotranslocated back to the cytoplasm, where they are degraded by the proteasome in a process termed ER-associated degradation (ERAD) [99-105].

1.6.1 Endoplasmic Reticulum Associated Degradation

Proteins that fail to achieve the correct state are targeted by ERAD for protein degradation via the ubiquitin proteasome pathway. The process of ERAD contains six main steps: selection of substrate, targeting to ERAD, retrotranslocation of substrate into the cytosol, ubiquitylation/ de-ubiquitination and ultimately proteasomal degradation (Figure 1.6) [106].

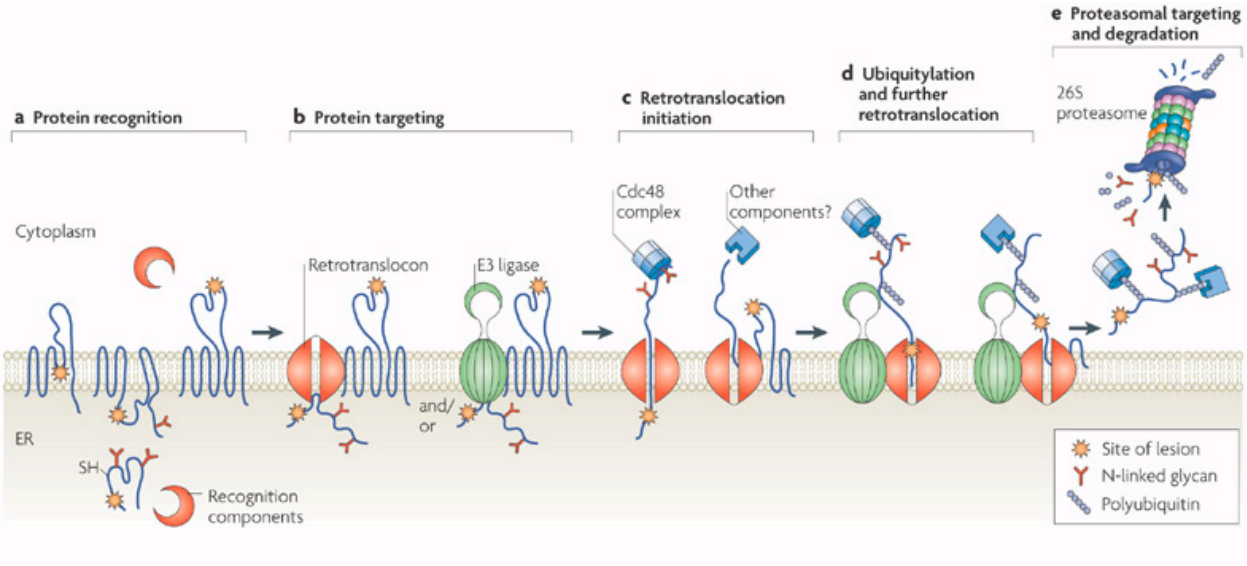

Figure 1.6 ERAD Mechanism

A. ERAD begins with recognition of target substrate. B. Substrate is targeted to retrotranslocation machinery (E3 ligase). C. Retrotranslocation is initiated resulting in translocation of substrate into the cytoplasm. D. Proteins are polyubiquintylated and further retrotranslocated from the ER into the cytoplasm. E. Substrates are targeted for degradation by the 26S proteasome. Image adapted from Vembar and Brodsky (2008) [106].

Recognition of potential ERAD substrates is incompletely understood. However, misfolded proteins maybe recognized and targeted to ERAD by displaying immature glycans, hydrophobic regions, or incorrect disulfide bonds. As previously described, *N*-linked glycosylation is important for the correct adoption of the glycoprotein's native structure. In this process, terminally misfolded proteins are extracted from the calnexin/calreticulin cycle and targeted for degradation by calnexin/calreticulin or EDEM (ER degradation enhancing alpha-mannosidade-like protein). These factors have been reported to accelerate ERAD of glycoproteins, however the exact mechanism is still unknown [107-109]. Substrate recognition may also involve exposure of hydrophobic regions [110]. If a protein is folded correctly then hydrophobic regions are usually located within the interior of the protein [110]. However, in an unfolded protein these regions may become exposed, leading to recognition by molecular chaperones that then target the misfolded protein for ERAD.

Lastly, substrate recognition may involve the formation of disulfide bonds. In the oxidizing environment of the ER oxidoreductases help establish disulfide bonds between thiol groups of cysteine pairs in the newly synthesized polypeptide. Disulfide bonds play an important role in the folding and stability of some proteins into their native state. The formation of disulfide bonds may require multiple breaks and reformation, which are catalyzed by disulphide isomerases. Disulphide isomerases have been suggested to work through a substrate-binding domain, which is vital in recognizing substrates for ERAD [111, 112].

Once the substrate is recognized as a misfolded protein, it is targeted for retrotranslocation to the cytosol where it is ultimately destroyed by the proteasome.

ERAD degrades a variety of misfolded proteins, which differ in structure, conformation and physical properties. Studies in yeast show, depending on the location of the substrate, different components of the ERAD pathway are utilized for targeting substrates for degradation. For instance, proteins with misfolded luminal domains are monitored by ERAD- luminal (ERAD-L) pathway. ERAD-L substrates seem to require ER to Golgi transport, the molecular chaperone BiP, the transmembrane protein Der1p, and Hrd1p (E3 ubiquitin ligase) [113]. ERAD-L substrates interact with BiP/GRP78, which targets the protein to Der1p for translocation into the cytosol and ultimately degradation by proteasome. In contrast, substrates with misfolded cytosolic domains are monitored by ERAD-cytosolic (ERAD-C) pathway. ERAD-C differs from ERAD-L in a variety of ways: substrates are not transported from the ER to the Golgi, and ERAD-C utilizes Doa10p as its E3 ubiquitin ligase [114]. Furthermore, substrates with misfolded membrane domains are monitored by ERAD-membrane (ERAD-M) pathway. ERAD-M is mostly undefined, but it appears that lesions on the membrane-spanning domain use the E3 ligase, similar to that used in ERAD-L. Furthermore, certain ERAD substrates require overlapping components, suggesting these processes are not mutually exclusive [115-117].

The ubiquitin-proteasome system (UPS) is the final destination for all ERAD substrates. However, the UPS is located in the cytoplasm, therefore, terminally misfolded proteins have to be retrotranslocated from the ER into cytoplasm. Two separate protein complex candidates have been identified in involvement in the retrotranslocation channel, Sec61 and Derlin [118-121]. However, like many components of ERAD, the retrotranslocation mechanism and components are still being

investigated, and those likely depend on the substrate being translocated into the cytosol. Additionally, the cell-division cycle (Cdc48) complex has been found to play an important role in the retrotranslocation of substrates [122]. Cdc48 is a hexameric AAA-ATPase that associates most commonly with the adapters ubiquitin fusion degradation 1 (Ufd1) and nuclear protein localization 4 (Npl4). This complex is recruited to the ER membrane and binds with a large number of ER-resident components (Der1p, Hrd1, GP78 (in mammals), and Doa10 (yeast)). The Cdc48 complex transports substrates from the ER into the cytosol utilizing its ATPase activity.

The last step in ERAD involves the degradation of the substrate by the UPS and is discussed in detail in section 1.7.1. Overall ERAD is a protein quality control process that results in the degradation of misfolded proteins from the ER. Substrates are identified and targeted by a variety of molecular chaperones that ultimately result in the ubiquitination of substrates. The substrates are retrotranslocated into the cytosol where they are degraded by the ubiquitin proteasome system. ERAD appears to be highly conserved in higher organism yet many of the specific components are still being investigated and defined [106].

1.6.2 Unfolded Protein Response

The unfolded protein response (UPR) is a cellular stress response that becomes activated once ERAD is overwhelmed. It is an intracellular signaling pathway with two main goals; initially to restore normal function to the cell by halting protein translation and then to activate signaling pathways that lead to increasing the production of molecular chaperones involved in protein folding [123-125] (Figure 1.7). The target

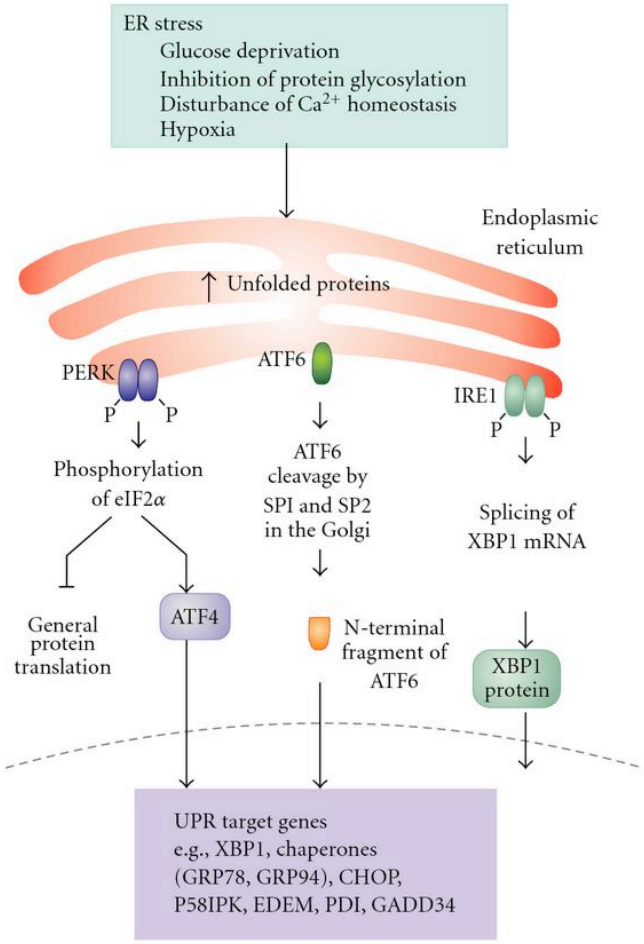

Figure 1.7 Unfolded Protein Response

ER stress stimulates the activation of PERK, ATF6 and IRE1. PERK phosphorylates eIF2α, which inhibits general protein translation. PERK also allows the translation of ATF4, which activates transcription of chaperones such as BiP. ATF6 undergoes specific proteolysis in the Golgi apparatus, which leads to activation of target genes such as XBP1. IRE1 catalyzes the alternative splicing of XBP1 mRNA leading to expression of the active XBP1 transcription factor. Image adapted from Fulda et al. (2010) [126]

genes of the UPR encode factors that are involved in many different processes, such as phospholipid biosynthesis, protein maturation in the ER, and secretory pathway function [127].

UPR is initiated by the activation of the transmembrane serine kinase endonuclease, IRE1. Current studies are indentifying factors involved in the activation of IRE1. One model suggests, that in the presence of high levels of misfolded protein, BiP/GRP78 dissociates from IRE1, which allows BiP/GRP78 to become available to bind to misfolded proteins [128]. The release of IRE1 from its complex with BiP/GRP78 results in the activation of IRE1 [128, 129]. A second model proposes that unfolded proteins interact directly with IRE1 ER-lumenal domain, resulting in the activation of IRE1 [130]. Regardless of the method, IRE1 activates itself through transautophos-phorylations, resulting in an activated domain, which is able to then cleave a mRNA substrate of XBP1 (X-box binding protein). Cleavage of XBP1 results in removal of a 252bp intron. The removal of the intron allows the transcription factor XBP1 to be efficiently translated [131, 132]. The now activated XBP1 transcription factor is translocated into the nucleus and upregulates stress genes by binding to stress element promoters in the nucleus. [127].

In addition to the activation of IRE1, two other stress receptors (PERK and ATF6) are activated during ER stress. PKR-like ER kinase (PERK) is an ER transmembrane kinase that phosphorylates the α subunit of eukaryotic initiation factor 2 (eIF2α) which leads to the reduction of translation initiation complexes and therefore general protein translation. Paradoxically, this allows eIF2α-independent translation of ATF4 (activating transcription factor 4), current studies suggest this is due to internal ribosome entry

sequence (IRES), which may confer translational advantage to mRNA under certain cellular conditions, such as when global translation is down regulated [133]. ATF4 in turn activates transcription of protein chaperones such as BiP/GRP78. Furthermore, activating transcription factor 6 (ATF6) undergoes proteolysis in the Golgi membrane leading to its activation of target genes such as XBP1. Together these three stress receptors (IRE1, PERK, & ATF6) block protein translation, increase protein chaperone expression and enhance ERAD pathways allowing for a reduction in accumulated misfolded proteins (Figure 1.7).

1.7 CELLULAR MECHANISMS FOR DEGRADATION OF PROTEINS

An important cellular process is the maintenance of proteins in their native structure. It is estimated that ~25% of all newly synthesized secretory proteins misfold and are subsequently degraded [105]. There are a number of cellular mechanisms that degrade unnecessary (damaged or modified) proteins in eukaryotic cells. The following sections will discuss the proteasomal and autophagic degradation pathways.

1.7.1 Ubiquitin Proteasome System

In the cytosol, the majority of proteins are eliminated by the ubiquitin (Ub) proteasome system [134]. The UPS is a complex system that requires two major steps for degradation of targeted proteins. Step one is selection of target proteins by covalent attachment of ubiquitin, targeting the protein substrate for degradation. Step two involves the degradation of targeted proteins by the 26S proteasome [135-139].

1.7.1.1 Poly-Ubiquitination of target substrates

Proteins targeted for degradation by UPS are first tagged with Ub [135-139]. Ubiquitin is a small 76 amino acid protein that is abundantly expressed in all eukaryotic cells. Ubiquitination is an enzymatic, post-translational modification in which an isopeptide linkage between the C-terminal glycine of ubiquitin and usually an amino group of a lysine residue in the target protein [139]. The process of protein substrate ubiquitination occurs in a series of steps. First ubiquitin is activated in an ATP requiring reaction by an E1 ubiquitin-activating enzyme. This initial step ultimately results in a thiol ester linkage between the C-terminal carboxyl group of ubiquitin and the E1 cysteine sulfhydryl group [136]. The second step is the transfer of ubiquitin from E1 to the active site cysteine of a ubiquitin conjugating enzyme E2. The E2 enzyme acts as a carrier of ubiquitin that, with the help of E3 ligase, transfers the ubiquitin to targeted substrates. E3 ligase can function in the transfer of ubiquitin onto the substrate, or it can function as an adaptor to facilitate the positioning and transfer of ubiquitin from the E2 directly onto the substrate. E3 enzymes are therefore responsible for the specificity of the target selection for ubiquitination [135-139]. Both E2 and E3 enzymes exists as large families, therefore in the ubiquitination cascade, an E1 can bind to dozens of E2's, which can bind to hundreds of E3s. Once a protein is monoubiquitinated, additional ubiquitins can be added resulting in the formation of a polyubiquitinated chain (Figure 1.8). Specifically, polyubiquitinated chains form from the C-terminal gly-76 covalently linking to one of seven lysine residues (K6, K11, K27, K33, K48 and K63) [140]. Lys-48 and lys-11 are the most common linkage sites, while lys-63 appears to have a non-proteolytic role. Of important note, studies in yeast investigating lys-11 have shown that when ER stress is

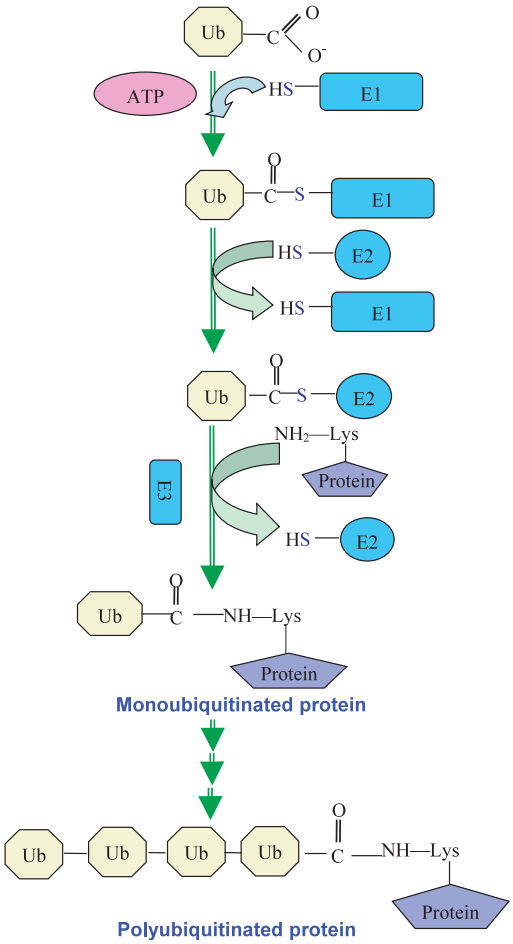

Figure 1.8 Protein Ubiquitination Pathway

Ubiquitin (Ub) is activated by E1 enzymes that transfers Ub to E2 carrier, which interacts with E3 ligase to target the protein substrate for degradation. Polyubiquitination of substrate is required to target proteins for destruction by the proteasome. Figure adapted from Nandi et al. (2006) [139]

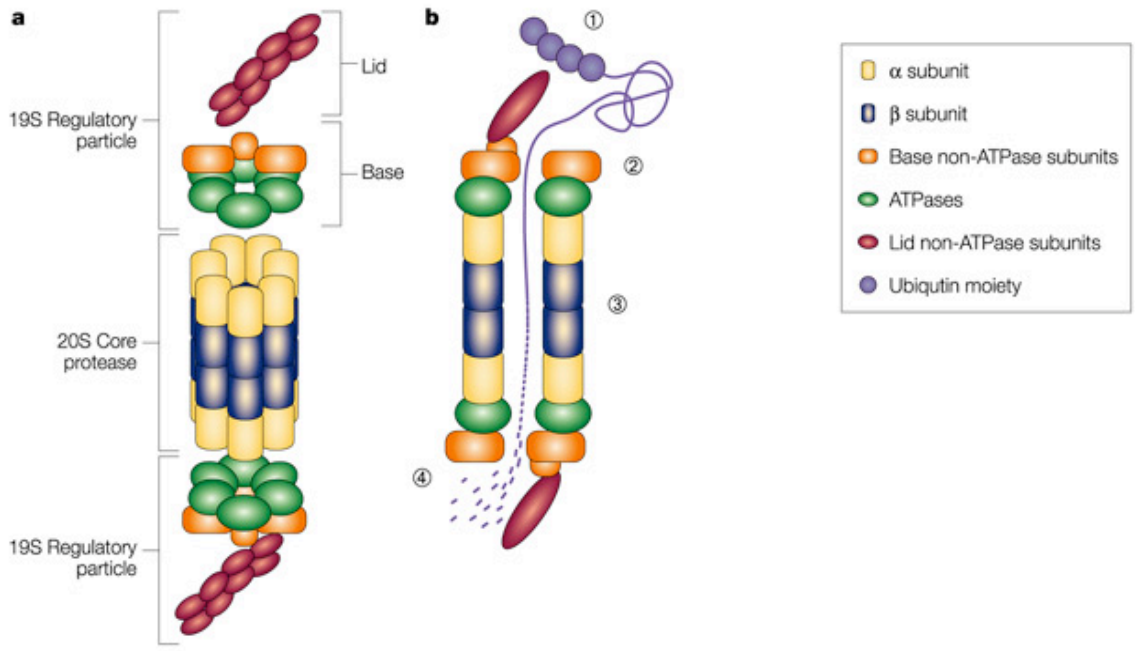

Figure 1.9 26S Proteasome

The 26S proteasome is essential in the degradation of proteins that have been tagged with ubiquitin. A. Structure of the 26S proteasome composed of the 20S core protease complex (yellow and blue) and the 19S regulatory particle that is composed of the lid and base components (green, orange, red). B.1. 19S regulatory particle (red) recognizes the polyubiquintylated protein (purple). B.2. The tagged protein is unfolded and translocated through the base complex into the 20S core particle. B.3. Once inside the 20S core the protein is exposed to proteases and broken down. B.4. The short peptides are then released to be reused by the cell in the formation of new proteins. Figure adapted from Sullivan, Shirasu, Deng (2003) [141]

artificially induced lys-11 linked chains are enhanced, additionally the mutation K11R results in growth defects and activation of UPR [140]. These results suggested that lys-11 plays an important role in ERAD [140] [136].

1.7.1.2 Degradation of polyubiquitinated substrate by 26S proteasome

The 26S proteasome recognizes, processes, and ultimately degrades target protein substrates. The 26S proteasome is an ~2.5 MDa complex that is comprised of different subunits that function together to degrade proteins into short (7-8) amino acid peptide sequences that are recycled for use within the cell [136, 139, 142]. The 26S proteasome is comprised of two 19S regulatory caps and a 20S core catalytic complex structure (Figure 1.9). The 19S regulatory cap is composed of two distinct structures the lid and base units (Figure 1.9). The lid recognizes ubiquitinated proteins while the base is responsible for unfolding and threading the protein into the 20S core. Therefore, the 19S structure allows for the recognition of polyubiquitinated proteins, de-ubiquitination, unfolding, and then transfer of those proteins into the lumen of the 20S catalytic core for destruction, thus preventing nonspecific proteolysis [137, 139, 142-144]. The 20S core contains the proteolytic activity that is ultimately responsible for the destruction of the target proteins [145]. The 20S core is a hollow barrel shaped structure comprised of four (2 α and 2 β) stacked heptameric rings (Figure 1.7) [137, 139, 142]. Once the targeted protein enters the 20S core, three catalytic sites (trypsin, chymotrypsin, and caspase sites) degrade target substrates resulting in short amino acid peptides sequences that are recycled for use in the cell [137, 139, 141, 142].

1.7.2 Autophagic Pathway

Eukaryotic cells have two conserved mechanisms to degrade proteins, the proteasome (described above) and the lysosome. The lysosome is designed to degrade larger and more complex substrates [146-148]. The lysosome is a double membrane organelle that contains different hydrolyases and proteases that work in an acidic environment to non-discriminately degrade proteins transported into the compartment. Autophagy is the process that transports macromolecules into the lysosome during times of nutrient starvation or other physiological conditions [139, 142, 149]. Autophagy is a tightly regulated process that plays a normal part in cell growth, development, and homeostasis. A variety of autophagic processes exist (macroautophagy, microautophagy, chaperone mediated autophagy (CMA)) all having in common the degradation of intracellular components via the lysosome.

Briefly, macroautophagy involves the sequestering of cytosol, organelles, and/or proteins in a double-membrane vesicle called an autophagosomes. Autophagosomes form from the elongation of precursors and is initiated by class III phosphoinositide 3-kinases and autophagy-related gene (Beclin-1) [150]. The autophagosome is a transport vesicle, and is targeted to the lysosome. The outer membrane of the autophagosomes fuses in the cytoplasm with the lysosome to form the autophagolysosome. The inner membrane vesicle (autophagic body) is released into the lumen of the lysosome where the contents are degraded [151]. Macroautophagy is activated during nutrient starvation, and it becomes the initial source of amino acids and other essential macromolecules [149]. Conversely, microautophagy involves the

sequestering of cytosol, organelles, and/or proteins, however, instead of an autophagosome (macroautophagy) the engulfing membrane is the lysosome itself [152]. Microautophagy has been associated with degradation of long-lived proteins within the cells and appears unresponsive to starvation as a stimulus [153]. CMA functions similarly to macroautophagy and microautophagy, however substrate proteins are directly translocated through the lysosomal membrane into the lumen without the formation of intermediate vesicles.

Autophagy is essential in helping to maintain the balance of proteins in the cell. Regardless of the form of autophagy it is mediated through the lysosomal degradation pathway. Autophagy can be induced by both external and internal stimuli (such as nutrition or mTOR inactivation). The autophagic response has been described in various pathophysiological conditions, including ATD.

1.8 *C. elegans* AS A MODEL SYSTEM

Studies designed to understand the mechanism of ATZ-induced liver disease have lead to significant insights into the cellular responses to misfolded or aggregation-prone proteins, which include characterization of disposal and ER-stress induced signaling pathways (mentioned above). However, additional studies are required to understand how genetic modifiers influence how ATZ is processed, secreted, and/or degraded. Although transgenic mouse lines, cell culture and yeast models are useful for studying ATD, there are some disadvantages: for instance both yeast and cell culture lack advanced multicellular processes, whereas mouse lines are expensive and time

consuming to study for long term effects. Therefore, we sought to develop a different *in vivo* model that would permit a more comprehensive evaluation of the genes involved in the cellular response to and disposal of ATZ. For this reason we have developed a *C. elegans* model of ATZ.

Sydeny Brenner in the early 1970's completed groundbreaking research into the molecular and developmental biology of *C. elegans* establishing it as a model organism [154]. There are many advantages to utilizing *C. elegans* as a model for ATD: 1) the small size (~1000 cells; ~1.5 mm in length as an adult), 2) the transparency (cells can be visualized using a standard dissecting microscope), 3) the ease of propagation (over 300 progeny can be hatched from a single worm), 4) the ease of animal manipulation, 5) large numbers that can be grown, 6) the short life cycle (3 days), 7) the short life span (20 days), 8) the knowledge of the entire genome, 9) ease of genetic screens (mutagenesis and RNAi) and 10) the cost efficiency [155]. Furthermore, transgenic animals are generated with relative ease and provide a wealth of information regarding how a gene is regulated and function it performs within the context of a whole organism. In a null mutant background, altered (mutated) copies of a gene can be easily reintroduced to study structure-function relationships. In some cases where a null fails to yield an overt phenotype, overexpression of a gene may provide insights into protein function [156]. Transgenes fused to one or more fluorescent proteins or affinity tags can be exploited for the study protein-protein interactions and target protein identification [157].

1.8.1 *C. elegans* a Model for Studying Human Diseases

The number of human disease-related genes that share at least modest homology ($E < 10^{-10}$ on BLASTP searches) with *C. elegans* genes ranges from 40-75% [158-163]. However, this degree of relatedness may still be an underestimate as the rapid divergence of non-essential domains and exon shuffling may impair the ability of the BLASTP algorithm to detect high-scoring segment pairs between orthologous genes [164]. For example, the *C. elegans* orthologue of vertebrate *P53*, *cep-1*, which also contains the five signature domains and residues commonly mutated in human malignancies, was detected only after using a combination of the squid P53 as the query, PSI-BLAST and the Block Maker tool [165]. Moreover, even if a human disease-related gene does not have an orthologue in *C. elegans*, there is still a high likelihood that a homologous gene, a protein domain or the constituents of an associated biochemical pathway (especially if it encompasses a core cellular function like signal transduction, synaptic transmission or membrane trafficking) are conserved to the extent that this model system can be exploited to lend insight into human pathobiology [166, 167].

The *C. elegans* model system has been used to study a variety of human diseases including Alzheimer's disease, Parkinson's disease, Huntington's disease and Muscular Dystrophy [168]. The majority of these models involve the accumulation of a misfolded protein that results in a disease phenotype. For instance, Parkinson's disease (PD) is a neurodegenerative disorder that has been characterized by the abnormal accumulation of alpha-synuclein (*α*-syn) protein in the brain [169]. Recently a *C.*

elegans model of PD has been used to identify gene products that were neuroprotective [170]. Specifically, this model over expresses the α-syn protein resulting in the accumulation of α-syn in the neurons of the worms. Utilizing this model ~900 possible targets were screened through RNAi methods, resulting in 20 candidate gene products that when inhibited led to an enhanced misfolding of α-syn in the worm. Ultimately this research led to the identification of VPS41, which encodes a conserved protein necessary for lysosomal biogenesis and ultimately a potential target for therapeutic treatments of PD [171].

C. elegans has also been used to gain an understanding of Huntington's disease (HD). HD is caused by repeated stretch of glutamines in the polyQ region of the Huntington gene, *HTT*. The normal range of glutamine repeats is fewer than 36, however when that number is exceeded, the *HTT* gene has different characteristics resulting in the gradual damage to specific areas of the brain. In *C. elegans* most of the research has been based upon the toxicity associated with polyglutamine repeats. This transgenic approach uses different polyglutamine (polyQ) repeat lengths fused directly with GFP and a promoter that drives expression in body wall muscle of the worm [172]. Expression of GFP::Q82 resulted in aggregate formation and induction of stress response proteins. Furthermore, a large scale RNAi screen identified genetic modifiers of the polyQ accumulations, which included a large set of genes involved in protein folding and degradation [173]. This research suggests that modeling human diseases in *C. elegans* may provide insights into the mechanism of cellular injury and the endogenous mechanisms that have evolved to regulate protein folding [168].

1.9 DISSERTATION OVERVIEW

The best-studied serpinopathy is ATD, which is most commonly caused by a mutation that results in a substitution of the amino acid, glutamic acid at position 392 to a lysine (known as the Z mutation). Since α1-AT is the predominant serine peptidase inhibitor in extracellular fluids, decreased α1-AT secretion results in a loss-of-function phenotype manifest by peptidase-inhibitor imbalance, connective tissue matrix destruction and susceptibility to chronic obstructive lung disease. In contrast, the accumulation of aggregation-prone ATZ in liver cells leads to a toxic gain-of-function phenotype characterized by liver failure and carcinogenesis. Only ~10% of all ATZ homozygous individuals develop severe liver disease [174]. This observation suggests that other genetic and/or environmental factors play key roles in determining disease severity and outcome [175]. Our current understanding of these factors is incomplete and effective therapeutic options are very limited. This work describes the development of a *C. elegans* model of ATZ deficiency, characterization of the phenotypes associated with ATZ accumulation, the targeted investigation of protein quality control, and an unbiased RNAi screen to identify modifier genes important for ATZ disposition.

2.0 THE DEVELOPMENT, CHARACTERIZATION, AND VALIDATION OF A *C. elegans* MODEL OF THE SERPINOPATHY, α-1 ANTITRYPSIN DEFICIENCY

2.1 INTRODUCTION

The serpinopathies are a group of conformational diseases in which a genetic mutations facilitate serpin protein misfolding, polymerization, and aggregation [43]. The accumulation of misfolded serpins lead to tissue damage and degenerative diseases [41-44]. Examples include a1-antitrypsin (AT) deficiency, hereditary angioedema, familial encephalopathy with neuroserpin inclusion bodies (FENIB), and thrombophilia. Most serpinopathies are a result of mutations occuring most frequently in or near the hinges of the reactive site loop and the shutter region that underlies the opening of the β-sheet A [41].

The best-studied serpinopathy is AT deficiency (ATD). ATD is caused most commonly by a mutation that results in a substitution of the amino acid, glutamic acid at position 342 to a lysine (known as the Z mutation). This change in charge destabilizes the hinge region, making the AT protein more susceptible to polymerization. These protein polymers are poorly secreted and accumulate within the ER of liver cells [6]. Since AT is the predominant serine peptidase inhibitor in extracellular fluids, decreased AT secretion results in a loss-of-function phenotype manifested by peptidase-inhibitor imbalance, connective tissue matrix destruction, and susceptibility to chronic obstructive

lung disease. In contrast, the accumulation of aggregation-prone α1-antitrypsin Z (ATZ) in liver cells leads to a gain-of-toxic-function phenotype, characterized by liver failure and carcinogenesis [82]. Indeed, ATD is the most common genetic cause of pediatric liver disease and the most frequent diagnostic indications for liver transplantation during childhood.

Curiously, only 10% of all ATZ homozygous individuals develop severe liver disease [174]. This observation suggests that other genetic modifiers and/or environmental factors play key roles in determining disease severity and outcome. Our current understanding of these other factors is incomplete and effective therapeutic options are limited. Model systems have provided valuable insights into different human diseases associated with aggregation-prone proteins. For example, transgenic worms and *Drosophila* have enhanced our understanding of Alzheimer's disease, Parkinson's disease, Huntington's disease, Duchenne muscular dystrophy and diabetes [173, 176]. Thus, the simple model organism, such as *C. elegans,* may be useful for unraveling genetic modifiers associated with ATD. Moreover, *C. elegans* is becoming the system of choice to study cell biological processes *in vivo* and may provide insights into the cellular mechanisms that protect against protein misfolding.

C. elegans are a well-established model organism with a proven track record. Their small size (1.5 mm as an adult), short life cycle (2–3 days), high fecundity (300 progeny in 3 days), easy genetic manipulation, and ease of culture, makes them an excellent, low-cost, alternative to other model organisms [154]. Transgenic animals can be generated with relative ease and well-established reverse and forward genetic tools are available. This chapter will focus on the development, characterization, and

validation of the *C. elegans* model of α1-antitrypsin deficiency. Emphasis is given to comparing the *C. elegans* model with the ER transport defect in hepatocytes that are associated with the human disease [6].

2.2 MATERIALS & METHODS

2.2.1. AT Constructs

Overlap extension PCR introduced synthetic introns in AT cDNA. Briefly, large oligonucleotides primers consisting of ~50 nt of synthetic intron and ~22 nt complementary sequence to AT coding region were used to amplify small regions of the AT cDNA. The amplified fragments were joined together utilizing overlap extension PCR to generate larger fragments that contained intronic regions. The resulting PCR product contains the entire AT fragment with inserted synthetic introns (~70 bp) that enhance transgene expression in the worm. The completed AT fragment was flanked with *Kas 1* recognition sites and cloned into a modified pPD95.85 expression vector (A. Fire, Stanford University) which generated $P_{nhx\text{-}2}$*sGFP::ATM*. To create the Z mutation of AT, site-directed mutagenesis of $P_{nhx\text{-}2}$*sGFP::ATM* with Quickchange II (Stratagene, CA) with primers (F:GGCTGTGCTGACCATCGATAAGAAAGGGACTGAAGCTGC) and (R:GCAGCTTCAGTCCCT TTCTTATCGATGGTCAGCACAGCC) was used to change Glu 342 to Lys. All PCR reactions used in these studies utilized Phusion high fidelity DNA polymerase (New England Biolabs, MA). All of the constructs were sequenced confirming correct constructs.

2.2.2. Creation of Transgenic Strains

Standard microinjection techniques were used to generate AT transgenic *C. elegans* [177]. Briefly, animals were co-injected with $P_{myo\text{-}2}$mRFP (10 ng/μl) and either sGFP::ATZ or sGFP::ATM (70 ng/μl) expression constructs into the gonad of adult N2 (wild type) hermaphrodites. For each DNA construct, injections yielded multiple transgenic lines propagating extra-chromosomal arrays.

2.2.3. Creation of Integrated Strains

Extrachromosomal arrays were integrated by exposure of transgenic animals to gamma irradiation. Approximately 300 L4 transgenic animals with ~25% transmission frequency were washed with Phosphate Buffered Saline (PBS; NaCl 8 g/l, KCl .2g/l, Na_2HPO_4• $2H_2O$ 1.44 g/l, KH_2PO_4 .24g/l, pH 7.4) and irradiated with 3500 Rads of gamma radiation. Animals were transferred to NGM/OP50 plates for recovery. Positive transgenic lines were identified and selected on the basis of 100% transmission to subsequent generations. To remove background mutations that may have arisen from irradiation, integrated lines were outcrossed to N2 (WT) animals at least 6 times before experimentation.

2.2.4. Strains and Culture Conditions

Strains used in this experiments were N2 (Bristol strain), CB4856 (Hawaiian polymorphic strain), VK413 ($P_{nhx\text{-}2}$*GFP*), VK414 ($P_{nhx\text{-}2}$*sGFP*), VK689 ($P_{nhx\text{-}2}$*sGFP::ATM*), VK694 ($P_{nhx\text{-}2}$*sGFP::ATZ*), and VK472 ($P_{nhx\text{-}2}$*sATZ*). Standard conditions were used for *C. elegans* culturing, propagation, and maintenance at 22 °C as described by Brenner [154]. Worms were cultured on nematode growth medium (NGM) plates seeded with *E. coli* OP50 (NGM/OP50) [154].

2.2.5. Chromosome Mapping

A SNP-based mapping strategy with the Hawaiian *C. elegans* strain CB4856 was utilized to determine the chromosomal location of a transgene integration site [178]. Hawaiian CB4856 males were crossed into sGFP::ATM and sGFP::ATZ animals. Fifty GFP animals and fifty non-GFP animals from the self-progeny of sGFP::AT/CB4856 heterozygote hermaphrodites were picked into separate tubes, each containing 20 μL single-worm lysis buffer (50 mM KCl, 10 mM Tris pH 8.3, 2.5 mM $MgCl_2$, 0.45% IGEPAL CA-630, 0.45% Tween 20, 0.01% (w/v) gelatin, 60 ug/ml proteinase K). They were lysed by freezing at -80 °C followed by incubation at 65 °C 1 hour and 95 °C 15 minutes to inactivate the proteinase K. The DNA was added to a PCR master mix containing 424 μL water, 52 μL 10X PCR buffer (10X: 22.5 mM $MgCl_2$, 500 mM Tris-HCl, 140 mM $(NH_4)_2SO_4$, pH 9.2 at 25 °C), 10.4 μL 10 mM dNTPs, and 3.12 μL Taq polymerase (5 units/μl). Ten uM of each primer and 9.8 μL of the mutant mix or the non-mutant mix

was aliquoted into single PCR tubes. The DNA was amplified by PCR using the cycling conditions: 2' at 94 °C, 35 cycles of (15" at 94 °C, 45" at 60 °C, 1' at 72 °C), and a final incubation for 5' at 72 °C. After amplification, PCR products were digested in the tubes with the restriction enzyme *Dra*I (New England Biolabs). Digestion reactions were incubated at 37 °C at least 4 hours. Samples were loaded onto a 1.0% agarose gel. The resulting gel displayed all 18 SNP markers, from left to right and from chromosome I to X. Each Mutant SNP was compared side-by-side to its non-Mutant control, so that the entire genome could be scanned for linkage. Chromosome mapping was completed for each isolated integrated AT transgenic line [178].

2.2.6. Imaging of Transgenic Lines

Fluorescence expression patterns were observed utilizing a Zeiss Axioskop microscope (Thornwood, NY) equipped with DIC, polarization, and fluorescence optics. Adults were immobilized by mounting in 0.1 M sodium azide solution on a 2% agarose pad. Images used for fluorescence were captured at the identical exposure times, brightness, and contrast.

Transmission electron microscopy was used to determine the subcellular location of ATZ accumulations. Transgenic adult animals were selected, washed in PBS buffer, fixed, and embedded by standard methods [179]. Thin sections (~50 nm) were collected and examined on a transmission electron microscope (JEOL 12-10 TEM, Massachusetts). Results were obtained by examining over 25 micrographs from each worm line.

2.2.7. Biochemical Characterization

Nematode protein extracts were prepared by resuspending frozen worm pellets in PBS with a protease inhibitor cocktail (Roche, Indianapolis) and were sonicated intermittently for a total of 15 seconds (Sonifier 450 Output: 6). To remove cell debris, extracts were centrifuged at 16,000 rpm for 20 min at 4^{o}C, and the supernatant collected. The supernatant (12 μl) was mixed with 3ul of 5x dissolving buffer (5 ml glycerol, 2.7 ml H_20, 2.13 ml of 0.5 M Tris pH 6.8) and analyzed on 7.5% native PAGE.

Alternatively, protein extracts were prepared from whole animal pellets in PBS containing proteinase inhibitors (Roche, Indianapolis). Samples were boiled 10 min with sample buffer containing 2% SDS and 200 mM DTT, and fractionated on a 10% SDS/PAGE gel. Both Native and SDS-PAGE gels were transferred to PVDF membranes. Blots were probed with a 1:1000 dilution of anti-GFP peptide polyclonal antiserum (Sigma), 1:10,000 dilution of anti-α1-antitrypsin (DiaSorin Inc, Stillwater) or 1:1,000 anti-tubulin polyclonal antiserum (Sigma), respectively; and visualized by binding of horseradish peroxidase-coupled secondary antibody and chemiluminescence (ECL Lumi-Light, Roche, Germany).

2.2.8. Phenotypic Characterizations

2.2.8.1. Longevity Assay

Twenty-five L4 larvae from each strain were transferred to NGM/OP50 plates. Following transfer (day 0), lifespan plates were incubated at 22 °C until final scoring for survival

was completed (survival was scored every day until all animals were dead). Animals were considered dead when there was no response to platinum wire prodding. Animals were transferred to fresh NGM/OP50 plates every 3 days to prevent starvation, and to maintain original adult population. Animals that crawled off the media or desiccated were censored. Each lifespan assay were repeated at least three times and showed similar trends in relative lifespan effects. The data were plotted with Kaplan- Meier survival curves and statistical analysis was competed utilizing the Logrank (Mantel-Cox) test.

2.2.8.2. Brood Size Assay

Ten L4 animals were individually placed onto separate NGM/OP50 plates and incubated at 22 ^{o}C. Animals were transferred to fresh plates daily for 5 successive days or until animals stopped producing eggs. The number of eggs produced by each worm was recorded daily, and the total number of eggs summed to give brood size. The mean brood size and standard deviation of a particular strain was calculated and significance was calculated using the Student's *t*-test.

2.2.8.3. Slow Growth Assay

25 gravid adult hermaphrodites were transferred to fresh NGM/OP50 plates and allowed to lay eggs for approximately 2 hours at 22 ^{o}C. The original 25 adults were removed from plates and the eggs were allowed to develop for 48 hours at 25 ^{o}C. Plates were

examined under a Leica dissecting microscope at 5X magnification to determine developmental stage. All adult and L4 animals were removed and plates were incubated for another 48 hours. After a total of 96 hours the plates were reexamined to determine if embryos had reached adulthood. The growth defects mean result and standard deviation was calculated from three separate trials, and *P*-values were calculated using the Student's *t*-test.

2.3 DEVELOPMENT OF AT TRANSGENIC ANIMALS

C. elegans is a powerful genetic and physiological system for modeling human diseases. As such, we created a *C. elegans* model of ER transport defect associated with ATD. Considerations for generation of AT transgenic animals included means to optimize transgene expression, promoter choice, and the use of a translational reporter (fluorescent protein). Many human genes are too large to be introduced efficiently by germline injection. Moreover, many human cDNAs are larger than some *C. elegans* genes. Studies in many species show that transgene expression is enhanced by the presence of intronic sequences [180, 181]. For that reason, synthetic introns were inserted into human AT cDNA by overlap extension PCR. The amplified AT fragment, containing synthetic introns, was cloned into the expression vector pPD95.85; which contains a multi-cloning site, flanking introns, and a 3' UTR. Additionally, the pPD95.85 vector has a synthetic signal peptide, which directed transgene expression to the secretory pathway (Figure 2.1).

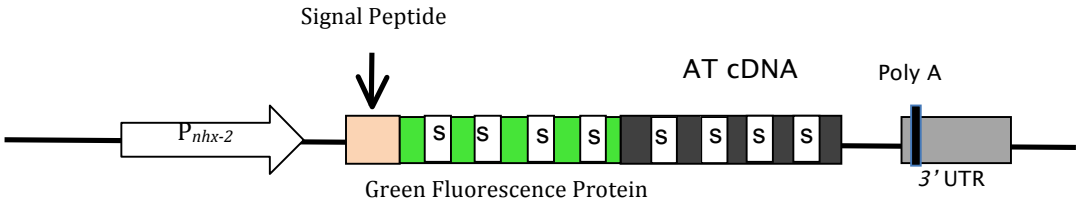

Figure 2.1 AT Expression Vector

Represents a schematic of the expression vector for expression of α1-antitrypsin in *C. elegans*. The *nhx-2* promoter (P_{nhx-2}) is used to drive expression of the transgene in the intestinal cells of the worm, while the synthetic signal peptide directs transgene expression to the secretory pathway. Both the GFP and α1-AT cDNA had synthetic introns inserted to increase transgene expression. s = synthetic intron, utr = untranslated region

The promoter selection was based on directing expression to cells that most closely resemble the biological environment in which the human protein is synthesized. The majority of human AT is produced in hepatocytes; however, nematodes do not have a liver. In *C. elegans,* the intestine acts as the metabolic center and performs biosynthetic and secretory functions of the worm [182]. Therefore, we utilized the intestinal specific promoter *nhx-2* (P_{nhx-2}), which drives expression through all stages of postembryonic development (Figure 2.1) [182].

To follow the cellular disposition of ATZ in intestinal cells we elected to fuse the serpin to a fluorescent reporter (FR). FR tags obviate the need for fixation and antibody staining, and provide real time monitoring of proteins in live animals [157]. We fused the green fluorescent protein (GFP) to the 5' end of the AT transgene creating a translational GFP::ATZ fusion gene (Figure 2.1). Since one mechanism of ATZ polymerization involves insertion of the reactive site loop of one molecule into β-sheet A of another ATZ molecule [40], we fused GFP on the N-terminal side of AT, to avoid interfering with this process.

The ATM and ATZ constructs were introduced by microinjection into the gonad of the worm. Specifically, sGFP::ATM or sGFP::ATZ plasmids (~70 ng/μl) were injected into the gonads of young N2 adult hermaphrodites (Figure 2.2 B). Multiple independent transgenic lines were isolated, which showed variable transmission rates and transgene expression patterns (Figure 2.2 C). As an independent means to help identify transgenic animals, a co-injection marker was used. Co-injection marker transgenes are incorporated concomitantly into the extrachromosomal array. Co-injection markers often make use of a promoter that is specific to an anatomical structure remote from the

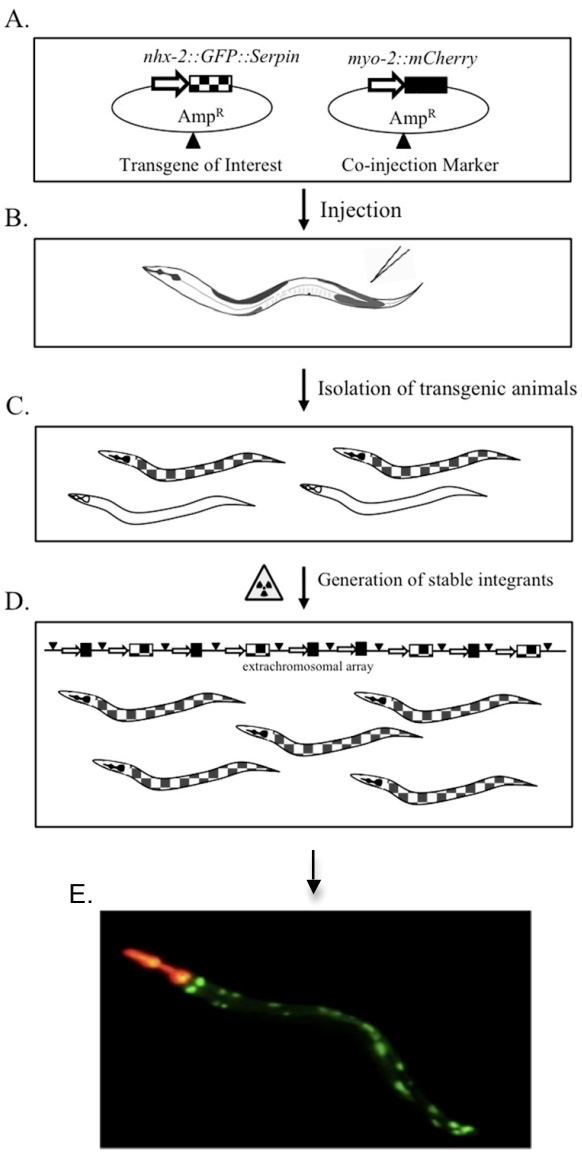

Figure 2.2 Flow Chart of Transgenesis

A. Expression vectors were created expressing the transgene of choice. B. Plasmid DNAs (for the transgene of choice had a co-injection marker) were injected into the gonad of adult hermaphrodites. C. Multiple lines of transgenic progeny were isolated. D. Gamma radiation was utilized to integrate transgene. E. Fluorescent image of sGFP::ATZ transgenic animals (Coloration red=mRFP, green=GFP) Figure adapted from Long et al., (2011) [183].

region of interest. Additionally, co-injection markers are usually tagged with a different FR to minimize interference during multicolor imaging. Therefore, we utilized the head muscle promoter, *myo-2* (P_{myo-2}), tagged with mRFP. This co-injection marker was very distinctive, allowing for easy identification of transgenic animals (Figure 2.2 A). Successful injections resulted in transgenic animals displaying an mRFP expressing head region and GFP expression in the intestine (Figure 2.2 E).

After isolation of stable transgenic lines, the transgenes were integrated into the genome of the animals. Injected DNA plasmids form large extrachromosomal arrays that are passed onto subsequent generations in a non-Mendelian inheritance pattern [184]. Integration of transgenes results in stable and consistent (100%) transgene expression. We generated integrated lines by exposing transgenic animals to high doses (3500 Rads) of gamma radiation (Figure 2.2 D). This ionizing radiation causes double-stranded DNA breaks [177]. Upon repair of these breaks, the extrachromosomal array may be incorporated into DNA of the animal. However, the radiation may also cause unintended mutations in other genes. Following the isolation of integrated transgenic lines, outcrossing was completed six times to remove any background mutations. Individual F1 strains were selected based on transgene expression levels and were expanded. Lastly, Single Nucleotide Polymorphism (SNP) mapping was completed on the different integrated transgenic lines to determine the relative location of the integration site (Figure 2.3, Table 2.1). In SNP-mapping, chromosomal specific SNP polymorphisms between wild-type N2 and CB4856 Hawaiian DNA are used as genetic markers to map the transgenic insertion site [178].

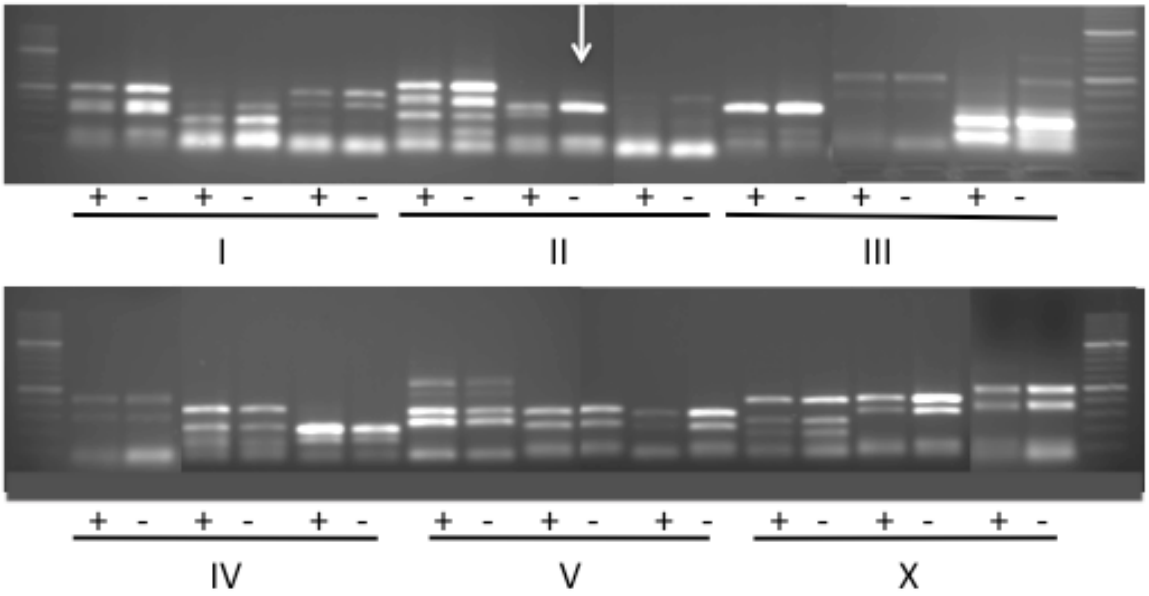

Figure 2.3 Chromosome Mapping of Integrated Transgene

Each pair of lanes shows results from SNP mapping at the indicated genetic map position, using DNA from either the GFP (+) or the non-fluorescent (-) F2 animals DNA derived from a N2 X Hawaiian cross. Linkage is visible as an increase in the proportion of closely linked N2 Bristol DNA in (+) lanes compared to the (–) lanes, and is visible in chromosome II (white arrow) for the ATZ transgenic line VK694.

Table 2.1: Summary of Independent AT Transgenic Lines

Name	Strain ID	Expression/description	Outcrossed 6X	SNP mapped
MR13.6		med. posterior globules		
MR14.5		no globules	√	Chr 2.2
MR17.1	VK689	small posterior globules	√	Chr X.2
MR18.1		high posterior globules		
Z6.1		med/high expressor	√	Chr 1.3
Z7.1		med/high expressor (slow growing)		
Z15.4		med/high expressor		
Z19.4		low/med expressor	√	Chr X.2
Z24.5		low/med expressor/posterior globules		Chr 1.3
Z26.6		medium expressor	√	Chr 3.1/3.2
Z2.3.1		medium expressor / posterior globules		
Z25.3.1		medium expressor / mutiple globules	√	Chr X.2
Z13.1.1		medium expressor / posterior globules		
ZR10.4	VK694	high expressor / multiple globules	√	Chr 2.2
ZR20.3		high expressor / multiple globules	√	Chr X.2
ZR21.4.2		medium expressor		
ZR30.1		medium expressor	OC 2X	Chr X.2

Chromosome mapping identifies chromosomal location [178]. Through these techniques, multiple independent transgenic lines were created, integrated, outcrossed, and SNP-mapped (Table 2.1).

2.4 CHARACTERIZATION OF AT TRANSGENIC ANIMALS

The second target of this study was the comprehensive characterization of AT transgenic animals. We wanted to confirm that the *in vivo* model of ATZ recapitulated the pathogeneses of ATD in humans. This characterization was broken down into several independent studies including cellular accumulation and secretion studies, biochemical characterization of AT protein, and phenotypical characterization of sGFP::ATZ transgenic animals.

2.4.1. Cellular Accumulation and Secretion

Control transgenic animals expressing $P_{nhx\text{-}2}$*::GFP* showed homogenous diffuse expression of GFP throughout the intestine of the animal (Figure 2.4 A). Whereas $P_{nhx\text{-}2}$*sGFP* showed diffuse GFP expression in the pseudocoelomic space outside of the intestine (Figure 2.4 B). These results suggest that the synthetic signal peptide was sufficient for directing GFP to the secretory pathway, resulting in the accumulation of GFP in the pseudocoelomic space. Transgenic animals expressing sGFP::ATM, the wild type AT protein, showed secretion of the GFP in the pseudocoelomic space with no

detectable intracellular accumulations (Figure 2.4 C). In contrast, sGFP::ATZ, developed large intracellular inclusions with no detectable secretion of ATZ (Figure 2.4 D).

DIC imaging was used to determine if the globules present in sGFP::ATZ animals were caused by an accumulation of mutant ATZ or aggregating GFP. Transgenic $P_{nhx\text{-}2}$*::ATZ* animals were created and imaged. Results from this imaging showed dilated cisternae in animals expressing ATZ alone, similar to what was visualized in sGFP::ATZ (Figure 2.4 E).

Transmission electron microscopy was used to characterize the location of the sGFP::ATZ accumulations to the ER of intestinal cells. Transgenic adult animals were selected, washed in PBS buffer, fixed, and embedded by standard methods [179]. Animals were examined under a transmission electron microscope. Similar to DIC imaging, large intracellular accumulations were observed in the intestinal cells of sGFP::ATZ transgenic animals (Figure 2.5 B, C, D). These accumulations appeared to be surrounded by ribosomes, suggesting that the retention of ATZ is located in dilated rough ER cisternae (Figure 2.5 D). In contrast, no irregular structures were observed in the intestinal cells of animals expressing sGFP::ATM (Figure 2.5 A).

2.4.2. Biochemical Characterization

Studies show that human ATZ polymerizes within hepatocytes [3, 185]. Therefore, we determined whether ATZ protein within *C. elegans* was in the polymerized form, utilizing non-denaturing gels. Under native conditions, sGFP::ATZ exhibited the properties of

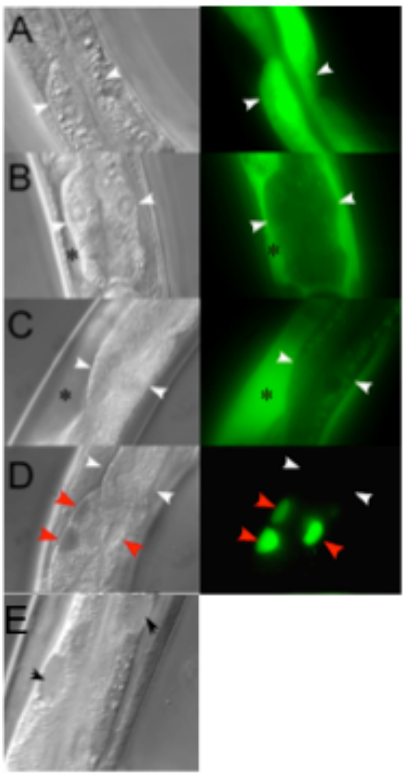

Figure 2.4 Fluorescent and DIC Imaging of Transgenic Animals

A. Adult worm harboring P*nhx-2GFP* showed diffuse intracellular GFP expression within the intestinal cells. B and C. P*nhx-2sGFP* and P*nhx-2sGFP::ATM* transgenic animals secreted GFP into the extracellular pseudocoelomic space (asterisks). D. P*nhx-2sGFP::ATZ* animals accumulated ATZ within intestinal cell cytoplasm (red arrowheads) and failed to secrete detectable amounts of fusion protein into the pseudocoelomic space. ***E***, P*nhx-2ATZ* showed prominent intracellular inclusions (black arrowheads) that are comparable to those of the GFP accumulations shown in P*nhx-2sGFP::ATZ* animals. For orientation in each paired set of figures, white arrowheads indicate corresponding basal surfaces of intestinal cells. (Figure Imaged by Stephen C. Pak, unpublished data)

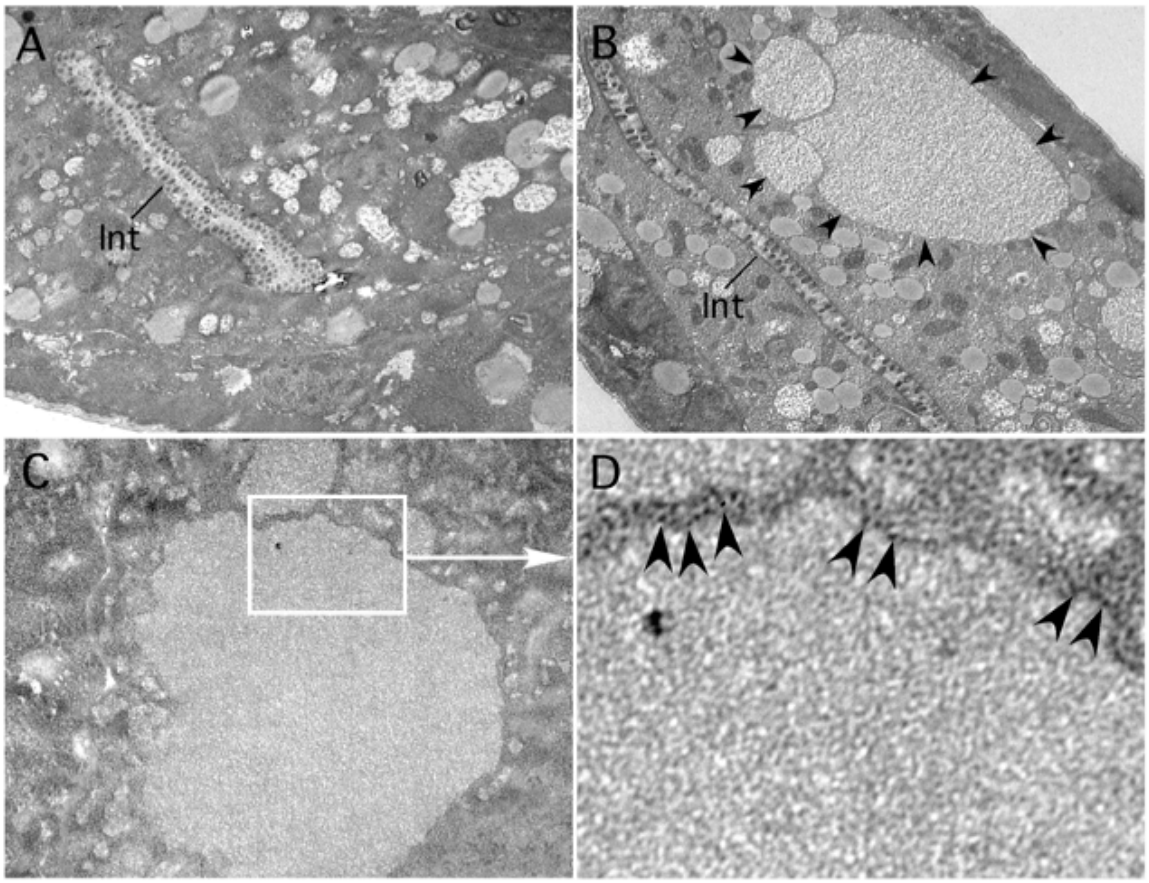

Figure 2.5 Electron Micrographs of ATZ Globule-containing Intestinal Cells of Transgenic Animals.

Cross and transverse sections of early larval stage worms expressing A. sGFP::ATM or B. sGFP::ATZ transgenes. Arrowheads point to large intracellular inclusions. C. Close-up of an ATZ inclusion. D. Higher magnification of the boxed area from C. Arrowheads point to ribosomes of the dilated ER. *Int* = intestinal lumen. (Figure Imaged by Stephen C Pak, unpublished data)

monomers, soluble oligomers, and higher order polymers (Figure 2.6 A). In contrast, sGFP::ATM was soluble with mobility relative to its molecular mass (Figure 2.6 A).

Furthermore, SDS-PAGE were used to confirm fusion protein production of sGFP::AT. Under denaturing conditions, total worm lysates were fractionated by SDS-PAGE. Proteins were transferred to nitrocellulose membranes and AT, GFP, and tubulin (loading control) protein bands were visualized by probing with anti-AT, anti-GFP, and anti-tubulin antibodies, respectively. (Figure 2.6 B). As expected, the lysates of the parental N2 worms did not react with anti-GFP or AT but only with the loading control tubulin (lane 1). In contrast, a protein band migrating at ~80 kDa was detected in the lysates of animals expressing sGFP::ATM (lane 6) and sGFP::ATZ (lane 2-5) in parallel blots for AT and GFP (Figure 2.6 B). This finding showed that no cleavage of the fusion protein occurred within the animals.

2.4.3. Phenotypic Characterization

In humans ATD can be associated with severe disease phenotypes [6, 40, 186-188]. Therefore, we assessed the overall health of sGFP::ATZ transgenic animals by assessing lifespan, brood size, and growth of transgenic animals.

2.4.3.1 Longevity

For longevity experiments, twenty-five L4 animals were placed onto OP50/NGM plates. The number of alive and dead animals was recorded daily. Death of the animal was characterized by a lack of response to touch. Upon completion of the study, Kaplan-

Figure 2.6 Biochemical Characterizations of AT

A. Higher ordered polymer formation was analyzed by native gel electrophoresis. Worm lysates from ATZ transgenic animals showed similar polymer formation as control lane containing human AT polymers (p). Similarly worm lysates from ATM transgenic animals showed monomer formation similar to control recombinant AT monomers (m). N2 animals were the negative control showing no AT protein. B. Immunoblot of worm lysates after SDS-Page gel probed with anti-human AT, anti-GFP , and anti-tubulin (loading control). Lanes 1= N2, Lane 2-5 are separate transgenic sGFP::ATZ lines (2=ZR20.30, 3=Z19.4, 4=ZR10.4, 5=Z25.3.1), Lane 6= sGFP::ATM. Lane 7 is recombinant AT protein at ~60 kD. The GFP and AT fusion proteins have a combined weight of ~87 kD. Tubulin is ~55 kD.

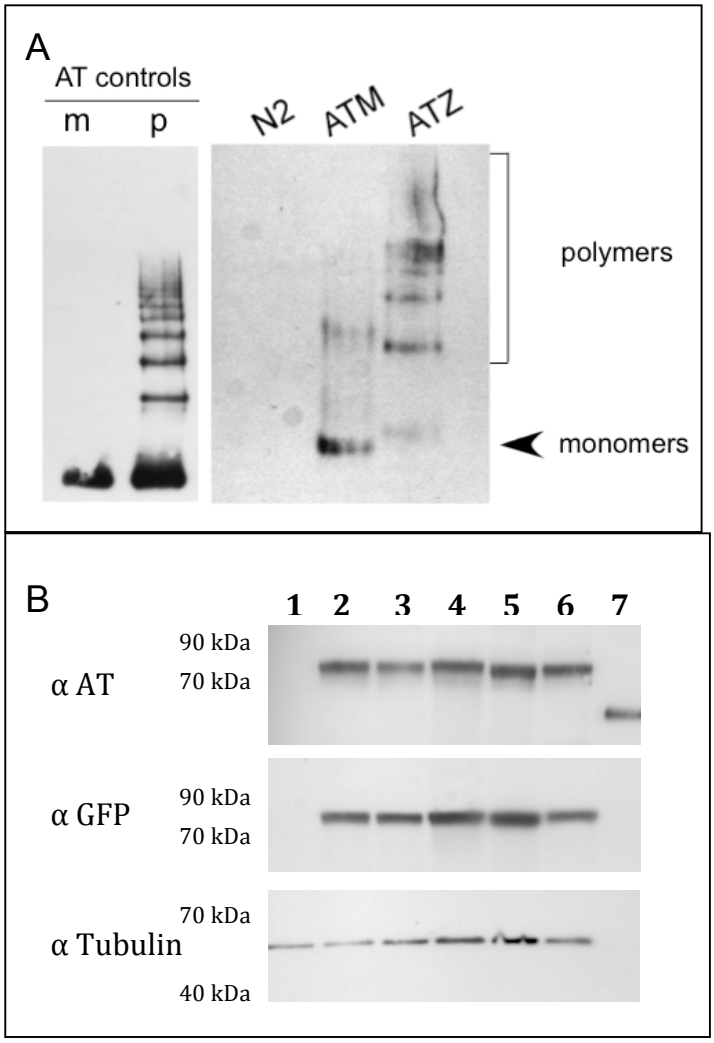

Figure 2.6 Biochemical Characterizations of AT

Meier survival curves showed that expression of sGFP::ATZ transgene resulted in a decreased lifespan ($p<0.001$, Log-Rank test (Figure 2.7 A) [189].

2.4.3.2 Brood Size

Brood size was ascertained by measuring the total number of embryos laid over a five-day period. Ten L4 animals were placed onto individual OP50/NGM plates and incubated at room temperature. The adults were transferred to new OP50/NGM plates daily. The number of progeny were counted daily and totaled to determine brood size (Figure 2.7 B). Animals expressing sGFP::ATZ transgene exhibited a significant reduction in brood size compared with animals expressing sGFP::ATM ($p<0.001$, one-tailed *t*-test). Additionally, sGFP::ATM showed a decrease compared to N2 animals, suggesting that overexpression of wild type AT had a negative effect on the health of the animal ($p<0.01$).

2.4.3.3 Growth

To test the effects of sGFP:ATZ on *C. elegans* development we measured the time of progression from embryo to adult. Whereas ~100% of wild-type (N2) embryos progressed to adulthood in 48 hours, only 10% of sGFP::ATZ transgenic embryos progressed to the L4/young adult stage (Figure 2.7 C). The sGFP::ATZ animals often required up to 96 hours to reach adulthood (Figure 2.7 D). In contrast, expression of sGFP::ATM had a minimal effect on developmental timing.

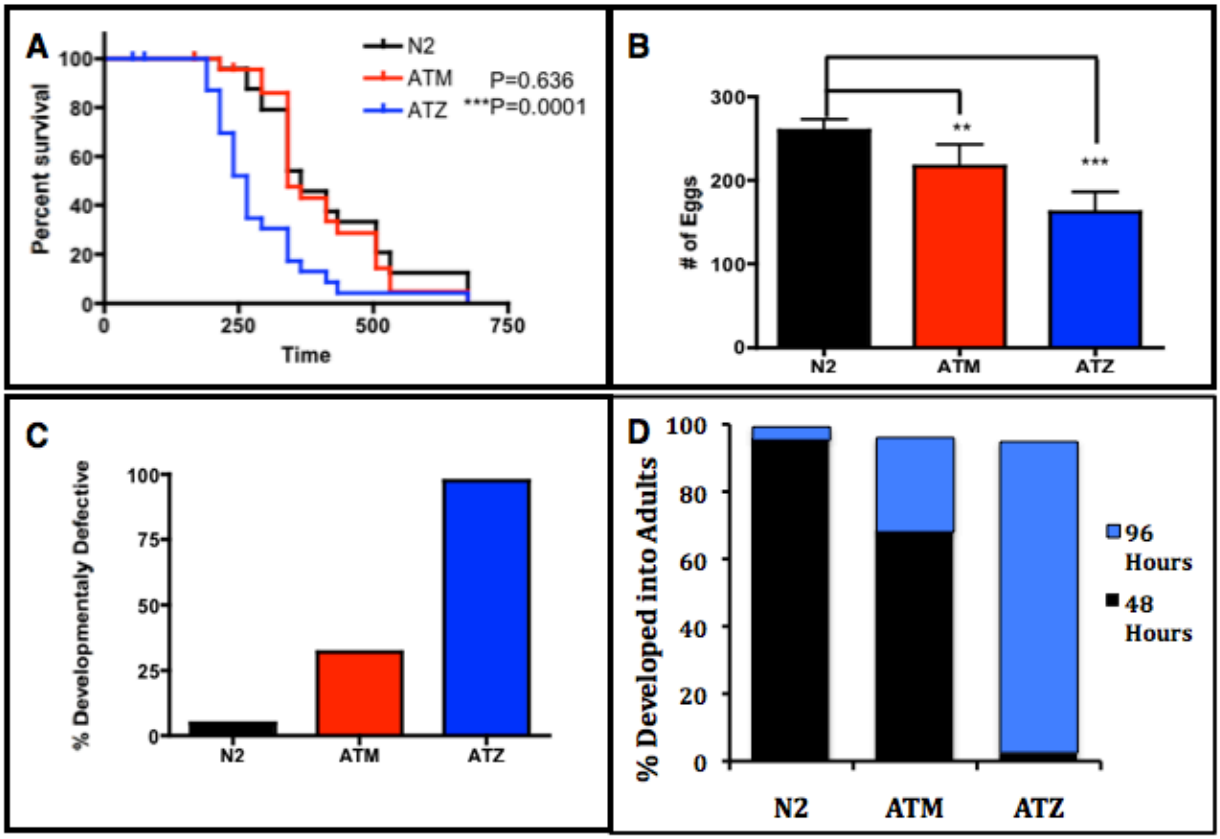

Figure 2.7 Phenotypic Analysis of Transgenic Animals

A. Kaplan-Meier curve showing sGFP::ATZ transgenic animals displayed a significant decrease in lifespan compared with sGFP::ATM and N2 animals. B. sGFP::ATZ animals showed decrease brood size ($p<0.01$). C. Post embryonic developmental delay assay showing ATZ animals exhibit severe developmental delays. D. Development of transgenic animals 96 hours after being laid, showing that ATZ animals enter into adulthood

2.5 DISCUSSION

Modeling aspects of human disease phenotypes in *C. elegans* allows for the dissection of complex molecular pathways that contribute to the disease process. For these reasons, we have produced transgenic *C. elegans* strains that model the ER transport defect associated with the liver disease of ATD patients. In humans, ATD is caused commonly by a genetic mutation (Z) resulting in protein misfolding, oligomerization and aggregation [3, 40, 185]. The accumulation of abnormal ATZ proteins within the liver cells leads to tissue injury and degenerative diseases in humans [40]. Consistent with the role the Z mutation plays in human disease, transgenic sGFP::ATZ animals develop intracellular accumulation in the intestinal cells with no discernible secretion of ATZ (Figure 2.4 D). In contrast, sGFP::ATM transgene was secreted into the pseudocoelomic space surrounding the intestinal cells (Figure 2.4 C). These studies indicated that the fate of ATM and ATZ in *C. elegans* recapitulates that which occurs in humans: secretion of ATM and intracellular retention of ATZ.

To exclude the possibility that the observed phenotypes were specific to intestinal cells, our laboratory also developed sGFP::ATM and sGFP::ATZ transgenic animals that expressed these proteins in hypodermal seam cells [156]. The $P_{srp\text{-}2}$sGFP::ATZ animals displayed a similar GFP accumulation phenotype in the hypodermal seam cells as $P_{nhx\text{-}2}$*sGFP::ATZ* displayed in the intestinal cells (data not shown). These studies showed that the accumulation of sGFP::ATZ was not unique to intestinal cells, but was a general feature of the aggregation prone protein, ATZ.

Although unlikely, it was conceivable that aggregation of sGFP::ATZ was due to GFP and not ATZ in this system. To test this possibility, we generated $P_{nhx\text{-}2}$*ATZ* transgenic animals. DIC imaging showed dilated cisternae, similar to what was visualized in sGFP::ATZ (Figure 2.4 E). These images showed that the intracellular inclusions are caused by the agregating ATZ, and not GFP (Figure 2.6 A).

In humans, ATZ aggregates are retained within the ER [1, 186]. In *C. elegans* transmission electron microscopy (TEM) and immunohistochemical studies showed that sGFP::ATZ was also retained within dilated ER cisterna (Figure 2.5 B,C,D). These studies support sGFP::ATZ accumulated in the ER of intestinal cells, which is similar to what is observed in humans with ATD.

Biochemically, ATZ polymerizes in hepatocytes [3, 5, 40, 185, 190, 191]. Protein lysates from transgenic sGFP::ATZ and sGFP::ATM animals showed that retained sGFP::ATZ and secreted sGFP::ATM were also in polymerized and monomeric forms, respectively (Figure 2.6 B). Taken together these studies suggest that sGFP::ATZ exhibited cellular and biochemical properties similar to those observed in humans with ATD.

ATZ accumulation in humans can be associated with severe liver disease [6, 40, 186-188]. Therefore, we determined whether expressing sGFP::ATZ affected the overall health and well being of the animals. The accumulation of mutant ATZ, in *C. elegans,* results in decreased life spans, decreased brood sizes and increased embryonic developmental delays (Figure 2.7 A,B,C,D). Overall, these studies indicated that expression of mutant ATZ in *C. elegans* was harmful to the animals. Some of these observations resemble those observed in the PiZ mouse, and in humans with ATD [3,

60, 78-81].

By developing a transgenic model that recapitulates the ER transport defect associated with ATD, we are better equipped to identify genes that modify the ATZ phenotypes. Studies show that the proteasomal pathway is responsible for the elimination of misfolded soluble proteins, whereas the autophagy-lysosome pathway is specialized for degradation of insoluble aggregates and higher order polymers [70, 76, 85-88]. Therefore, we next want to determine if the disposal mechanism of sGFP::ATZ in *C. elegans* parallels those in mammalian systems (Chapter 3). Furthermore, the robust expression of sGFP::ATZ transgene makes this system a candidate for a high-throughput genome-wide RNAi screening, to determine if any additional genes or pathways play a pivotal role in the disposal of sGFP::ATZ in *C. elegans* (Chapter 4).

Acknowledgments: This work was supported by grants from NIH/NIDDK (DK079806 and DK084512) and Hartwell foundation.

Portions of this chapter were adapted from: *Using Caenorhabditis elegans to Study Serpinopathies.* Methods in Enzymology, 2011; Volume 499: 259-281. **Olivia S. Long**, Sager J. Gosai, Joon Hyeok Kwak, Dale E. King, David H. Perlmutter, Gary A. Silverman, and Stephen C. Pak

3.0 PATHWAY DIRECTED IDENTIFICATION AND CHARACTERIZATION OF GENETIC MODIFIERS AFFECTING ATZ ACCUMULATION

3.1 INTRODUCTION

α-1 antitrypsin (α1-AT) is an secreted glycoprotein that is synthesized predominantly by hepatocytes, and acts as the major inhibitor of neutrophil elastase in extracellular fluids [60, 192]. Classical α-1 antitrypsin deficiency (ATD) is an autosomal recessive disorder caused by the Z (E342K) mutation (ATZ) [1]. This non-conservative mutation results in protein misfolding and the accumulation of ATZ in the endoplasmic reticulum (ER) of hepatocytes [3, 6]. Consequently, ATZ is poorly secreted with plasma levels <10% of normal. ATD patients can present with a loss-of-function phenotype characterized by elastase-mediated chronic obstructive pulmonary disease [2] and/or a gain-of-function phenotype characterized by aggregation prone protein mediated hepatic injury [3, 6, 40, 42, 191, 193-196].

The expression of liver disease among homozygous ATZ patients is highly variable [4, 5]. This heterogenity suggests that additional genetic and/or environmental factors play an important role in development of liver disease. Studies designed to understand the mechanism of ATZ-induced liver disease have lead to significant insights into the cellular responses to misfolded or aggregation-prone proteins, which include characterization of disposal and ER-stress induced signaling pathways.

However, additional studies are required to understand how genetic modifiers influence how ATZ is processed, secreted, and/or degraded.

Studies in yeast, mammalian cell lines, and transgenic mouse models indicate that there are multiple ATZ elimination pathways. Werner and colleagues showed that a portion of ATZ is eliminated by the ubiquitin proteasome system (UPS) [71]. In this study, a yeast expression system was utilized to monitor degradation of ATZ during pulse-chase experimentation. Specifically, wild-type yeast strains degraded the majority (~94%) of ATZ, while a yeast proteasome mutant (*pre1-1 pre2-2)* strain cleared less than half (~39%). The reduced clearance of ATZ provides evidence that the proteasome plays a role in ATZ degradation. Qu et al., showed a similar role of the proteasomal degradation pathway in the elimination of ATZ in a cell culture model [72]. Specifically, human fibroblast cell lines transfected with ATZ showed inhibition of ATZ degradation when its cell lines were exposed to proteasome inhibitors [72].

The study by Werner et al. also showed that ATZ can serve as a substrate for the endoplasmic reticulum associated degradation (ERAD) pathway [71]. ERAD is a process in which proteins that fail to achieve their correct conformational state are subjected to degradation via the UPS pathway. ERAD is comprised of specific steps including the selection of ERAD substrates, the targeting of substrates for degradation, and the retrotranslocation of the substrates into the cytoplasm where ubiquitination and proteasomal degradation of the targeted substrates occur [71, 197, 198]. However, ERAD chaperones and proteins that identify ATZ as a substrate, and the components that target and mediate its retrotranslocation into the cytoplasm for degradation have not yet been completely delineated [103, 104, 199, 200].

In addition to the degradation of ATZ via the ERAD pathway, the autophagy-lysosome pathway has also been identified as a quality control system associated with the degradation of ATZ [201-203]. In studies by Teckman and Perlmutter, a transfected fibroblast cell lines expressing ATZ, but not wild-type AT protein (ATM), contained a large number of autophagosomes [64]. Additionally, an increased number of autophagosomes were identified in both the liver cells of the ATZ mouse model as well as in patients with ATD [64, 204].

Several investigations have been focused on elucidating the molecular components in both the ERAD/ proteasomal and autophagy pathways that facilitate the degradation of ATZ. Since misfolded ATZ accumulates in hepatocytes as oligomers, polymers, and higher order aggregates it was not surprising that multiple degradation pathways are required for its elimination. In mammals, it appears that aggregated or insoluble proteins are degraded via the autophagic pathway [64, 77]; whereas, the soluble misfolded monomers and oligomers are degraded via the proteasomal pathway [70, 76, 85-88].

Although ATZ misfolds and accumulates in the ER, in some systems it does not appear to induce the unfolded protein response (UPR) [205]. The UPR is a ER stress response pathway that initiates an intracellular signaling network that transcriptionally up-regulates a specific set of genes whose role is to alleviate ER stress by increasing the elimination of unfolded proteins [123-125]. Typically, the UPR becomes activated once ERAD is overwhelmed by the accumulation of misfolded proteins. Currently, it is unknown why ATZ does not activate the UPR. One hypothesis attributes this lack of response to inherent properties of ATZ that results in it not being recognized as a

misfolded protein capable of triggering the UPR sensors [205]. A better understanding of why ATZ does not trigger the UPR may lead to the identification of other genetic modifiers that modulate ATZ accumulation.

Utilizing the *C. elegans* ATZ model, the goal of my dissertation is to help elucidate the genetic modifies of ATZ accumulation and degradation. This model should provide essential insights into protein synthesis, trafficking, and degradation, as these pathways are well conserved between *C. elegans* and humans [206-213]. Earlier studies validated the *C. elegans* model of ATZ pathogenesis (Chapter 2 and unpublished data). Therefore, by using the *C. elegans* ATZ model to identify genetic modifiers that affect the disposition of ATZ, we can gain additional insight into the human disorder. In this chapter, I utilized RNAi-based experimentation to specifically knockdown genes from the different degradation pathways. The results show that ATZ is partially degraded by both the proteasomal degradation pathway and autophagy response, confirming past studies. Furthermore, I provide new data showing that ATZ is also partially degraded through a novel pathway.

3.2 MATERIALS AND METHODS

3.2.1 Worm Strain and Culture Conditions

N2, CB360 (*unc-51(e369)),* RB545 (*pek-1(ok278)),* and RE666 (*ire-1(v33))* strains were obtained from Caenorhabditis Genetics Center (CGC), (http://www.cbs.umn.edu/CGC/),

which is supported by NIH funding. Strains VK694 ($P_{nhx\text{-}2}$*sGFP::ATZ*), VK643 ($P_{nhx\text{-}2}$*sGFP::AT$_{Saar}$*), VK1223 ($P_{nhx\text{-}2}$*sGFP::AT$_{NHK}$*), VK1267 ($P_{nhx\text{-}2}$*CPL-1::YFP*), VK1269 ($P_{nhx\text{-}2}$*CPL-1$_{PPM2}$::YFP),* VK737 ($P_{hsp\text{-}4}$*::GFP)* were all generated by co-injecting the plasmid with $P_{myo\text{-}2}$::*mRFP* at a final concentration of 70 ng/μl and 10 ng/μl, respectfully into the gonad of adult N2 hermaphrodites. Strains VK1093 ($P_{nhx\text{-}2}$*mCherry::lgg-1),* VK1243 ($P_{nhx\text{-}2}$*UB::R::mCherry)* and VK1244 ($P_{nhx\text{-}2}$*UB::M::mCherry)* were generated by co-injecting the plasmid with $P_{myo\text{-}2}$::GFP at a final concentration of 70 ng/μl and 10 ng/μl. Strains VK1751 ($P_{nhx\text{-}2}$*sGFP::ATZ;pek-1(ok278))* and VK1757 ($P_{nhx\text{-}2}$*sGFP::ATZ;ire-1(v33))* were generated by standard genetic crosses. Animals were maintained at 22 ^{o}C on nematode growth medium (NGM) plates spotted with *Escherichia coli* OP50 (NGM/OP50) [214].

3.2.2 Preparation of Animals for RNAi Screening

Twelve to fifteen adult transgenic animals were placed on two 10 cm NGM/OP50 plates. Approximately 7 days later, early-staged larval animals were isolated by differential sedimentation and then transferred to five 50 cm NGM/OP50 plates. The larvae were incubated at 22 ^{o}C until the majority of the animals were in the L4 larval stage, approximately 30-48 hours later depending on the transgenic strain.

3.2.3 Animal Sorting Using the COPAS^{TM} BIOSORT

The use of the COPAS^{TM} BIOSORT (Union Biometric, Holliston, MA) allowed for the reduction in assay variability due to the selection of a more homogenous population of animals based upon size and fluorescence intensity [215]. Animals were cultivated as described above and sorted using the COPAS^{TM} BIOSORT as described with the following modifications: PBS was used to wash the animals and as sheath fluid for sorting using the COPAS^{TM} BIOSORT [215]. Furthermore, animals were sorted onto NGM plates not into microtiter plates. Approximately 300 L4/young-adult animals were sorted for each treatment.

3.2.4 RNAi Bacterial Preparation and Induction

All RNAi clones were obtained from the Ahringer RNAi feeding Library (Geneservice Limited, Cambridge, UK), except for *unc-51(RNAi)* and *hrd-1(RNAi)* which were purchased from Open Biosystems (Huntsville, USA). RNAi cultures were grown as previously described with slight modifications [216]. Briefly, 1 ml of an overnight bacterial RNAi culture was inoculated into a 50 ml culture of Luria Bertani broth (LB; containing 10 g tryptone, 5 g yeast extract, 10 g NaCl and 50 μg/ml ampicillin per liter). These cultures were incubated, by shaking, at 37 ^{o}C until an OD_{600} of 0.5 was obtained. IPTG (4 mM final concentration) was added to cultures, which were then incubated at RT for 3-4 hours to induce production of dsRNA. Induced cultures were centrifuged at

5,000 rpm for 10 minutes to pellet bacteria. Pellets were resuspended in 5 ml of fresh LB and stored at 4 ^{o}C.

3.2.5 RNAi Assay Procedure

Induced RNAi cultures were inoculated onto 15 mm NGM plates containing 50 mg/L amp, 4 mM FUDR, and 1 mM IPTG [216]. Plates were incubated overnight. Approximately 300 larval stage 4 (L4) or young adult (YA) transgenic worms were sorted onto each RNAi plate seeded with a specific RNAi culture. Plates were incubated in a 22 ^{o}C for 48 hours. Animals were imaged utilizing the ArrayScan V^{TI}. Due to their severe growth defect only 100 P$_{nhx-2}$*sGFP::ATZ;Unc-51(e1369),* were sorted to each RNAi plate.

3.2.6 Image Acquisition

Worms were washed off RNAi plates and pelleted by gravity settlement. Approximately 100 animals were transferred into three separate wells of a 96-well optical bottom plate and anesthetized with a 4 mM Levamisole solution prior to image capture. Images were acquired with the ArrayScan V^{TI} HCS Reader (Cellomics, Thermofisher, Pittsburgh, PA, USA) fitted with a 5x objective and a 0.63x coupler. The images were captured utilizing a 2-channel (TRITC and GFP) assay previously described [215]. Valid objects (adult worms) were automatically selected using the SpotDetector BioApplication (Cellomics). All strains utilized the above method except for the P$_{nhx-2}$*sGFP::ATZ;Unc-51(e369),*

Approximately 30 animals were placed into three separate wells of a 384-well optical bottom plate and imaged utilizing the 2.5x objective imaging one field capturing the entire well.

3.2.7 Statistical Analysis

Statistical analysis of data was performed using PrismH (Graphpad Software). Statistical significance of the spot total area between various transgenic lines and empty vector (L4440) feed controls were determined utilizing an unpaired, two-tailed, *t*-test.

3.3 DEVELOPMENT OF *C. elegans* STRAINS FOR CONTROL OF RNAi INDUCED MODULATION OF DEGRADATION AND SIGNALING PATHWAYS

I utilized RNAi clones corresponding to gene sets involved in different degradation pathways to determine whether transgenic *C. elegans* strains use these pathways to eliminate ATZ. RNAi-mediated gene silencing has become a useful genetic tool for the analysis of gene function in *C. elegans* and other species [217]. RNA interference (RNAi) is a process where double-strand RNA is introduced into cells, which triggers the degradation of mRNA. As a consequence, the corresponding protein is depleted or knocked down, leading to the loss of protein function (the mechanism is detailed in Chapter 4) [218, 219]. In *C. elegans,* animals can be fed bacteria expressing dsRNA, which triggers a systemic RNAi response throughout the worm [220, 221]. However,

before investigating the disposal mechanisms of ATZ, it was important to develop a set of control strains to ensure that feeding the corresponding RNAi bacterial clone elicited the desired RNAi effect. The following sections established transgenic *C. elegans* strains that control for the function of the ERAD, UPS, UPR and autophagy pathways (Table 3.1).

3.3.1 ERAD Substrate Controls

ER luminal or transmembrane proteins that fail to achieve their correct conformational state are identified, targeted, and translocated to the cytosol where they are eliminated via the UPS [71]. This ERAD pathway eliminates a variety of malfolded proteins, which differ in structure, conformation and physical properties [222-225]. Studies in yeast show that depending on the location of the substrate, different components (E3 ubiquitin ligases and molecular chaperones) of the ERAD pathway are utilized for targeting substrates for degradation [115-117, 198].

Since ATZ is a secreted glycoprotein retained in the ER lumen and based on previous data in other models, it should serve as an ERAD substrate in *C. elegans* [226-228]. However, before assessing this possibility it was necessary to determine how RNAi of different ERAD components would effect the disposition of known luminal ERAD substrates. Therefore, we developed three separate control transgenic strains expressing well-described luminal ERAD substrates (α1-AT mutant Null Hong Kong, α1-AT mutant Saar, and a cathepsin L mutant), each of which is described and validated in the following sections.

3.3.1.1 α1-AT mutants as ERAD substrates

Studies of α1-AT null mutants Hong Kong and Saar show that they are possible ERAD luminal substrates and are targeted for degradation via the proteasome [83, 229-232]. Null Hong Kong (NHK) results from a frameshift mutation causing the synthesis of a truncated protein [233]. This thirty-three C-terminal amino acids truncation results in a protein that is devoid of the RSL and several β-strands in the C-sheet [233]. In humans, NHK is associated with a total lack of circulating α1-AT [233]. α1-AT variant Saar is caused by a point mutation that introduces a premature stop codon, and leads to truncation of the C-terminus of α1-AT. Similar to NHK, Saar results in a dysfunctional misfolded serpin that is completely retained in the ER, does not form insoluble polymers or aggregates, and is efficiently degraded by ERAD [229, 230].

We generated transgenic *C. elegans* strains expressing $P_{nhx\text{-}2}$*sGFP::AT*$_{NHK}$ (NHK) and $P_{nhx\text{-}2}$*sGFP::AT*$_{Saar}$ (Saar) after mutagenesis of the $P_{nhx\text{-}2}$*sGFP::ATZ* construct (detailed in Chapter 2). Specifically, the NHK construct had a deletion of leucine at position 318 causing a frameshift, resulting in a premature stop codon at amino acid position 334. The Saar constructs were created by frameshift mutation at position 363, resulting in the addition of 13 spurious residues followed by a premature stop codon. As expected, transgene expression of both NHK and Saar is relatively low, with similar expression patterns of small accumulations in the posterior intestinal region in N2 animals (data not shown).

I utilized transgenic animals expressing NHK and Saar to investigate the effectiveness of ERAD RNAi knockdown of gene function (Figure 3.1 A,C). Both NHK and Saar showed significant accumulation following RNAi treatment for some (*cdc-48,*

3.1. Transgenic Control Lines

Control	Transgenic Construct	Abbr.	Fluorescent Tag	Baseline description	RNAi knockdown of pathway
ERAD					
	P_{nhx-2}*sGFP::AT*$_{NHK}$	NHK	GFP	Low level diffuse expression intestinal cells	Increase in accumulation
	P_{nhx-2}*sGFP::ATZ*$_{Saar}$	Saar	GFP	Very low levels of expression, small accumulations in intestinal cells	Increase in accumulation
	P_{nhx-2}*CPL-1*$_{PPM2}$*::YFP*	PPM2	YFP	Accumulated in intestinal cells	Increase in accumulation
Proteasome					
	P_{nhx-2}*Ub::R::mCherry*	Ub::R	mCherry	Low signal	Increase in accumulation
	P_{nhx-2}*Ub::M:mCherry*	Ub::M	mCherry	Diffuse signal throughout worm	No change
UPR					
	P_{hsp-4}*::GFP*	Hsp-4	GFP	Normal expression in spermatheca	Under ER stress conditions diffuse signal throughout body of the worm
Autophagy					
	P_{nhx-2}*mCherry::lgg-1*	Lgg-1	mCherry	Diffuse signal throughout intestinal cells	Change in diffuse to punctate pattern in intestinal cells

Figure 3.1 Inactivation of *cdc-48, sel-1,* and *hrd-1* Results in the Accumulation of ERAD Substrates

Transgenic animals expressing different ERAD substrates fused to fluorescent tags were exposed for 48 hours to ERAD RNAi's (n=300 worms for each condition). Animals were anesthetized and imaged utilizing the ArrayScan V^{TI}. Panels A, C, & E show quantification of fluorescence in intestinal cells upon RNAi inactivation of ERAD genes (x-axis). Panels B, D, & F show florescence images after each transgenic line was exposed to control (vec) or ERAD RNAi's: *cdc-48, sel-1,* or *hrd-1*. A&B. NHK transgenic animals, C&D. Saar transgenic animals, E&F. PPM2 transgenic animals. Note: Inactivation of *cdc-48, sel-1,* or *hrd-1* results in the accumulation of ERAD substrates. Error bars represent standard deviations from a representative experiment; statistical significance determined using unpaired, two-tailed, *t*-test; ***p<0.001, **p<0.01.

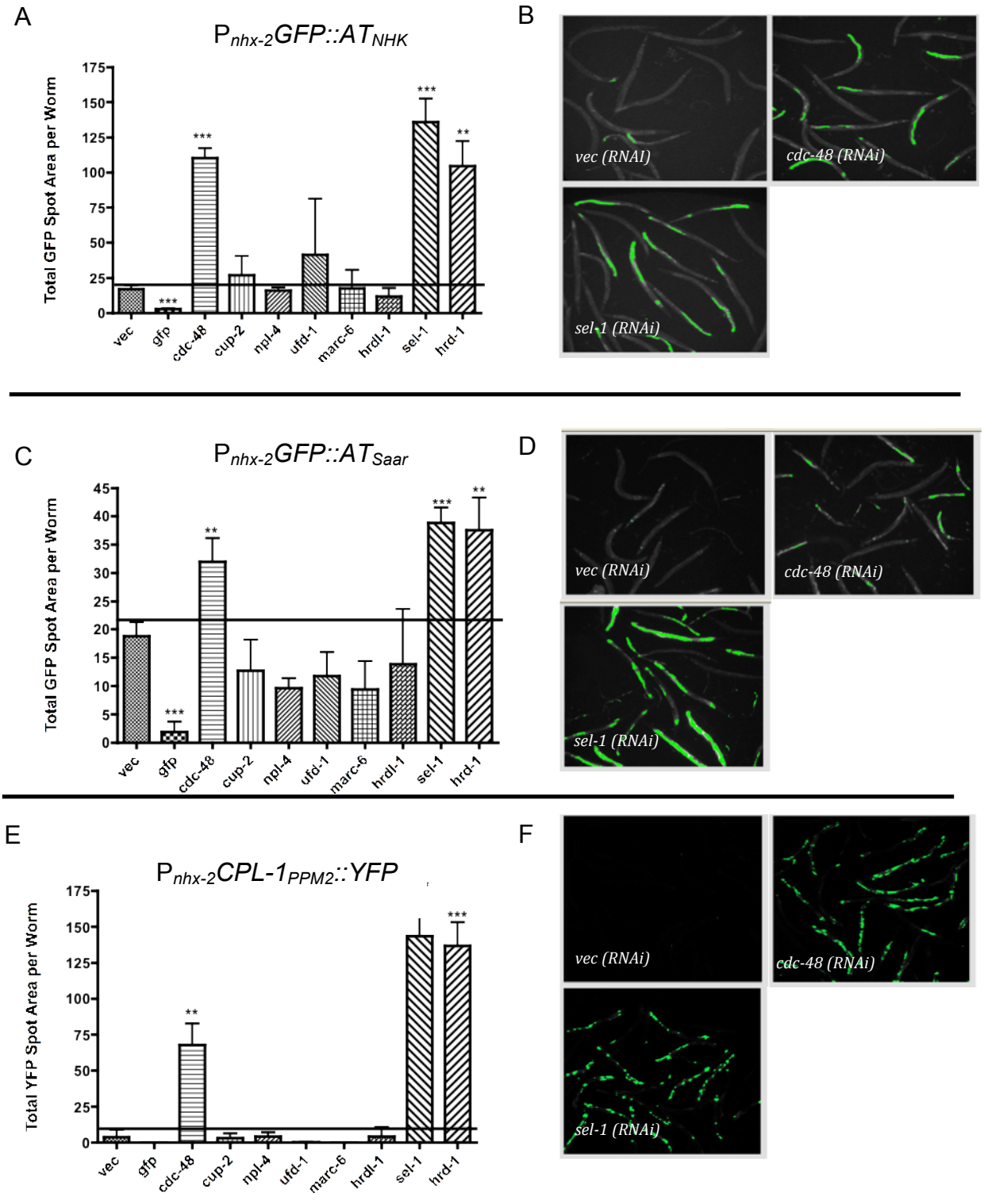

Figure 3.1 Inactivation of *cdc-48, sel-1,* and *hrd-1* Results in the Accumulation of ERAD Substrates

sel-1, or *hrd-1*) but not all ERAD associated genes. These studies suggested the null mutants of α1-AT are eliminated by the *hrd-1* E3 ligase complex and follow a classical *cdc-48* pathway to the proteasome (Figure 3.1 A-D). Accumulation of GFP in the intestine of transgenic animals was quantified via the ArrayScan V^{TI} (Figure 3.1 B,D).

3.3.1.2. Pre-Pro mutant of cathepsin L as an ERAD substrate

Cathepsins are cysteine aspartic or serine proteases found in membrane bound structures [234]. The cysteine cathepsins are primarily targeted to the lysosome in mammalian cells and are activated by a combination of the acidic pH and post-translational processing [235, 236]. The cathepsins are synthesized in the ER as inactive preproenzymes prior to lysosomal delivery. The N-terminal pre-region contains the signal sequences whereas the pro-region has been shown to control catalytic activity and enzymatic targeting [236, 237].

The pro-region of the protein is also necessary for correct folding. Mutational analysis of the preproregion of cathepsin L-like proteases showed that three tryptophan residues are essential for proper folding of the prodomain (W28, W31 and W52). Proteins containing these mutations are retained in ER and eliminated by ERAD, with a combination of W28 and W31 causing the most severe misfolding [236].

ClustalW alignments between mammalian and *C. elegans* cathepsin L proteins showed that the three tryptophan residues were conserved (Miedel, M. T., Silverman G. A. and Luke, C. J., unpublished). Thus, we created transgenic *C. elegans* strains expressing either wild-type cathepsin L (CPL-1) or a mutant CPL-1 (W28A and Y31A, collectively known as PPM2) (Miedel, M. T., Silverman G. A. and Luke, C. J.,

unpublished). These transgenes were driven by *nhx-2* promoter and yellow fluorescence protein (YFP) was fused to the C-terminus for visualization of transgene expression. The wild-type CPL-1 ($P_{nhx\text{-}2}$*CPL-1::YFP*) transgenic worms showed diffuse punctate fluorescence that co-localized with lysotracker or Alexa-Fluor647 Dextran (10 KDa MW), suggesting progression of CPL-1 through the secretory pathway and eventual targeting to the late endosomal and lysosomal compartments. Additionally, some of the CPL-1::YFP was seen in the pseudocoelomic space and in the oocytes suggesting that a portion of the wild-type CPL-1 was secreted and taken up by the eggs (Miedel, M. T., Silverman G. A. and Luke, C. J., unpublished).

Conversely, transgenic animals expressing $P_{nhx\text{-}2}$*CPL-*1_{ppm2}*::YFP*, accumulated YFP in the intestinal cells of worms. Co-injection of the $P_{nhx\text{-}2}$*CPL-*1_{ppm2}*::YFP* with a $P_{nhx\text{-}2}$*dsRED::KDEL* plasmid (KDEL is a ER-retention signal, resulting in dsRED expression in the ER of the worms) showed that CPL-1_{ppm2}::YFP co-localized with the dsRED fluorescence, suggesting that the CPL-1_{ppm2}::YFP was accumulating in the endoplasmic reticulum of the intestinal cells. There was no detectable trafficking of CPL-1_{ppm2}::YFP to the lysosomal compartment or the pseudocoelomic space.

I investigated the effect of ERAD RNAi on CPL-1_{ppm2}::YFP disposition. The $P_{nhx\text{-}2}$*CPL-*1_{ppm2}*::YFP* animals showed marked accumulation following treatment with *cdc-48 (RNAi), sel-1(RNAi),* or *hrd-1(RNAi),* results similar to those shown for strains expressing NHK and Saar (Figure 3.1 E,F). Taken together these studies suggested that the CPL-1_{ppm2}::YFP was a serviceable ERAD substrate in *C. elegans*.

3.3.2 Ubiquitin Tagged mCherry as a Marker of Proteasome Activity

The UPS is the final destination for most ERAD substrates [139]. The degradation of targeted proteins by the UPS requires two significant steps. First, proteins are targeted to the proteasome by the covalent attachment of ubiquitin. Second, the targeted proteins are deubiquitinated and then degraded by the 26S proteasome (described in section 1.7) [135].

Ubiquitin fusion degradation (UFD)-targeted fluorescent reporters allow for the functional analysis of the UPS within cells [135]. UFD-targeted reporter constructs utilize a fluorescent protein reporter (such as GFP or mCherry) fused to the C-terminus of ubiquitin [135]. Normal expression of the reporter is relatively low, due to the fast turnover of ubiquitinated products. However, inhibition of the UPS allows for the accumulation of the reporter proteins, which are detected by fluorescence microscopy [238, 239]. Some UFD-targeted reporter constructs have been modified to use the N-end rule signals to target reporter substrates for degradation [240]. Briefly, the N-end rule states that certain N-terminal amino acids trigger ubiquitination of the protein, which are subsequently targeted for degradation [238, 241].

Based on these findings, we have created transgenic *C. elegans* strains expressing $P_{nhx\text{-}2}$*Ub::R::mCherry.* This construct contains an UFD-targeted reporter (mCherry), which was fused to the C-terminus of UB. Expression was targeted to the intestine by using the *nhx-2* reporter. Specifically, this $P_{nhx\text{-}2}$*Ub::R::mCherry* transgene was constructed by mutation of a residue (V77R) just after the C-terminal gly-gly residues of ubiquitin. The resulting product can be targeted directly for degradation (UFD substrate) or deubiquitination and reubiquitination (N-end rule substrate) [238]. As

expected, the transgenic animals expressing P_{nhx-2}*Ub::R::mCherry* showed no detectable accumulation of mCherry under normal conditions (Figure 3.2 B (vector)). As a control, I also constructed a P_{nhx-2}*Ub::M::mCherry* construct, which contains the mutation (V77M). This protein is deubiquitinated but the N-terminal methionine residue does not trigger ubiquitination and therefore stabilizes the mCherry protein in the cytosol [238]. As expected, this control showed diffuse mCherry fluorescence throughout the intestine of the worm (Figure 3.2 D vector).

I then utilized the P_{nhx-2}*Ub::R::mCherry* and P_{nhx-2}*Ub::M::mCherry* transgenic animals to test the effects of RNAi on proteasomal activity. The transgenic animals were fed RNAi for 48 hours and then imaged to determine changes in fluorescence. Knocking down a proteasome subunit by *rpt-5 (RNAi)* resulted in a significant increase in fluorescence in P_{nhx-2}*Ub::R::mCherry* animals (Figure 3.2 A,B) and, as expected, had no effect on the P_{nhx-2}*Ub::M::mCherry* expressing animals (Figure 3.2 C,D). Interestingly, when certain components of ERAD (*cdc-48, npl-4, ufd-1*) were inhibited by RNAi, the transgenic P_{nhx-2}*Ub::R::mCherry* animals showed an increase in fluorescence (Figure 3.3 A,B). However, neither *sel-1* nor *hrd-1* showed an effect on fluorescence (data not shown). These data confirmed that *cdc-48* and its cofactors play a role in the elimination of cytosolic and or ER proteins targeted for degradation [242, 243].

3.3.3 P_{Hsp-4}::GFP as a Marker of UPR induction

BiP/ Grp78 is an ER molecular chaperone required for correct protein folding, sensing ER stress, and targeting unfolded proteins for degradation [91, 197, 244, 245]. The *C.*

Figure 3.2 RNAi's that Inhibit Degradation of $P_{nhx\text{-}2}$*Ub::R::mCherry*

A. Quantification and B. Fluorescence images of $P_{nhx\text{-}2}$*Ub::R::mCherry* transgenic worms (n=300) fed RNAi clones for the indicated genes (x-axis). Fluorescence of $P_{nhx\text{-}2}$*Ub::R::mCherry* worms fed RNAi clones were compared to the animals fed empty RNAi feeding vector (L4440). C. Quantification and D. Fluorescence images of $P_{nhx\text{-}2}$*Ub::M::mCherry* transgenic animals showed no variation in steady state levels of mCherry fluorescence. Error bars represent standard deviations from a representative experiment; statistical significance determined using unpaired, two-tailed, *t*-test; **p<0.01, *p<0.05.

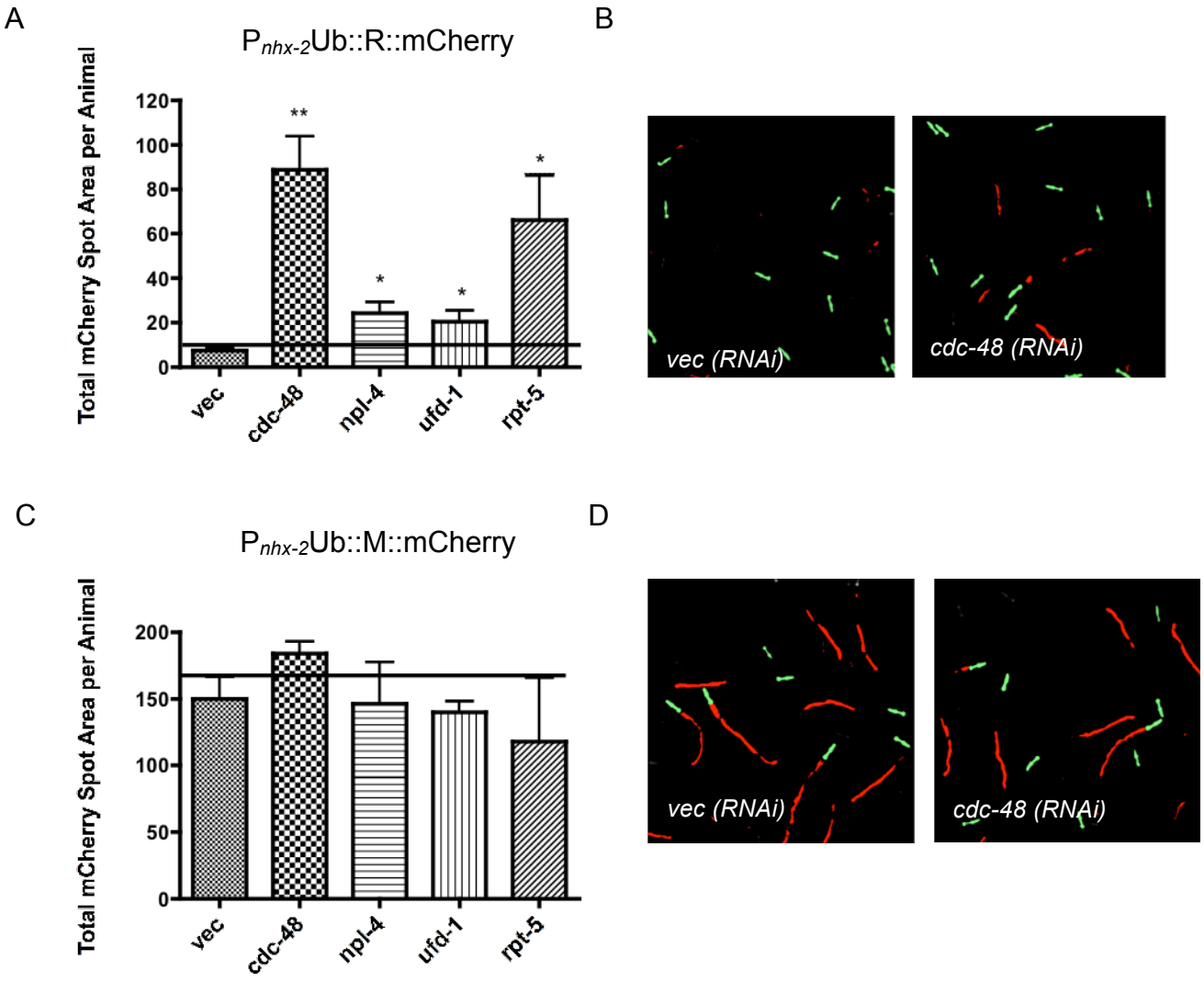

Figure 3.2 RNAi's that Inhibit Degradation of P*nhx-2*Ub::R::mCherry

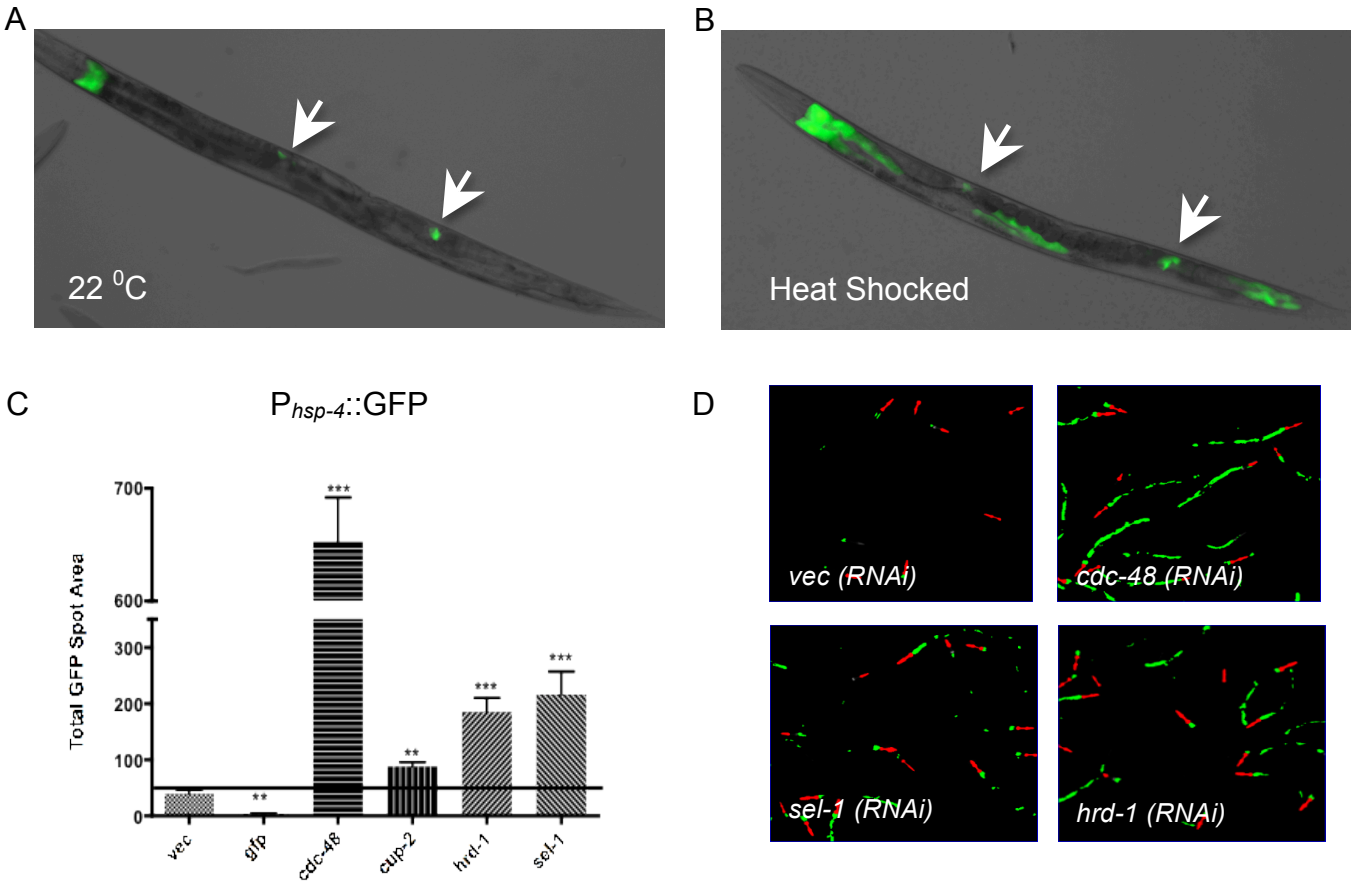

Figure 3.3 ER Stress Results in P_{hsp-4}::GFP Accumulation

A. Image of an adult wild-type worm expressing GFP under the UPR-inducible *hsp-4* promoter (P_{hsp-4}::GFP *)* under normal conditions. B. Image of an adult P_{hsp-4}::GFP transgenic worm after heat shock at 30 °C for 1 hour. White arrows (in panels A & B) indicate the spermatheca. C. Quantification and D. Images of GFP fluorescence of P_{hsp-4}*::GFP* transgenic worms (n=300) that were exposed to different ERAD (RNAi) of indicated genes (x-axis) for 48 hours. Fluorescence of P_{hsp-4}::GFP worms fed different RNAis were compared to animals fed empty RNAi feeding vector (L4440). Error bars represent standard deviations from a representative experiment; statistical significance determined using unpaired, two-tailed, *t*-test; ***p<0.001, **p<0.01.

elegans homolog of BiP is *hsp-4*. In previous studies, an *hsp-4::GFP* transcriptional reporter driven by the endogenous BiP (*hsp-4)* promoter shows low level of baseline expression (except for that in the spermatheca) but is transcriptionally upregulated in the gut and epidermises in response to ER stress, heat shock and activation of some of the UPR activators [206, 208, 210]. However, in the presence of ER stress, RNAi of *ire-1* or *xbp-1* blocks *hsp-4* expression [206].

As a control for UPR activation, we generated an GFP reporter driven by the *hsp-4* promoter. Under baseline conditions P_{hsp-4}*::GFP* expression was detected in the spermatheca (Figure 3.3 A) [206, 208, 210]. However, when the P_{hsp-4}*::GFP* animals were stressed by heat shock at 30^{o}C for one hour, P_{hsp-4}*::GFP* was markedly induced in the intestine of transgenic animals (Figure 3.3 B). Similarly, when UPR was activated by ERAD inhibition via RNAi (*cdc-48, sel-1, hrd-1 or cup-2*), P_{hsp-4}*::GFP* was induced in a manner similar to that of heat shock (Figure 3.3 C,D). These results confirmed that P_{hsp-4}*::GFP* can serve as a sensor for UPR activation.

3.3.4 Lgg-1 as a Marker of Autophagy

Autophagy is a cell stress response pathway that delivers cytosolic proteins and damaged organelles to lysosomes for degradation and recycling [126, 246]. Specifically, cytoplasmic components are surrounded by double-membrane that eventually forms a closed vesicle (autophagosome) and this structure fuses with late endosomes or lysosomes for degradation. LC3/Atg8 is a cytosolic protein that is processed and inserted into the initial membrane (phagophore). Thus, during enhanced

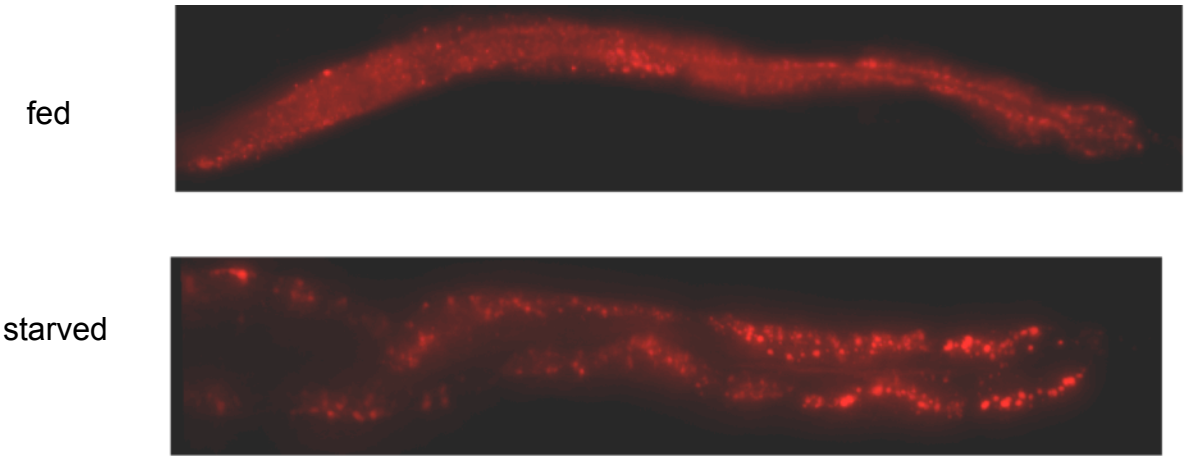

Figure 3.4 Induction of Autophagy by Starvation

Fluorescence images of $P_{nhx\text{-}2}$*mCherry::lgg-1* worms fed (upper panel) or starved (lower panel) for 48-hours.

autophagy, the distribution of LC3 changes from diffuse to punctate. This feature can be used to monitor an increase in the number of autophagosomes [247, 248].

Lgg-1/Atg-8 is the *C. elegans* homolog of LC3 [211]. We created *C. elegans* strains expressing the P_{nhx-2}*mCherry::lgg-1* (Lgg-1) transgene. This construct utilizes the *nhx-2* promoter to drive expression of the *lgg-1* in intestinal cells. Under normal conditions, transgenic animals displayed diffuse fluorescence pattern throughout the intestine of the worm (Figure 3.4, top panel). However, when autophagy is induced by starvation, the fluorescence became punctate, suggesting an increase in formation of autophagosomes (Figure 3.4, bottom panel).

3.3.5 Control for Promoter Expression

To determine if an RNAi clone had a nonspecific effect on the *nhx-2* promoter, we generated transgenic *C. elegans* strains expressing P_{nhx-2}*sGFP*. This control strain was created utilizing the *nhx-2* intestinal promoter to drive expression of GFP in the intestine of the worm. These transgenic animals display diffuse fluorescence throughout the intestine of the animals. Overall, the P_{nhx-2}*sGFP* transgenic animals showed relatively stable expression (Figure 3.5 A,B,C,D).

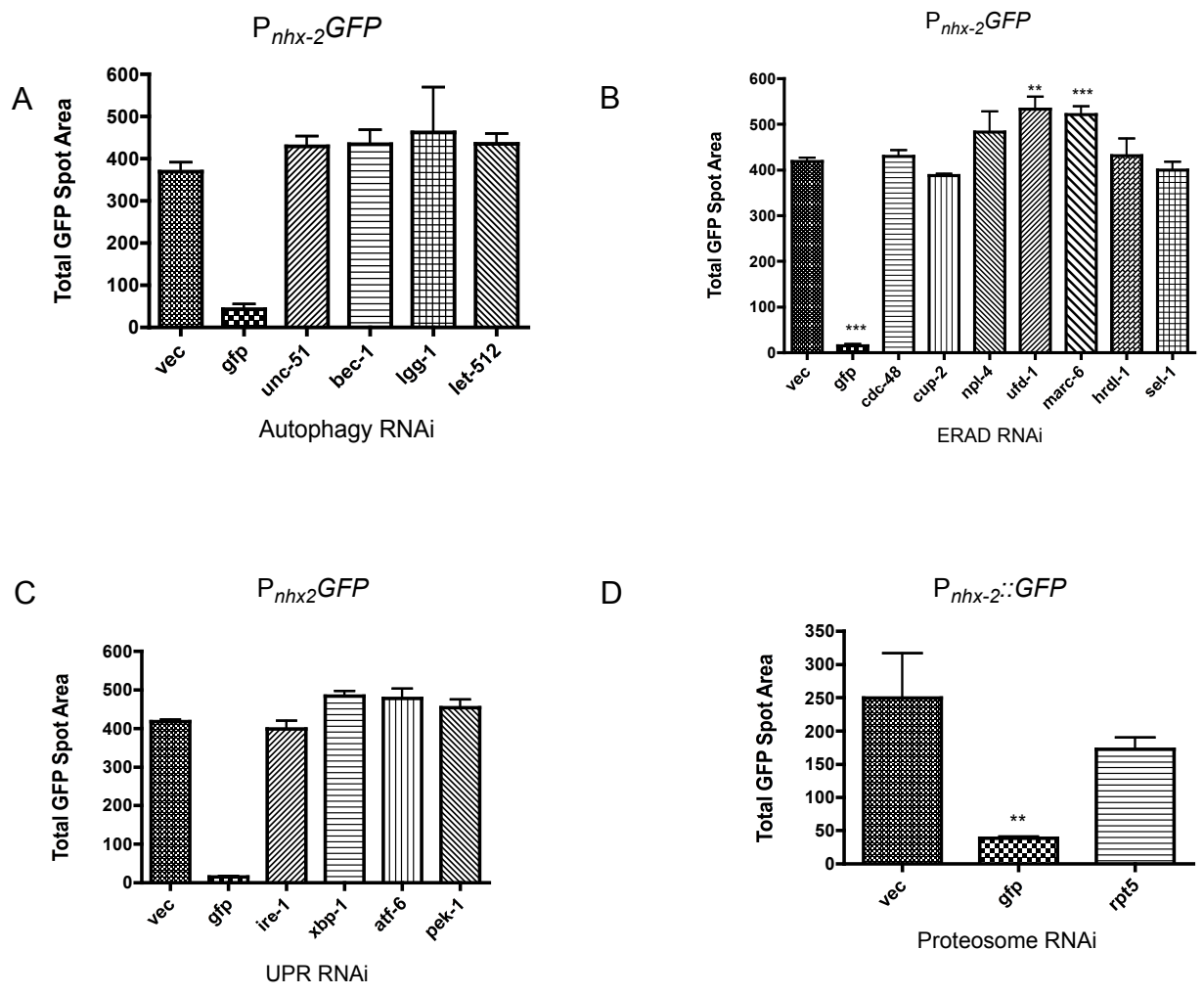

Figure 3.5 RNAi Effects on Promoter Expression

Quantification of fluorescence of P*nhx-2GFP* transgenic worms (n=300) that were exposed to different A. Autophagy, B. ERAD/proteasome, C. UPR or D. Proteasome RNAis (x-axis). Error bars represent standard deviations from a representative experiment; statistical significance determined using unpaired, two-tailed, *t*-test; ***p<0.001, **p<0.01, *p<0.05.

3.4 ATZ ACCUMULATION AFTER RNAi INDUCED MODULATION OF DEGRADATION AND UPR SIGNALING PATHWAYS

The goal of these investigations was to help elucidate the genetic modifies of ATZ accumulation and degradation by utilizing the *C. elegans* ATZ model in combination with RNAi-based knockdown of genes from the well-defined degradation pathways. The following sections present the results of the P_{nhx2}sGFP::ATZ transgenic animals upon RNAi-mediated gene silencing of the autophagy/ lysosomal and ERAD/UPS pathways. In addition, I analyzed the effects of ATZ accumulation on the UPR to determine if this signaling pathway was involved in directing the disposition of the non-canonical ERAD substrate.

3.4.1 ATZ Accumulation After Autophagy RNAi

The autophagy-lysosome pathway has been identified as a quality control system associated with the degradation of ATZ in other model systems [201-203]. To determine whether autophagy was responsible for effecting the disposition of sGFP::ATZ in *C. elegans*, I inhibited autophagy by RNAi in P_{nhx-2}*sGFP::ATZ* animals. If autophagy plays a role in the degradation of ATZ in *C. elegans,* then silencing genes critical for autophagy activation should result in an increase in ATZ accumulation. Transgenic animals expressing sGFP::ATZ were exposed to different autophagy RNAi's for 72 hours and then assayed for total florescence utilizing the ArrayScan V^{TI} imaging platform. *Bec-1(RNAi), lgg-1(RNAi), let-512(RNAi),* and *unc51(RNAi)* all resulted in a

significant increase in fluorescence (Figure 3.6 A,B). None of these RNAi's altered the expression of $P_{nhx\text{-}2}$*sGFP* (Figure 3.5 A). Thus, it is unlikely that these results were due to a transcriptional effect on the *nhx-2* promoter. In contrast to ATZ, inhibition of autophagy had no effects on the prototypical luminal ERAD substrates NHK and PPM2 (Figure 3.6 C,D). Taken together, these results suggested that a portion of misfolded sGFP::ATZ was eliminated via the autophagy pathway. These results are consistent to those observed in studies utilizing mammalian cell cultures and mouse models of ATZ [201-203].

3.4.2 ATZ Accumulation After ERAD RNAi

To determine whether ERAD was responsible for effecting the disposition of sGFP::ATZ, I performed *ERAD(RNAi)* on P_{nhx2}sGFP::ATZ animals. If ERAD plays a role in degrading ATZ, then silencing genes in the ERAD pathways should increase ATZ accumulation. Control strains and P_{nhx2}sGFP::ATZ were assayed for total fluorescence using the ArrayScan V^{TI} 48 hours after starting RNAi treatment. Knockdown of five genes (*cup-2, ufd-1, npl-4, sel-1,* and *hrdl-1)*, which are associated with different functions within the ERAD pathway, mediated a significant increase in fluorescence (Figure 3.7 A,B). Most notably, knockdown of the E3 ligase *hrdl-1*, the *C. elegans* ortholog of GP78, showed a modest but significant increase in fluorescence. This result suggested that at least a portion of misfolded sGFP::ATZ was eliminated via

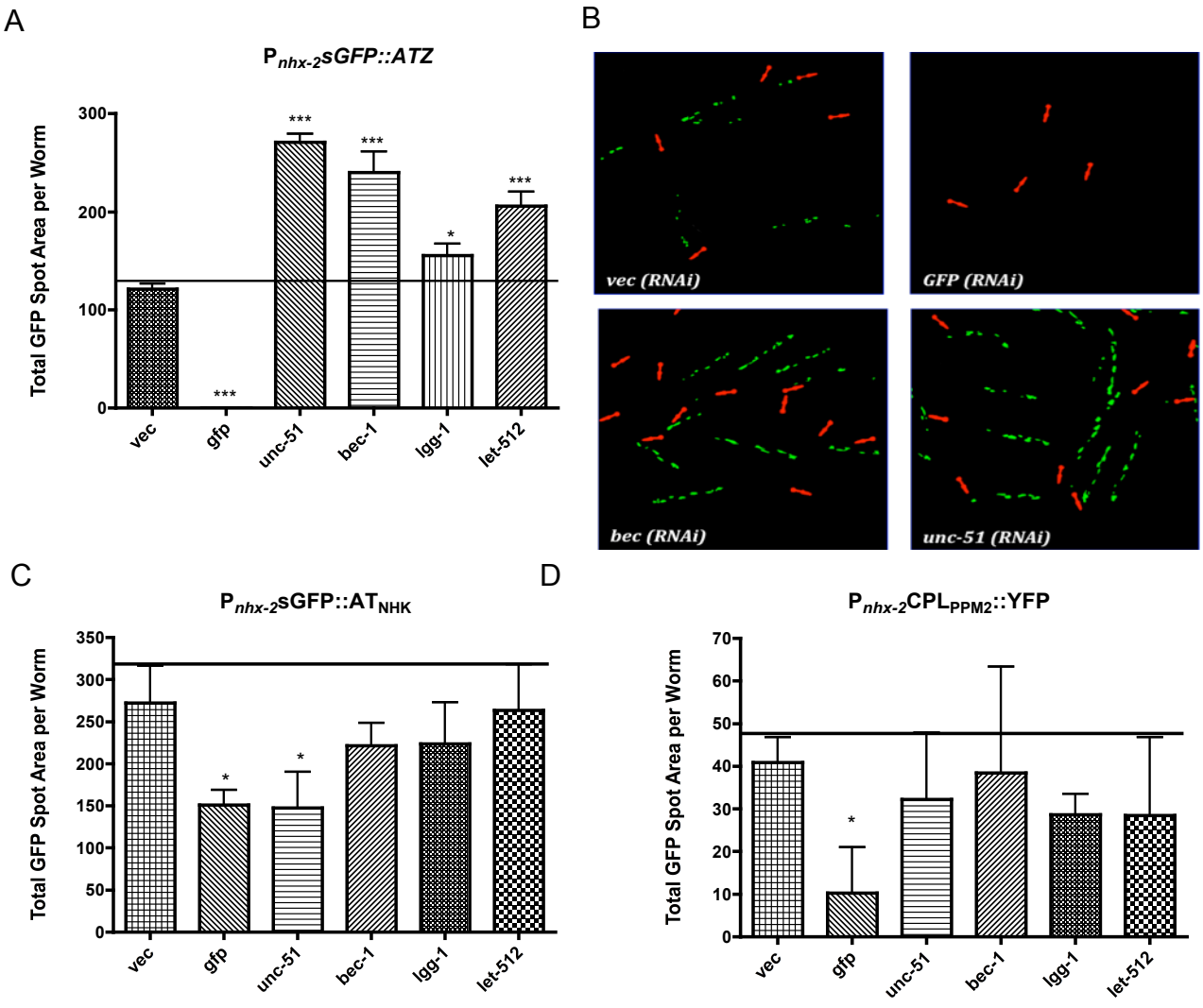

Figure 3.6 Response of P *nhx-2*sGFP::ATZ Animals to Autophagy RNAi's

A. Quantification and B. Fluorescence images of P*nhx-2sGFP::ATZ* transgenic animals (n=300) that were treated with *bec-1(RNAi), lgg-1(RNAi), let-512(RNAi),* or *unc51(RNAi)* (x-axis). All RNAi's resulted in a significant increase in fluorescence. C. Quantification of P*nhx-2sGFP::ATNHK* D. P*nhx-2sCPL-1PPM2::YFP* transgenic animals fed autophagy RNAi's (x-axis). Error bars represent standard deviations from a representative experiment; statistical significance determined using unpaired, two-tailed, *t*-test; ***p<0.001, **p<0.01 *p<0.05.

Figure 3.7 Response of P_{nhx-2}*sGFP::ATZ* Animals to ERAD RNAi's

Transgenic animals (n=300) expressing P_{nhx-2}*sGFP::ATZ* were exposed to ERAD RNAis for 48 hours. Animals were anesthetized and then imaged utilizing the ArrayScan Vti. A. Quantification and B. Images of GFP fluorescence of P_{nhx-2}*sGFP::ATZ* transgenic animals that were fed differing RNAi clones (x-axis). Inactivation of *cup-2, ufd-1, sel-1,* and *hrdl-1* by RNAi results in an increase in accumulation. *Cdc-48(RNAi)*, showed a significant decrease in sGFP::ATZ accumulation. Error bars represent standard deviations from a representative experiment; statistical significance determined using unpaired, two-tailed, *t*-test; ***p<0.001, **p<0.01

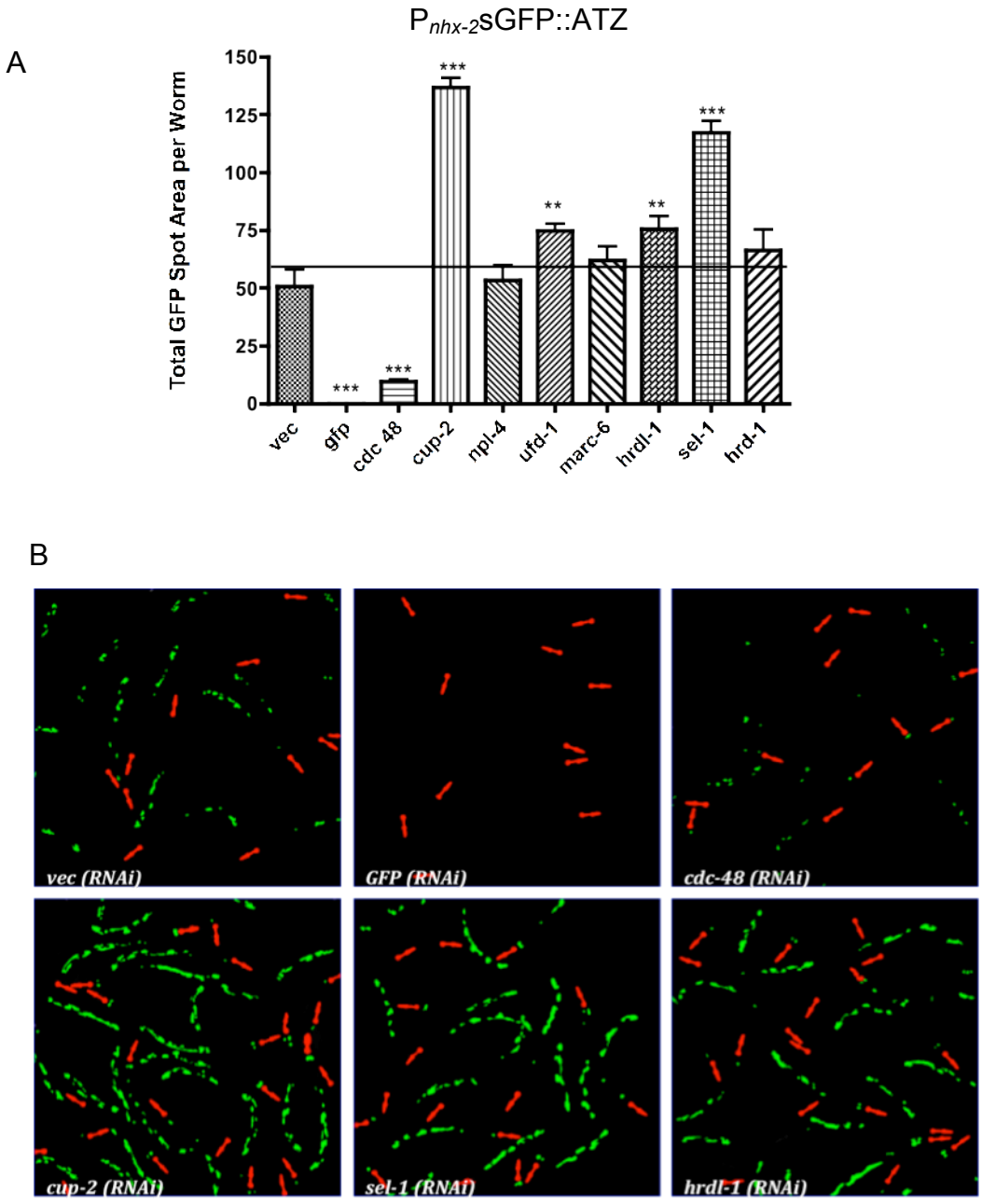

Figure 3.7 Response of P*nhx-2*sGFP::ATZ Animals to ERAD RNAi's

this E3-mediated ERAD pathway. Recent studies also suggested that gp78 may ubiquitinate and facilitate partial degradation of ATZ [227]. Of note, the increase in sGFP::ATZ after these RNAi clones was unlikely due to a transcriptional effect, as none of these RNA's, with the exception of *ufd-1* and *marc-6*, increase in $P_{nhx\text{-}2}$*sGFP::ATZ* expression (Figure 3.5 B).

One of the core components of ERAD is cdc-48/VCP/p97, which is the cytosolic AAA+ATPase involved in the retranslocation of misfolded proteins from ER to the cytosol [207, 249]. If ERAD was essential for eliminating a portion of ATZ, then *cdc-48.1*/ *cdc-48.2* (collectively known as cdc-48) RNAi should result in an increase in sGFP::ATZ. However, my results showed a significant decrease in sGFP::ATZ accumulation (Figure 3.6 A,B). This result was opposite of that observed with other ERAD substrates (NHK, SAAR, and PPM2) (Figure 3.1 A,C,D). Since ATZ is localized to the ER and *cdc-48* to the cytosol, this result suggested that down-regulation of *cdc-48* could have an indirect effect on ATZ disposition. Since ERAD inhibition activates the UPR and UPR signaling increases autophagy, I reasoned that the decrease in sGFP::ATZ in animals exposed to *cdc-48(RNAi)* was secondary to increased autophagy.

3.4.2.1 *Cdc-48* RNAi Does Not Stimulate the Elimination of ATZ by Autophagy

To determine if *cdc-48 (RNAi)* was activating autophagy, we crossed *unc-51* (autophagy deficient) mutants with sGFP::ATZ animals, which resulted in an autophagy deficient, sGFP::ATZ expressing line $P_{nhx\text{-}2}$*sGFP::ATZ;unc51(e369).* Since autophagy has been linked with disposal of ATZ, it was not surprising that the resulting P_{nhx2}*sGFP::ATZ;*

Figure 3.8 $P_{nhx\text{-}2}$*sGFP::ATZ*;*unc-51(e369)*

A. Fluorescence images of an adult $P_{nhx\text{-}2}$*sGFP::ATZ* animal (left) and an adult $P_{nhx\text{-}2}$*sGFP::ATZ; unc-519(e369)* (right) transgenic animal. B. Quantification and C. images of fluorescence of $P_{nhx\text{-}2}$*sGFP::ATZ;unc-51(e369)* transgenic worms that were fed different RNAi's (x-axis) for 48 hours (n=100). The quantification of fluorescence of $P_{nhx\text{-}2}$*sGFP::ATZ*;*unc-51(e369)* worms fed an RNAi clone was compared to that of the animals fed empty vector (RNAi). Error bars represent standard deviations from a representative experiment; statistical significance determined using unpaired, two-tailed, *t*-test; ***p<0.001, **p<0.01, *p<0.05.

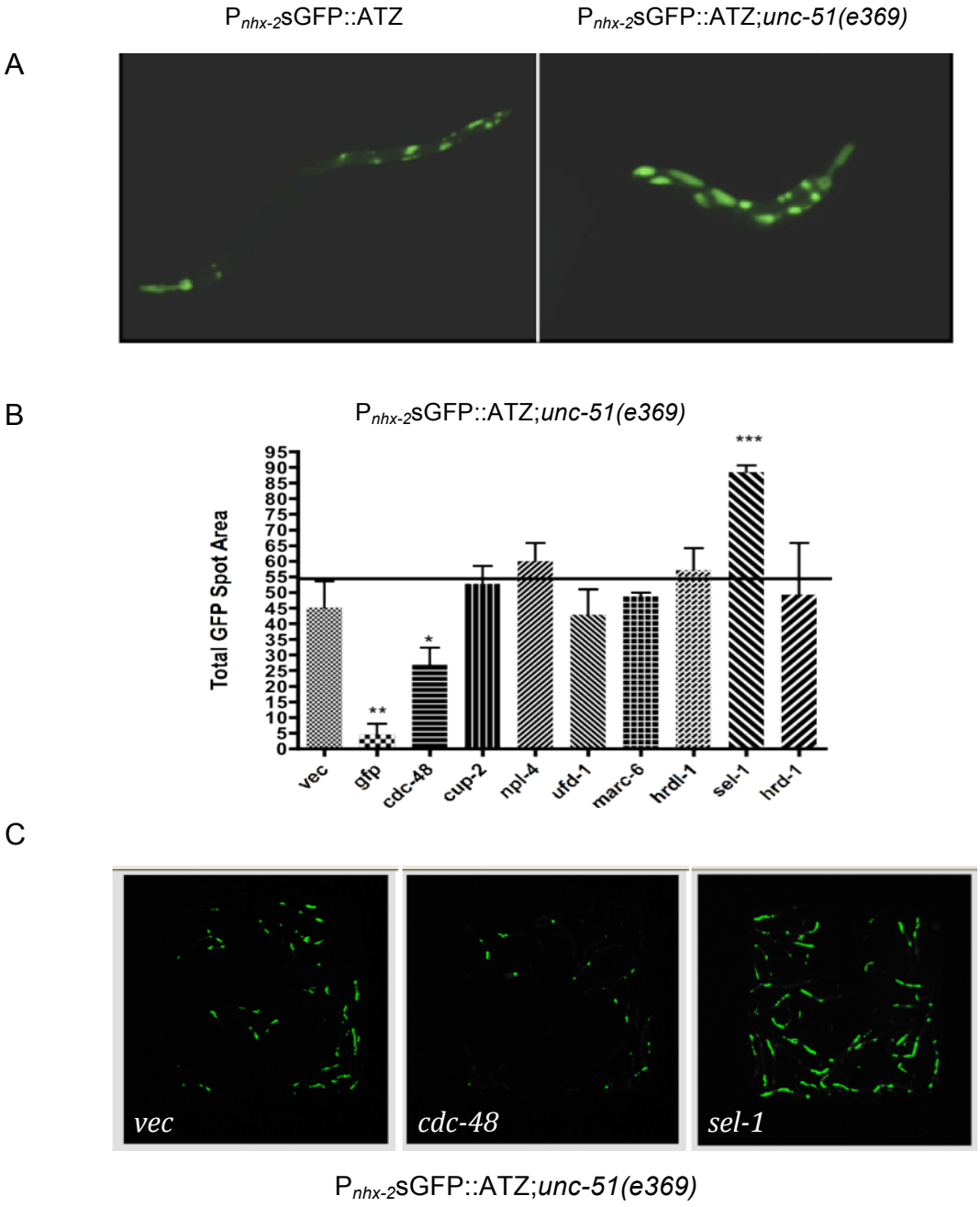

Figure 3.8 P*nhx-2*sGFP::ATZ;*unc-51(e369)*

unc51(e369) animals displayed an increase in sGFP::ATZ accumulation (Figure 3.7 A). When the $P_{nhx\text{-}2}$*sGFP::ATZ;unc51(e369)* animals were exposed to *cdc-48(RNAi)* they still showed a significant decrease in ATZ (Figure 3.7 B,C). These findings suggested that knockdown of *cdc-48* decreased the accumulation of ATZ by a non-autophagy and non-proteasomal pathway.

3.4.3 ATZ Accumulation After Proteasome RNAi

To determine whether the proteasome was involved in the disposition of sGFP::ATZ, I performed proteasomal (RNAi) on P_{nhx2}*sGFP::ATZ* animals. If the proteasome was important in the degradation of ATZ, then impairing proteasomal function by RNAi should result in an increase in ATZ accumulation. Control strains ($P_{nhx\text{-}2}$*Ub::R::mCherry* and $P_{nhx\text{-}2}$*Ub::M::mCherry*) and $P_{nhx\text{-}2}$*sGFP::ATZ* were exposed to *rpt-5(RNAi)* and *rpn-10(RNAi)* for 48 hours. Rpt-5 is a AAA ATPase base component of the 19S regulatory particle that is shown to reversibly bind to ubiquitinated proteins and deliver them to the 20S core particle for degradation. Rpn-10 is a non-ATPase base component of the 19S regulatory particle that recognizes polyubiquitinated proteins. Both *rpt-5* and *rpn-10* are essential for ubiquitin-mediated proteolytic degradation of targeted substrates [250, 251]. Knockdown of *rpn-10* resulted in no change in accumulation (Figure 3.9 A). However, the control line $P_{nhx\text{-}2}$*Ub::R::mCherry* showed no increase in fluorescence, suggesting that *rpn-10(RNAi)* was not effective (Figure. 3.9 B).

Figure 3.9 Response of $P_{nhx\text{-}2}$*sGFP::ATZ* animals to Proteasome RNAI's

A. Quantification $P_{nhx\text{-}2}$*sGFP::ATZ* transgenic animals (n=300) that were treated with *rpt-5(RNAi)* and *rpn-10(RNAi). Rpt-5(RNAi)* resulted in a significant decrease in fluorescence. B. Quantification $P_{nhx\text{-}2}$*Ub::R::mCherry* control transgenic animals (n=300) that were treated with *rpt-5(RNAi)* and *rpn-10(RNAi).* As expected *rpt-5(RNAi)* resulted in an increase in fluorescence, however *rpn-10* did not block the proteasome and therefore was eliminated from analysis. C. Quantification $P_{nhx\text{-}2}$*sGFP::AT*$_{NHK}$ and D. $P_{nhx\text{-}2}$*CPL-1*$_{PPM2}$*::YFP* transgenic animals (n=300) that were treated with *rpt-5(RNAi)* and *rpn-10(RNAi). Rpt-5(RNAi)* resulted in a significant decrease in fluorescence. Error bars represent standard deviations from a representative experiment; statistical significance determined using unpaired, two-tailed, *t*-test; ***p<0.001, **p<0.01, *p<0.05.

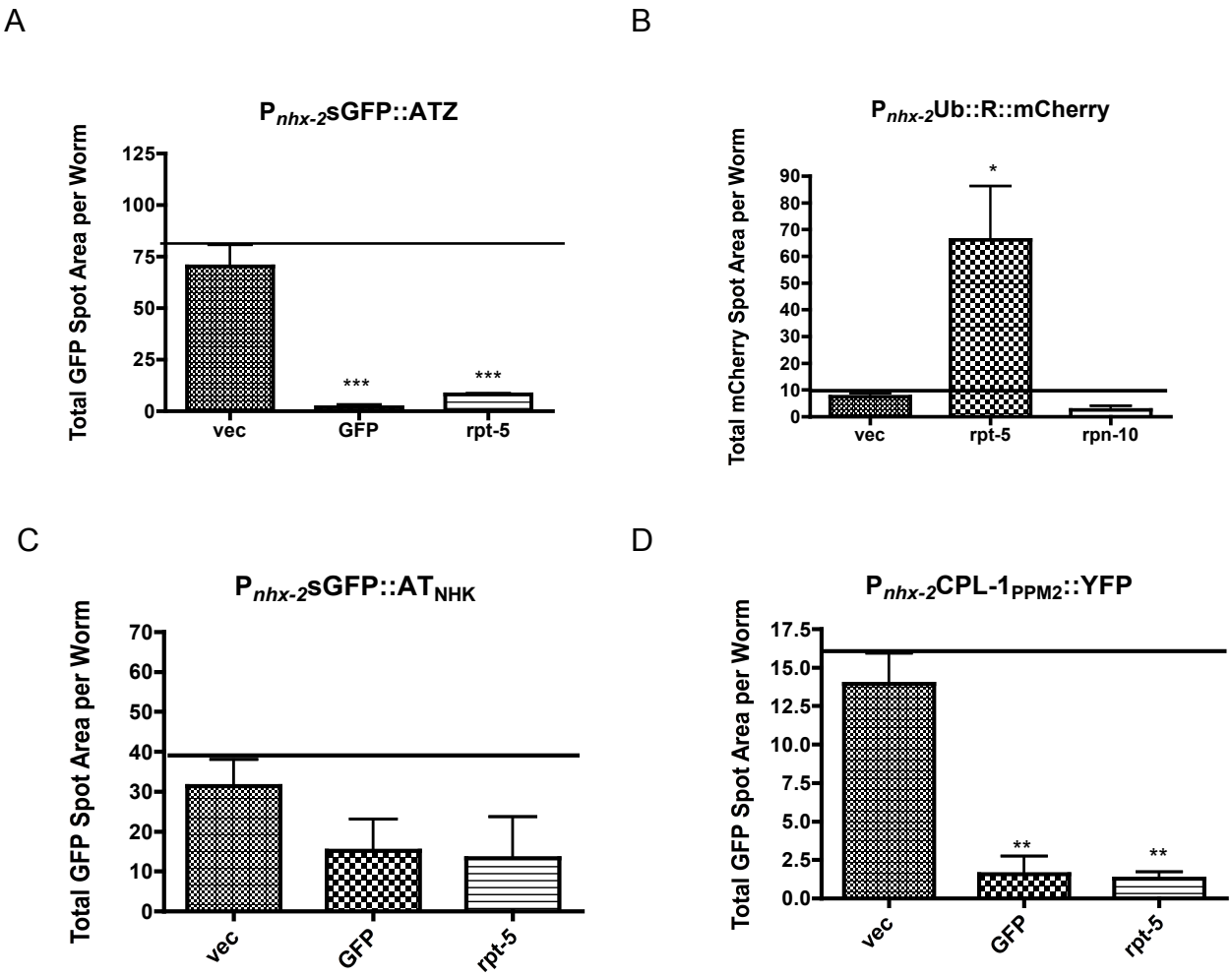

Figure 3.9 Response of P*nhx-2*sGFP::ATZ Animals to Proteasome RNAI's

Surprisingly, *rpt-5(RNAi)* resulted in a significant decrease in sGFP::ATZ accumulation (Figure 3.9 A). Since the control strain, P_{nhx-2}*Ub::R::mCherry*, showed an increase in accumulation, the *rpt-5*(RNAi) appeared to be effective in inhibiting proteasome function (Figure 3.9 B). These results suggest that the inhibition of proteasomal function may be having a complex effect on ATZ accumulation. Similar to ATZ, inhibition of proteasome had comparable effects on the prototypical luminal ERAD substrates, NHK and PPM2. When either control strains were treated with *rpt-5(RNAi)* it resulted in a decrease in expression of protein (Figure 3.9 C,D). These results suggest that proteasome inhibition may be having a complex effect on protein accumulation.

3.4.4 ATZ Accumulation After UPR RNAi

Although ATZ misfolds and accumulates in the ER, in some systems it does not appear to induce the unfolded protein response (UPR) [205]. To determine whether P_{nhx-2}*sGFP::ATZ* animals induce the UPR; we co-injected either the P_{nhx-2}*s*GFP::ATZ or P_{nhx-2}*sGFP::ATM* plasmid with P_{hsp-4}*::mCherry* plasmid. The latter construct served as a sensor for UPR activation. Transgenic animals expressing P_{nhx-2}*sGFP::ATZ;*P_{hsp-4}*::mCherry* showed a marked increase relative to control P_{nhx-2}*sGFP::ATM;*P_{hsp-4}*::mCherry* (Figure 3.10). These findings suggested that sGFP::ATZ expression in *C. elegans* constitutively activated the UPR.

If ATZ constitutively activated the UPR, and the UPR enhances both the ERAD-UPS and autophagy-lysosome protein degradation pathways, silencing of the UPR could result in an increase in sGFP::ATZ accumulation. Since UPR signaling is initiated

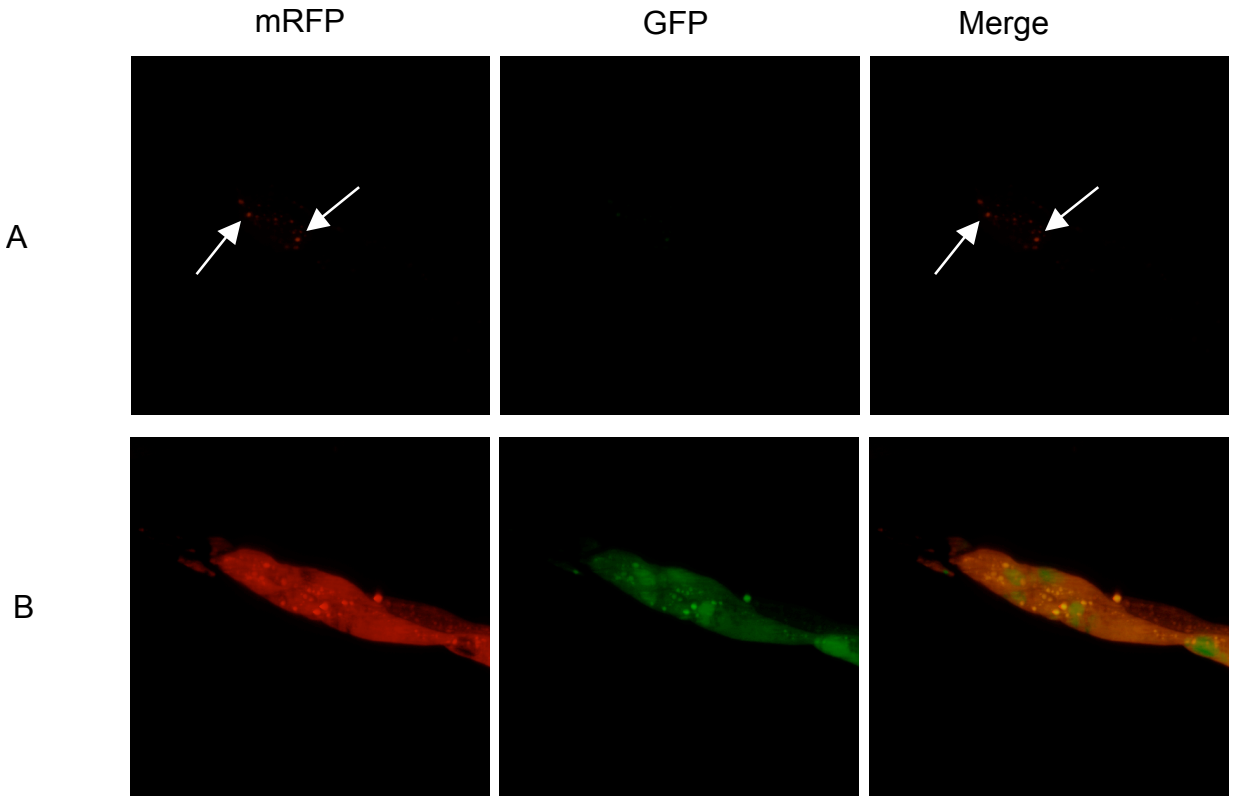

Figure 3.10 Constitutively Activated UPR in P*nhx-2*sGFP::ATZ;P*hsp-4*::*mCherry*

Fluorescence images of transgenic animals expressing A. P*nhx-2*sGFP::ATM;P*hsp-4*::*mCherry* (top three panels) or B. P*nhx-2*sGFP::ATZ;P*hsp-4*::*mCherry* (bottom three panels). Images illustrate UPR activation as demonstrated by high level of hsp-4::mCherry expression. White arrows represent the low level of hsp-4::mCherry expressed in the P*nhx-2*sGFP::ATM;P*hsp-4*::*mCherry* animals.

through three main activators, IRE-1, ATF-6, or PEK-1 [126], I first determined the effectiveness of their RNAi's on P_{hsp-4}*::mCherry* animals under basal conditions (no ER stress). Knockdown of *atf-6,* but not of *ire-1* or *pek-1* induced the *hsp-4* promoter (Figure 3.11). Thus under basal conditions inhibition of *atf-6* activated the UPR. Interestingly, knockdown of the ERAD or autophagy pathways resulted in significant increases in *hsp-4::*GFP expression, suggesting that the UPR was activated (Figure 3.11).

To determine if silencing of UPR activators altered sGFP::ATZ accumulation, transgenic animals expressing P_{nhx-2}*sGFP::ATZ* were exposed to different UPR RNAi for 48 hours and then assayed for total florescence utilizing the ArrayScan V^{TI} imaging platform. *Atf-6(RNAi)* did not alter sGFP::ATZ accumulation (Figure 3.12 A). However, *pek-1(RNAi)* resulted in a significant increase in sGFP::ATZ accumulation (Figure 3.12 A,B). Whereas, *ire-1*(RNAi) resulted in a significant decrease in sGFP::ATZ accumulation (Figure 3.12 A,B). In contrast to ATZ, inhibition of *ire-1* resulted in an increase in accumulation of CPL-1_{PPM2}::YFP, whereas inhibition of *xbp-1, atf-6, and pek-1* had no significant effect (Figure 3.12 C).

To confirm these effects of the UPR RNAi's, I crossed P_{nhx-2}*sGFP::ATZ* animals with *pek-1(ok275)* or *ire-1(v33)* loss-of-function mutants. Similar to RNAi, the P_{nhx-2}*sGFP::ATZ; pek-1(ok275)* displayed a significant increase in sGFP::ATZ accumulation (Figure 3.13 A vs. B, D). The P_{nhx-2}*sGFP::ATZ*; *ire-1(v33)* displayed a marked decrease in sGFP::ATZ accumulation, which was also consistent with the RNAi screening results (Figure 3.13 A vs. C). However, the P_{nhx-2}*sGFP::ATZ*; *ire-1(v33)*

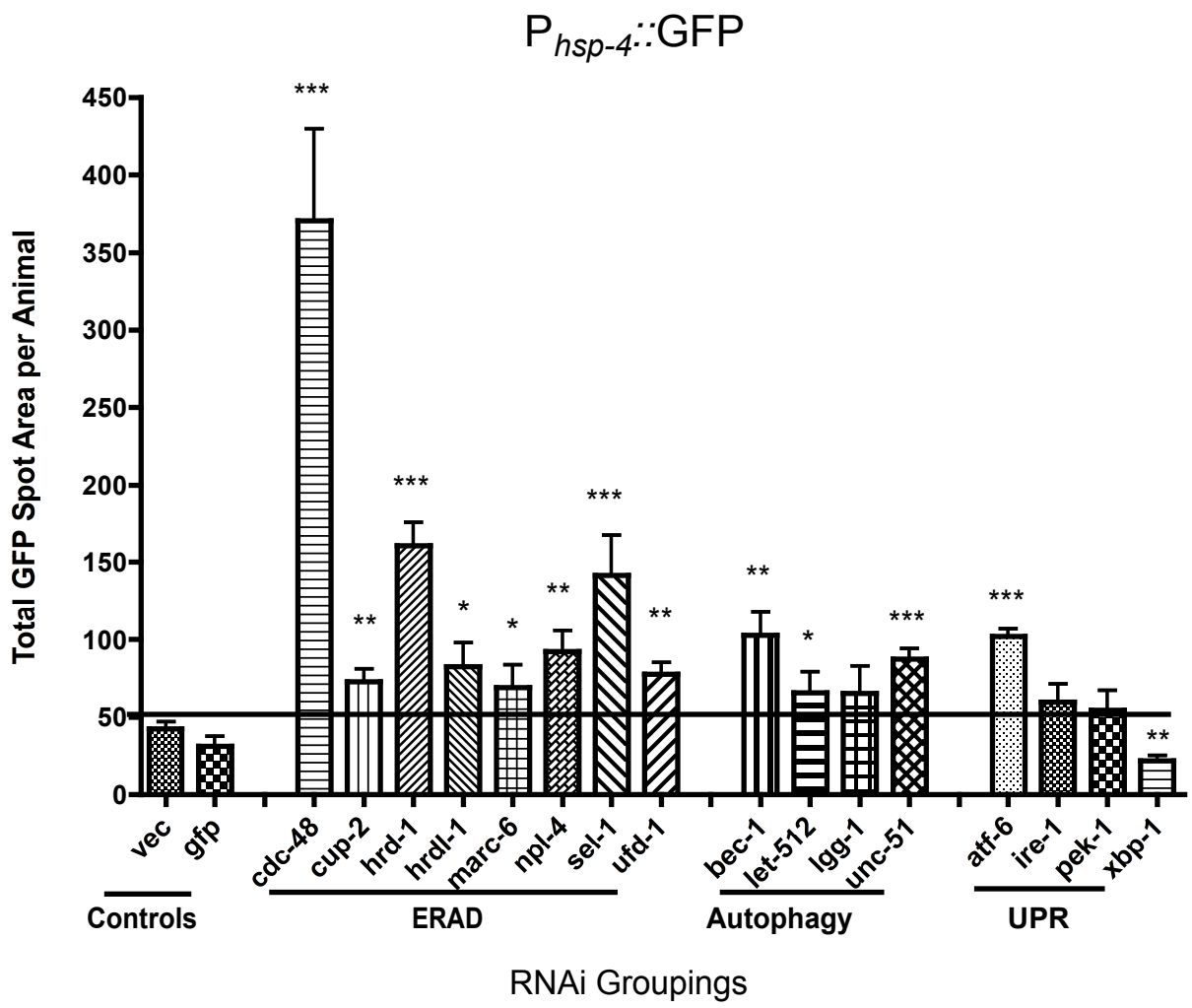

Figure 3.11 Response of P_{hsp-4}::GFP to RNAi's

Fluorescence quantification of P_{hsp-4}::GFP animals fed different RNAi's (x-axis) were compared to animals fed vector RNAi. Error bars represent standard deviations from a representative experiment; statistical significance determined using unpaired, two-tailed, *t*-test; ***p<0.001, **p<0.01, *p<0.05.

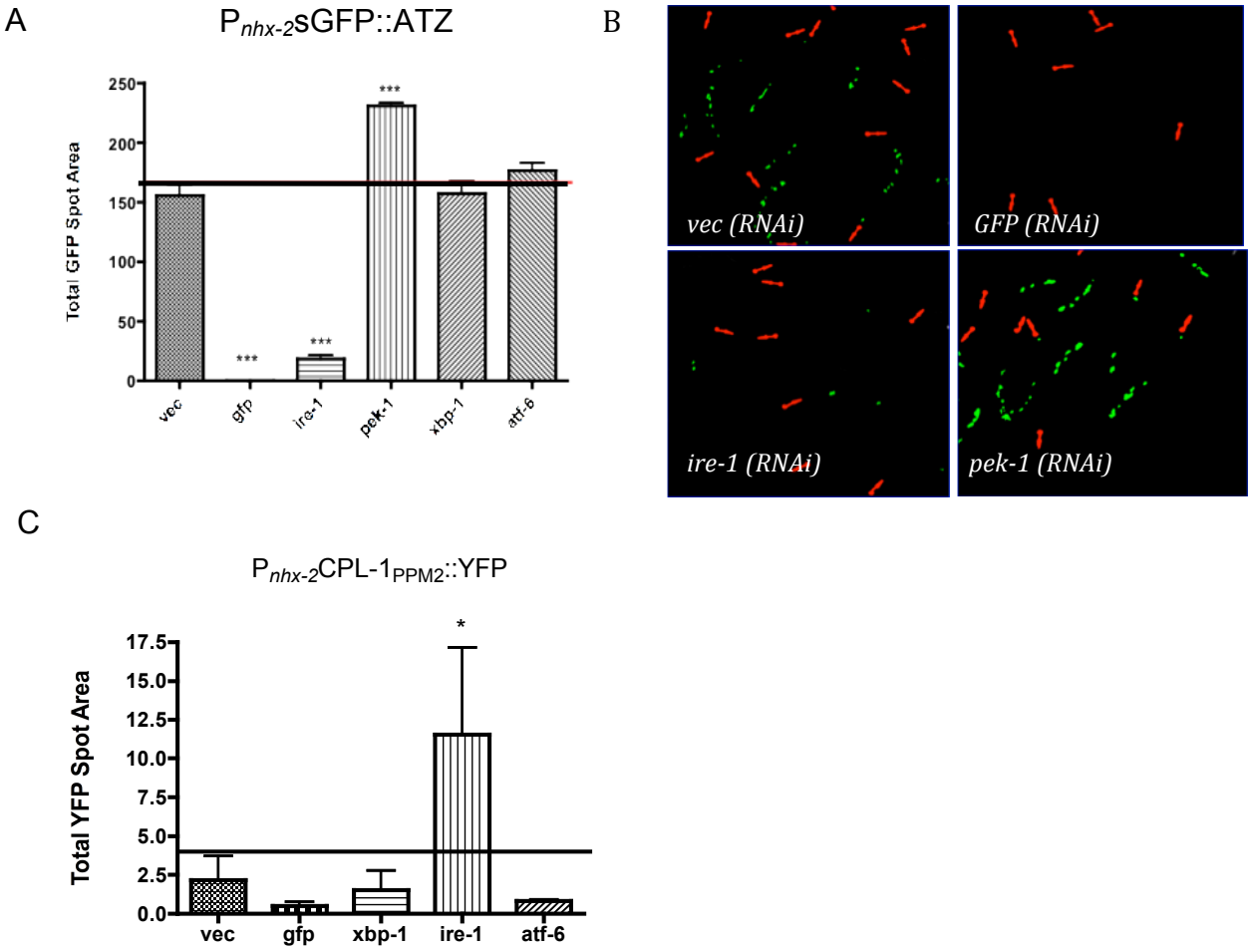

Figure 3.12 Response of P*nhx-2*sGFP::ATZ to UPR RNAi's

A. Quantification and B. images of fluorescence of P*nhx-2*sGFP::ATZ transgenic animals that were fed *ire-1(RNAi), pek-1(RNAi), xbp-1(RNAi),* and *atf-6(RNAi)). Ire-1* showed a significant decrease in fluorescence, while *pek-1* knockdown resulted in a significant increase in fluorescence. C. Quantification of P*nhx-2*CPL-1*PPM2*::YFP transgenic animals that were fed UPR RNAi's. Error bars represent standard deviations from a representative experiment; statistical significance determined using unpaired, two-tailed, *t*-test; ***p<0.001, **p<0.01, *p<0.05.

animals displayed severe growth defects and embryonic lethality making quantification of fluorescence difficult. Nevertheless, even at the earliest stages of development, the amount of sGFP::ATZ was qualitatively decreased relative to the same stage $P_{nhx\text{-}2}$*sGFP::ATZ* animals. Taken together these studies suggested that different components of the UPR had differential effects on sGFP::ATZ accumulation.

IRE-1 inactivation appeared to decrease sGFP::ATZ accumulation. Conceivably, this decrease was due to activation of the "blocked UPR" response, in which a non-canonical UPR system involving the scavanger-like receptor, *Abu* gene family, which facilitates the elimination of misfolded proteins [252]. Activation of the UPR via *ire-1* involves *ire-1* mediated activation of the transcription factor *xbp-1* and it is the down-regulation of this factor that triggers the blocked UPR response or up-regulation of the *Abu* genes. To determine whether the effect of *ire-1* knockdown on sGFP::ATZ accumulation occurred via decreased processing of *xbp-1*, I treated $P_{nhx\text{-}2}$*sGFP::ATZ* animals with *xbp-1(RNAi)* (Figure 3.12 A). Treatment did not affect sGFP::ATZ accumulation (Figure 3.12 A). These findings suggested that the *ire-1(RNAi)* decrease in sGFP::ATZ accumulation was not due to a decrease in *xbp-1* activation and up-regulation of the *Abu* genes.

Recent studies show that *ire-1* activation has a function independent of its nuclease activity, of which the latter cleaves the mRNA encoding *xbp-1* resulting in activation and translation of *xbp-1* [123-125]. This independent function, Regulated Ire1-Dependent Decay (RIDD), results in the rapid turnover of mRNAs separate of *xbp-1* activity [284]. RIDD studies indicate that both *ire-1* activation and ER stress are required for activation of this pathway [285]. Since, expression of ATZ in *C. elegans* induced

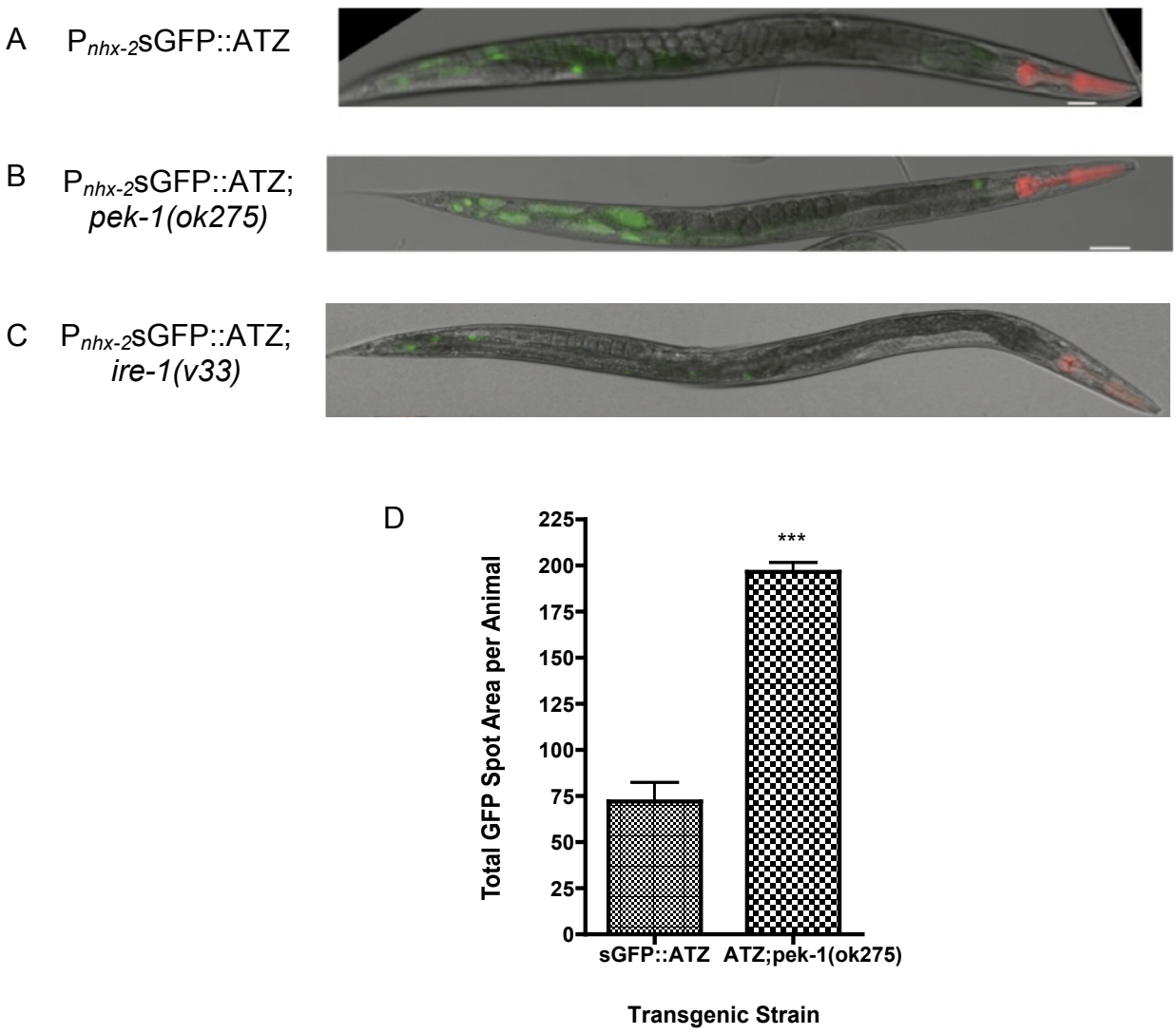

Figure 3.13 *Pek-1(ok275)* and *Ire-1(v33)* Mutations Alter ATZ Accumulation

Images of A. P_{nhx-2}*sGFP::ATZ* B. P_{nhx-2}*sGFP::ATZ*;*pek-1(ok275)* C. P_{nhx-2}*sGFP::ATZ*;*ire-1(v33)* D. Quantification of fluorescence. Note: quantification of P_{nhx-2}*sGFP::ATZ*;*ire-1(v33)* was not completed because of the severe embryonic lethality prevented growth of sufficient number of animals. Error bars represent standard deviations from a representative experiment; statistical significance determined using unpaired, two-tailed, *t*-test; ***p<0.001.

hsp-4 activation (i.e., *ire-1* activation), and knockdown of *ire-1* would further increase ER stress, it is conceivable that the residual *ire-1* activity activated the RIDD pathway, which could preferentially degrade ATZ mRNA.

3.5 DISCUSSION

The aim of this project was to use a targeted RNAi approach to identify genetic modifiers that effect ATZ accumulation. Although systemic RNAi in *C. elegans* is a powerful tool to study gene function, the effectiveness of each RNAi must be assessed by using appropriate controls. Thus, before studying the effects of different RNAi's on sGFP::ATZ accumulation, we constructed a series of transgenic lines to follow the effects of autophagy, ERAD, or UPR RNAi's on prototypical luminal ER substrates or cellular sensors.

My results indicated that sGFP::ATZ was partially degraded through the autophagy pathways. Knockdown of autophagy genes via RNAi resulted in significant increases in sGFP::ATZ accumulation, however no changes were observed in any of the ER luminal substrate controls (NHK/ PPM2). These results suggest that ATZ accumulation are processed differently than other ER luminal misfolded proteins. Furthermore, our results in *C. elegans* are consistent with studies on ATZ disposition in other systems [201-203].

ERAD is comprised of different components that specify the selection of ERAD substrates, the targeting of substrates for degradation, ubiquitination, and retrotranslocation of the substrates into the cytoplasm for proteasomal degradation [71,

197, 198]. HRD-1 is one of three RING finger E3 ubiquitin ligases found in *C. elegans [253].* In mammals HRD-1 is found in a stoichiometric complex with SEL-1, which stabilizes and modulates HRD-1 activity [122, 254, 255]. Additional studies have suggested that SEL-1 facilitates protein degradation through its interactions with transmembrane ERAD components CUP-2 (DERLIN1) as well as cytoplasmic CDC-48 (p97). Together, these data suggest that some ERAD substrates utilize the HRD-1/ SEL-1 complex to target substrates for ubiquitination and then subsequent targeting for retrotranslocation. Ubiquitinated proteins are degraded in the cytoplasm, therefore terminally misfolded proteins have to be retrotranslocated from the ER into cytoplasm. *Cup-2* is the *C. elegans* homolog of Derlin1, which is a transmembrane protein that has been implicated as a retrotranslocation channel [118-121]. Furthermore, the majority of misfolded proteins extracted from the ER require the cytosolic AAA+ATPase cell-division cycle (Cdc-48) complex [122]. The CDC-48 complex utilizes its ATPase activity to segregate ubiquitinated ERAD substrates and/or extract substrates from the ER into the cytosol for degradation by the proteasome [122, 255].

We constructed three different types of transgenic strains expressing luminal ERAD substrates where disposition has been well studied; α1-AT mutant Null Hong Kong, α1-AT mutant Saar, and cathepsin L mutant (PPM2). All three strains showed an increase in protein accumulation upon RNAi knockdown of the ERAD components; *hrd-1, sel-1, cup-2, and cdc-48*. Based on these data, all three transgenes encoded luminal ERAD substrate dependent upon ubiquitination by the HRD-1/SEL-1 ubiquitin ligase complex, retrotranslocation into the cytosol via the CUP-2 transmembrane protein, and then targeted to the proteasome via interaction with CDC-48 for destruction.

In direct contrast to the three “prototypical” luminal substrates (NHK, Saar, and PPM2), only a portion of sGFP::ATZ was eliminated by ERAD, and that occured with the utilization of different ERAD components. Most notably, knockdown of the E3 ligase *hrdl-1*, the *C. elegans* ortholog of GP78, showed a modest but significant increase in ATZ accumulation. This result suggested that at least a portion of misfolded sGFP::ATZ was eliminated via the gp78 E3-mediated ERAD pathway instead of the HRD-1 E3 ligase utilized by the other three ERAD substrates, including the α1-AT mutants NHK and Saar. Recent studies utilizing HEK 293 cells co-transfected with gp78 and ATZ resulted in a decrease in ATZ expression [227]. Furthermore, siRNA for gp78 also resulted in an increase in ATZ accumulation. This study suggests that gp78 could ubiquitinate ATZ which could help facilitate the partial degradation of ATZ [227].

In this work, *hrd-1* knockdown resulted in no effect on sGFP::ATZ degradation, suggesting that this E3 ligase was not essential for targeting ATZ with ubiquitin. However, HRD-1 binding partner, SEL-1, was found to have a significant effect on the accumulation of ATZ. Most commonly, SEL-1 has been associated with HRD-1 complex for degradation of glycoproteins through ERAD [256-258]. SEL-1 is a type-1 transmembrane glycoprotein with the bulk of the protein composed of repetitive copies of the short tetratricopeptide-like repeats, exposed to the ER lumen. Recent studies suggest that SEL-1 has other functions in the ER lumen, including interactions with the transmembrane ERAD components CUP-2 as well as cytoplasmic CDC-48 [256-258]. One interesting study compared Sel1L knockout mice with Hrd1L knockout mice, resulting in similarities and differences between the two mutants [258]. Importantly severe growth defects and morphological brain abnormalities in Sel1L mutants are not

shown in Hrd1L mutants. This data suggests that Sel1L protein may also function in an Hrd1L independent manners [258]. Similarly, the $P_{nhx\text{-}2}$*sGFP::ATZ* transgenic animals showed a significant accumulation of sGFP::ATZ upon *sel-1 (RNAi)*, while *hrd-1 (RNAi)* showed no significant change in ATZ disposition. These data suggested that SEL-1 is interacting with ATZ in an HRD-1 independent fashion and most likely by utilizing the gp78 E3 complex.

One of the core components of ERAD is *cdc-48*, which is the cytosolic AAA+ATPase involved in the retranslocation of misfolded proteins from ER to the cytosol [207, 249]. Our results showed a significant decrease in sGFP::ATZ accumulation upon knockdown of *cdc-48 (RNAi).* This result was opposite that observed with other luminal ERAD substrates (NHK, SAAR, and PPM2). Since ATZ is localized to the ER and *cdc-48* to the cytosol, this result suggested that down-regulation of *cdc-48* had an indirect effect on ATZ disposition. Since ERAD inhibition activates the UPR, which in turn can stimulate autophagy, I hypothesized that the decrease in sGFP::ATZ in animals exposed to *cdc-48 (RNAi)* was due to increased autophagy. However, *cdc-48(RNAi)* of autophagy deficient ATZ transgenic animals ($P_{nhx\text{-}2}$*sGFP::ATZ; unc51(e369))* still resulted in a significant decrease in ATZ. This study suggested that knockdown of *cdc-48* decreased the accumulation of ATZ by a non-autophagy, non-proteasomal pathway. Future studies will be aimed at elucidating the mechanism that causes reduction of ATZ accumulation upon knockdown of *cdc-48.* For instance, *cdc-48* has been shown to complex with components outside of the ERAD pathway, including a phosphatase in the insulin/ insulin-like signaling pathway (IIS) [259].

In *C. elegans,* the IIS pathway is comprised of a phosphorylation cascade that ultimately modulates longevity, stress resistance, and reproductive development [260-263]. Briefly, insulin and IGF-I hormones signal through dimeric (*daf-2*) receptor tyrosine kinases to activate phosphoinositide 3-kinase, which in turn activates the serine/threonine kinases, AKT/PKB and PDK-1. AKT-1 phosphorylates DAF-16, which inhibits DAF-16 from entering the nucleus. Elimination of signaling through the DAF-2 pathway results in the dephosphorylation of DAF-16 and results in translocation into the nucleus. DAF-16 is a FOXO transcription factor that promotes the expression of many genes that mediate the effects of decreased IIS such as stress resistance and increased longevity [260, 264-266]. This cascade is highly regulated by different phosphatases. PP2A is a ubiquitously expressed phosphatase that dephosphorylates AKT-1 resulting in an activation of AKT-1, which in turn phosphorylates DAF-16 preventing its translocation into the nucleus [267]. If PP2A is overexpressed it causes AKT-1 to become less active. As a result, AKT-1 does not efficiently phosphorylate DAF16, resulting in an increase in the nuclear localization of DAF-16. This increase in the transcription factor DAF-16 promotes the expression of many genes including those associated with stress resistance. A recent study indicate that PP2A forms a complex with CDC-48 [259]. Our hypothesis is that if *cdc-48(RNAi)* is knocked down it causes a decrease in PP2A activity, resulting in deactivation of AKT1 consequentially DAF-16 enters the nucleus. Thus, this result would phenocopy the effects of decrease IIS and reduced IIS decreases the accumulation of other aggregation prone proteins [87]. Similarly, $P_{nhx\text{-}2}$*sGFP::ATZ*; *daf-2(e1370)* animals showed a decrease in sGFP::ATZ

accumulation (data not shown), suggesting that reduced IIS is having an effect in these animals as well.

I had next investigated the effect of proteasome inhibition through the use of the proteasomal RNAi *rpt-5*. Surprisingly, *rpt-5(RNAi)* resulted in a significant decrease in sGFP::ATZ accumulation (Figure 3.9 A). Since the control strain, P_{nhx2}*Ub::R::mCherry*, showed an increase in accumulation, the *rpt-5*(RNAi) appeared to be effective inhibiting proteasome function (Figure 3.9 B). These results suggest that the inhibition of proteasomal function may be having a complex effect on ATZ accumulation. Since *cdc-48* delivers ubiquinated substrates to the proteasome, inhibition of the proteasome could have a similar effect as *cdc-48* and paradoxically activate another elimination pathway. Alternately the 48 hour RNAi treatment may have been sufficient to decrease overall global protein synthesis, a known effect of proteasomal inhibition [122, 243]. Currently, we are developing a time-course experiment utilizing a fluorescent plate reader to allow for the monitoring of sGFP::ATZ accumulation in real-time.

Unlike the mouse model, transgenic animals expressing P_{nhx-2}*sGFP::ATZ* appear to activate the UPR response. Transgenic P_{nhx-2}*sGFP::ATZ;*P_{hsp-4}*::mCherry* showed a marked increase in *hsp-4* activation relative to P_{nhx-2}*sGFP::ATM;*P_{hsp-4}*::mCherry* suggesting that sGFP::ATZ expression in *C. elegans* constitutively activated the UPR. Interestingly, IRE-1 inactivation appeared to decrease ATZ accumulation that was not due to a decrease in *xbp-1* activation and up-regulation of the *Abu* genes. Recent studies show that *ire-1* activation has a function independent of its nuclease activity. This independent function, termed RIDD, results in the rapid turnover of mRNAs separate of *xbp-1* activity [284]. RIDD studies indicate that both *ire-1* activation and ER

stress are required for activation of this pathway [285]. Since, expression of ATZ in *C. elegans* induced *hsp-4* activation (i.e., *ire-1* activation), and knockdown of *ire-1* would further increase ER stress, it is conceivable that *ire-1* activity activated the RIDD pathway, which preferentially degrades ATZ mRNA. Results from the other ERAD luminal substrates (NHK and PPM2), showed that UPR was activated upon RNAi inhibition of *ire-1.* These data together suggest that ATZ accumulation is not processed in the canonical pathway as other ERAD luminal substrates.

Utilizing the *C. elegans* ATZ model, the goal of this research was to elucidate genetic modifies of ATZ accumulation and degradation using an RNAi based approach. I have identified several genes that when eliminated modified ATZ accumulation, suggesting that they play a role in the metabolism of ATZ (findings summarized in Table 3.2). Our data suggest a significant degree in conservation of the pathways associated with the disposal of aggregation prone proteins, as *C elegans,* yeast, and higher vertebrates use components of ERAD and autophagy pathways to help restore proteostasis. Moreover, the studies in *C. elegans* reveal the presence of an undefined pathway, animals treated with *cdc-48*(RNAi) showed a marked decrease in ATZ accumulation that did not involve autophagy or UPS (Figure 3.14).

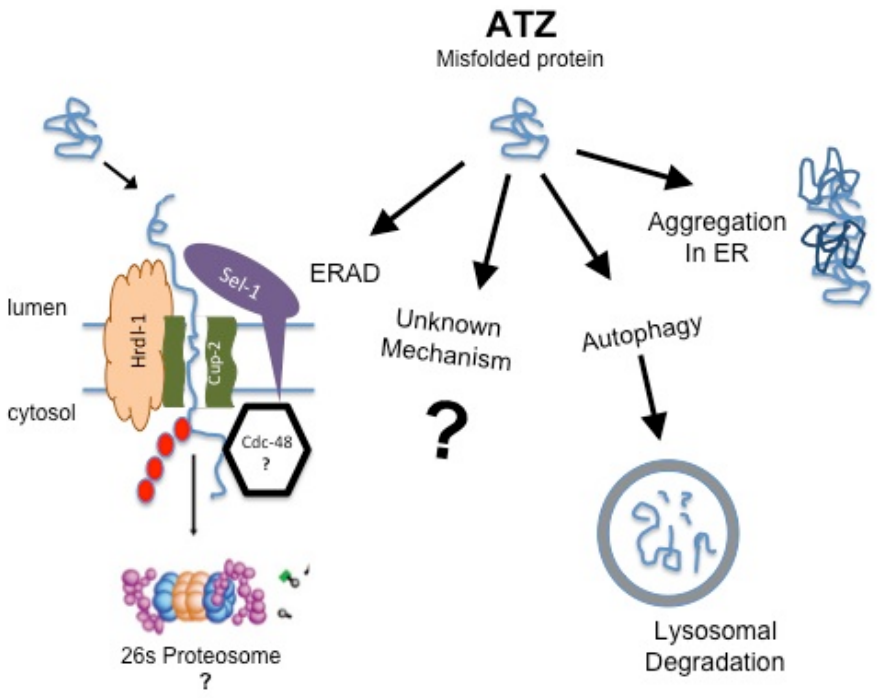

Figure 3.14 Fate of ATZ in Transgenic *C. elegans*

Generalized model showing the possible fate of misfolded ATZ (blue). The misfolded protein can be degraded via ERAD; utilizing the E3 ligase HRDL-1, ER membrane protein SEL-1, and retrotranslocated to the cytosol via the transmembrane protein CUP-2. After this point ATZ is probably polyubiquitinated (red circles= ubiquitin) and possibly interacts with CDC-48 to be targeted for destruction by the 26S proteasome. The misfolded ATZ is also degraded via a novel mechanism, the autophagy pathway and a portion is probably retained as accumulations in the ER.

Table 3.2. Summary of Effects Resulting from Knockdown of Genes (RNAi)

Gene	Description	Worm Line								
		AT-NHK	*AT-SAAR*	*PPM2*	*Ub::R*	*Ub::M*	*Hsp-4::GFP*	*Nhx-2::GFP*	*ATZ*	*ATZ;unc-51*
ERAD										
Cdc-48	VCP/p97; AAA+ATPase, retrotranslocation of misfolded proteins	+++↑	+++↑	+++↑	++↑	—	+++↑	—	++↓	+ ↓
Cup-2	Derlin-1; ER transmembrane protein, forms a receptor	—	—	—	+↑	—	++↑	++↓	++↑	—
Npl-4	Nuclear protein localization, binding partner of cdc-48	—	—	—	+↑	—	++↑	—	+↑	—
Ufd-1	Ubiquitin fusions degradation, binding partner of cdc-48	—	—	—	+↑	—	++↑	++↑	+↑	—
Sel-1	Hrd-3; E3 ligase adapter protein	+++↑	+++↑	+++↑	—	—	+++↑	—	+++↑	+++↑
Hrd-1	E3 ligase	+++↑	+++↑	+++↑	—	—	+++↑	—	—	—
Hrdl-1	GP78; E3 ligase	—	—	—	—	—	+↑	—	++↑	—
Marc-6	Doa10; E3 ligase	—	—	—	+↑	—	+↑	++↑	—	—
Autophagy										
Bec-1	ATG6; PI3 kinase complex	—	—	—			++↑	—	+++↑	
Let-512	Vps-34; Class III PI3 kinase	—	—	—			+↑	—	+++↑	
Lgg-1	ATG8; microtubule associated anchor protein	—	—	—			—	—	+ ↑	
Unc-51	ATG1; ser/thr protein kinase	—	—	—			+++↑	—	+++↑	
Proteasome										
Rpt-5	AAA+ATPase 19S regulatory particle proteasome base	↓	↓	++↓	+↑	—		—	+++↓	
UPR										
Ire-1	Ire-1 kinase related, transmembrane thr/ser kinase and endonuclulcease of Xbp-1	—	—	+↑			—	—	+++↓	
Atf-6	ATF6a, transcription factor that induces BiP associated anchor protein	—	—	—			+++↑	—	—	
Pek-1	Elongation initiation factor kinase	—	—	—			—	—	+++↑	
Xbp-1	bZip transcription factor; increases ERAD	—	—	—			++↓	—	—	

+++ = Strong change in fluorescence ++ = Moderate change in fluorescence + = Weak change in fluorescence
– = No change in fluorescence ↑= Increase in fluorescence ↓= Decrease in fluorescence

4.0 DETERMINING GENETIC MODIFIERS INVOLVED IN THE DISPOSITION OF ATZ THROUGH THE USE OF AN UNBIASED GENOME-WIDE RNAi SCREEN

4.1 RNAi IN *C. elegans*

RNAi-mediated gene silencing was discovered in *C. elegans* and is now used commonly to identify specific gene function. Over a decade ago, Fire and Mello discovered that microinjecting *C. elegans* with double stranded RNA (dsRNA) caused a specific gene silencing effect that spread systemically throughout the organism [218]. Furthermore, soaking worms in dsRNA solution and feeding worms with *E. coli* expressing dsRNA had the same effect [220, 268].

RNAi is initiated by the RNase III-like enzyme Dicer, which cleaves long double-stranded RNA molecules into short (~20 nucleotides) double stranded fragments, siRNAs [269-272]. Each siRNA is incorporated into an endoribonuclease-containing, RNA-induced silencing complex (RISC), and are unwound into two single-stranded RNAs (ssRNAs). The passenger strand is degraded, while the guide strand base pairs with a complementary sequence of messenger RNA (mRNA). Within the RISC complex, an argonaute protein degrades the mRNA [273]. Thus, RNAi is a form of post-transcriptional gene silencing (Figure 4.1).

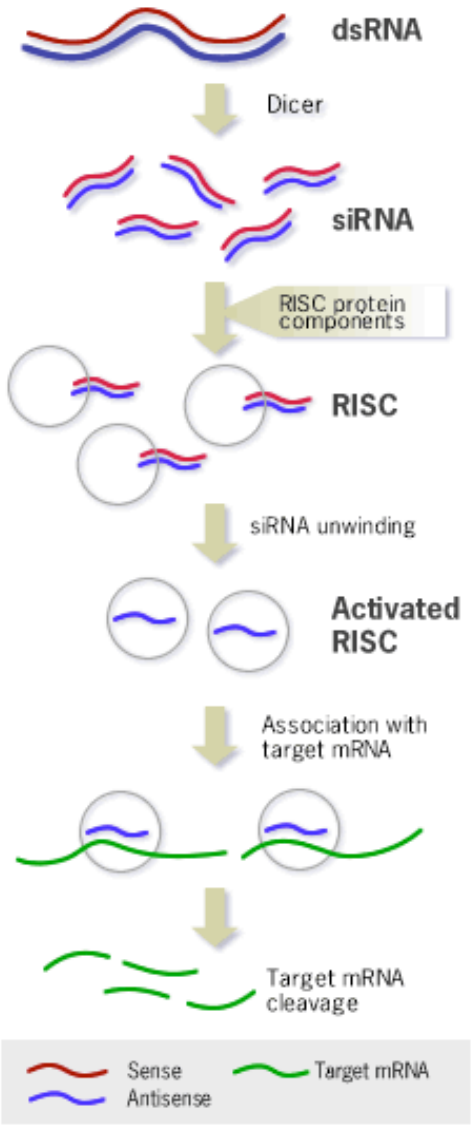

Figure 4.1: RNAi Process

RNAi processing in *C. elegans*. First, the dsRNAs is processed into siRNAs by the enzyme Dicer. Next the siRNAs assemble into RNA-induced silencing complexes (RISCs). The ssRNA strands subsequently guide the RISCs to complementary RNA molecules, where they cleave and destroy the mRNA. Adapted from Ambion's online appendix accessed: http://www.ambion.com/ techlib/append/RNAi_mechanism.html

4.1 PAST RNAi SCREENS

Different RNAi screening strategies have been used to interrogate the *C. elegans* genome; including at least 15 different genome-wide RNAi screens utilizing the RNAi feeding technique [274-280]. In addition, candidate-based approaches using a small (40-2000) subset of genes for analysis, have been instrumental in identifying a genes involved in aging, cell death, development, and other different cellular processes [217, 281-283].

The first genome-wide RNAi screen assayed for overt changes in *C. elegans* post-embronic growth, development, morphology and movement after feeding ~17,000 bacterial clones [217]. RNAi suppression of ~10% of the genes produced a detectable phenotype. In addition, this screen revealed functions for ~1200 genes that were previously unknown [217]. Other genome-wide RNAi screens in *C. elegans* identified genes important for embryonic development [217, 281], and aging [282, 283].

In addition to the identification of gene function through phenotypic analysis, genome-wide RNAi screens have been conducted utilizing markers for identification of specific phenotypes. For example, a genome-wide RNAi screen was used to identify genes regulating body fat storage [277]. Candidate genes were knocked down via RNAi and changes in fat storage were assessed by monitoring levels of Nile red staining, which visualizes fat storage droplets [277]. RNAi knockdown of 112 genes increased fat storage, while 305 genes reduced fat storage. Several of the new fat regulatory genes are conserved in humans [277]. These results identified inactivation of insulin, serotonin, and tubby signaling all of which increased body fat content. The results of this screen

helped to increase understanding about fat storage and obesity in addition to illustrating the importance of genome-wide RNAi screens in *C. elegans*.

Fluorescent protein expressing transgenic animals are another tool utilized in genome-wide RNAi screens. An example of this type of assay is illustrated in an RNAi screen for modifiers of poly-agglutination aggregation [173]. In this model, animals expressing polyglutamine stretches fused to the yellow-fluorescent protein (YFP) served as a model for the protein aggregation disorder, Huntington's disease. The misfolded protein accumulated in the muscle cells as illustrated by YFP expression. The screen identified 186 potential genes that modulate poly-Q accumulations [173]. The identified genes corresponded to five functional classes of polyglutamine regulators; translation, RNA metabolism, proteins synthesis, protein folding, and protein degradation [173].

4.2 CONSIDERATIONS FOR RNAi SCREENING

Although RNAi screens have become a powerful tool for unraveling molecular pathways in *C. elegans*, they are still labor intensive and technically challenging, especially if the changes in phenotype are subtle. Therefore, the initial goal of this study was to develop an automated high throughput genome-wide RNAi screening technology that would address current challenges in genome-wide RNAi screens. In the following section I will be addressing those current issues.

The three major technical challenges associated with past genome-wide RNAi screens are: 1) labor and time intensive 2) variability in screening results due to a narrow dynamic range (e.g. signal to background) and 3) operator bias and fatigue when manually selecting phenotypic outputs. As illustrated in Figure 4.2, the screening strategy developed in this chapter addresses these challenges by automating many of the labor-intensive components associated with past genome-wide RNAi screens.

Adapting RNAi screens to an all liquid workflow would greatly facilitate automation of the screening process. This was achieved by adapting current liquid culturing methods in combination with the COPAS^{TM} BIOSORT worm sorter and ArrayScan V^{TI} imaging platform to allow us to achieve a fast high throughput, non-subjective screen. The COPAS^{TM} BIOSORT worm sorter, which is a large particle (animal) flow cell, is used to automatically select animal of a designated size and/or fluorescence and dispense them into the wells of a 96-well microtiter plate. By using a combination of COPAS^{TM} BIOSORT and a integrated transgenic line the variability of expression associated with transgenic populations is minimized.

A third consideration is whether robust statistical methods can be used to calculate a dynamic range and confidently identify RNAi clones resulting in the desired effect. Many RNAi screens utilize a labor-intensive manual scoring system to identify phenotypic changes during the first round of screening. Manual scoring methods are susceptible to operator fatigue and subjective assessment, leading to a high number of false positives and/or a large number of unidentified hits. Utilizing the automated fluorescence microscope ArrayScan V^{TI} allows us to automate data acquisition and

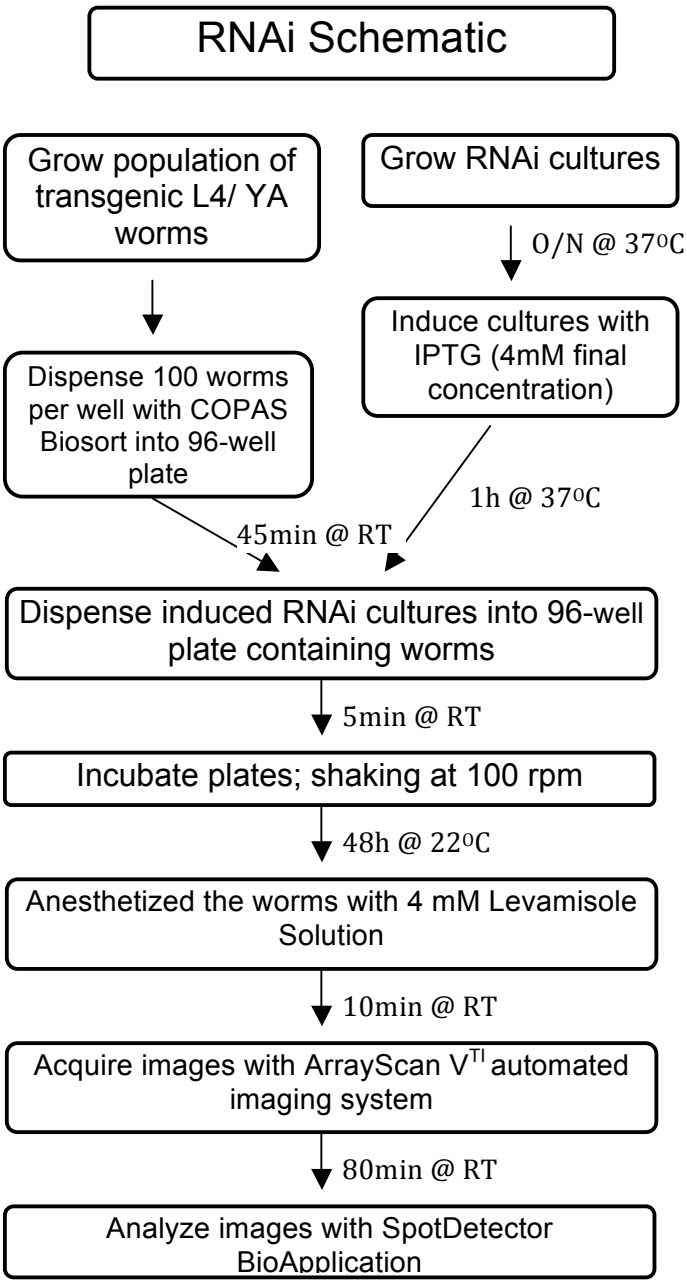

Figure 4.2: RNAi Schematic for High Throughput RNAi Screen

Worm preparation is performed concurrently with the preparation of the RNAi bacteria. The SpotDetector BioApplication analyzes the change in transgene expression (GFP). The data analysis output is stored indefinitely and can be reanalyzed at any time.

analysis. The instrument, ArrayScan V^{TI}, consists of an inverted light microscope (Axiovert 200M, Carl Zeiss) configured with a motorized objective turret with Plan-Neofluar objectives, a motorized 5-position filter cube turret, a mechanized stage, a 12-bit cooled CCD camera and controller software. Samples are illuminated for fluorescence imaging in up to 4 different spectra using a mercury-based light source. Different types of analysis modules (Thermo Scientific BioApplications) automatically convert 16-bit monochromatic images into numeric data [284]. Utilizing the ArrayScan V^{TI} in conjunction with a fluorescent reporter protein allows for the real time imagining and analysis of changes in fluorescence (protein accumulations) in the animals.

A further consideration is the reproducibility of an RNAi screen. Currently, there is poor reproducibility when comparing results between laboratories conducting genome-wide RNAi screens on similar phenotypes. Variations in screening methods are likely to account for these discrepancies. Therefore, the initial goal of this study was to develop an automated high throughput genome-wide RNAi screening technology that would reduce labor while improving overall sensitivity, specificity, and reproducibility. Successful development of this strategy was then utilized to complete a genome-wide RNAi screen for genetic modifiers of sGFP::ATZ protein accumulation in the worm.

4.3 MATERIALS AND METHODS

4.3.1 Worm Strains and Culture Conditions

Strain VK694 *(P$_{nhx-2}$sGFP::ATZ)* was generated by co-injecting YA with the plasmids P$_{nhx-2}$*sGFP::ATZ* and P$_{myo-2}$*::mRFP* at a final concentration of 70 ng/ul and 10 ng/ul, respectively. The extra-chromosomal array was integrated by gamma irradiation as described [177]. Animals were maintained at 22 ^{o}C on nematode growth medium (NGM) plates seeded with *Escherichia coli* OP50 (NGM/OP50) [214].

4.3.2 Preparation of Animals for RNAi Screening

Twelve to fifteen adult sGFP::ATZ transgenic animals were placed on five 10 cm NGM/OP50 plates. Approximately 7 days later, early-staged larval animals were isolated by differential sedimentation and then transferred to ten 50 cm NGM/OP50 plates. The larvae were incubated at 22 ^{o}C until the majority of the animals were in the L4 larval stage, approximately 48 hours later.

4.3.3 Animal Sorting Using the COPAS^{TM} BIOSORT

As previously described, the COPAS^{TM} BIOSORT (Union Biometric, Holliston, MA) allowed for the reduction in assay variability, which resulted in a tightly control population based upon size, and fluorescence intensity [215]. Animals were cultivated as described above and sorted using the COPAS^{TM} BIOSORT as previously described

[215] with the following modifications: PBS was used to wash the animals for sorting and as sheath fluid for sorting using the COPAS^{TM} BIOSORT. One hundred L4/young-adult animals were sorted into each well of a 96-well optical bottom plate (Figure 4.2). Approximately 50,000 transgenic worms were required for each 96-well plate and the sorting time was ~45 minutes per plate. Upon completion of sorting the induced RNAi cultures were added (vide infra).

4.3.4 RNAi Bacterial Preparation and Induction

RNAi clones were obtained from the Ahringer RNAi feeding Library (Geneservice Limited, Cambridge, UK) [285]. A sterile pinning device was used to replicate each RNAi library plate into a 96-well deep well plate containing 400 μl of Luria Bertani broth (LB), [containing 10 g Tryptone, 5 g yeast extract, 10 g NaCl and 50 μg/ml ampicillin per liter] [216] .

4.3.5 RNAi Assay Procedure

To each well of a 96-well plate seeded with animals 40 μl of the induced RNAi culture was added. Next, 5-fluorodeoxyuridine (FUDR) was added to each well to prevent eggs from developing. The addition of FUDR allowed only the original worm population to be scored. Plates were incubated in a 22 ^{o}C shaking incubator for 48 hours. To prevent evaporation, plates were placed into moist sealed plastic containers. Plates were imaged after 48-hours utilizing the ArrayScan V^{TI}.

4.3.6 Image Acquisition

Worms were anesthetized with a 4 mM Levamisole solution prior to image capture. Images were acquired with the ArrayScan V^{TI} HCS Reader (Cellomics, Thermofisher, Pittsburgh, PA, USA) fitted with a 5x objective and a 0.63x coupler. The images were captured utilizing a 2-channel (TRITC and GFP) assay previously described [215]. The data were normalized by dividing the total GFP area by the number of animals per well.

4.3.7 Analysis of Hits

A *z*-score was determined for each RNAi using each 96-well plate as its own intrinsic control. Since RNAi has been shown to have intrinsic variability, RNAi that has a *z*-score above or below 2.35 must be retested to eliminate false positives [287]. A *z*-score was calculated by subtracting the population mean from an individual raw sore and then dividing the difference by the population standard deviation as illustrated in the following equation: $z = (x - \mu) / \sigma$ where x= raw score, μ = mean of the population and σ = the standard deviation of the population.

4.3.8 Hit Verification

Utilizing the methods described in sections 4.3.2 – 4.3.7, RNAi clones yielding absolute *z*-score ≥ 2.35 were verified by repeating the assay in triplicate (n=300 animals. These values are then compared to the transgenic strain fed on control RNAi (L4440 feeding vector) for statistical significance through a Students two-tailed *t*-test.

4.4 RNAi SCREEN PARAMETERS

4.4.1 Controls for RNAi Screen

To identify genes that alter the accumulation of sGFP::ATZ, I used a *C. elegans* strain expressing the transgene, $P_{nhx\text{-}2}$*sGFP::ATZ* (detailed explanation in Chapter 2). The use of a sGFP::ATZ fusion protein enables the assessment of misfolded protein accumulation. We utilized the promoter, *nhx-2,* which drives expression of $P_{nhx\text{-}2}$*sGFP::ATZ* transgene in the intestinal cells, as such sGFP::ATZ accumulates in the intestinal cells of the animal (Figure 2.3). sGFP::ATZ accumulations are seen as early as the L1 stage and continue to be displayed throughout all developmental stages.

To determine if changes in sGFP::ATZ fluorescence could also be identified after RNAi exposure, a time course experiment using *GFP(RNAi)* was conducted to determine the rate and extent of sGFP::ATZ elimination. *E. coli* strains expressing double-stranded RNA for GFP, was fed to L4/YA sGFP::ATZ animals. The animals were imaged utilizing the ArrayScan V^{TI}. Based on these studies, sGFP::ATZ had a half-life of ~24 hours and was undetectable within 48 hours of exposure to RNAi (Figure 4.3). These studies suggested that the accumulated sGFP::ATZ can be reversed by RNAi and that it occurs within a time frame that animals can survive in the liquid culture.

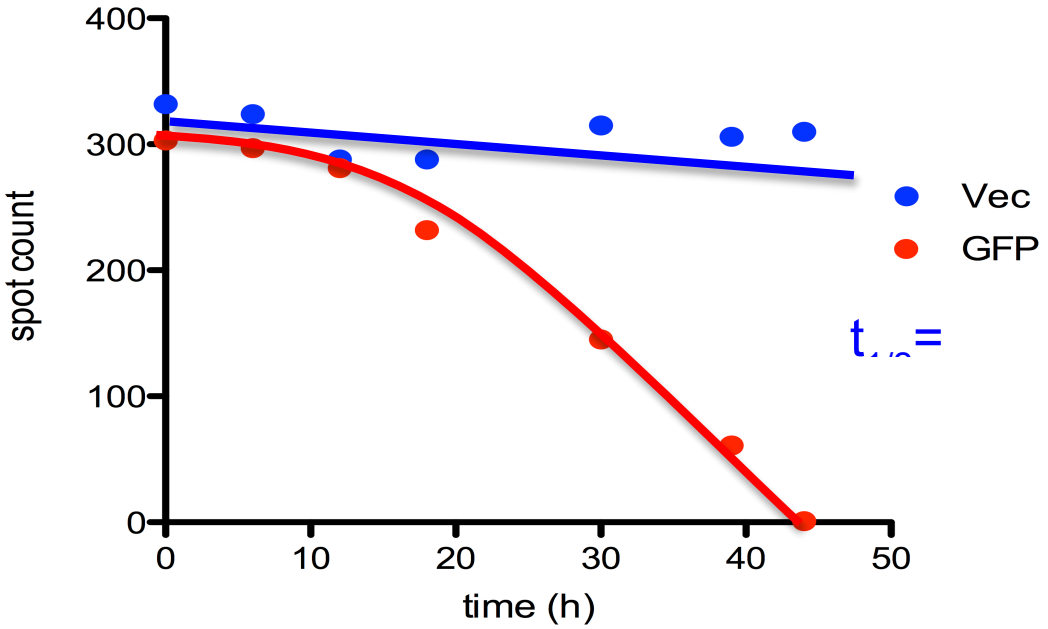

Figure 4.3: GFP Half-life

P*nhx-2*sGFP::ATZ animals were exposed to GFP RNAi for various lengths of time (X axis). At each time point worms were imaged for total amount of GFP spots (Y axis). Results show that almost all GFP accumulations are eliminated by 48 hours. Image adapted from work performed by Gosai, Kwak, Long, and Pak.

4.5 QUALITY OF HIGH CONTENT ASSAY

It was essential to verify that the screening method yielded reproducible results before proceeding with an entire genome-wide RNAi screen. To test the assay conditions, I harvested a large transgenic population of sGFP::ATZ animals. One hundred L4/YA animals, with similar GFP expression levels, were sorted using the COPAS^{TM} BIOSORT into each well of a 96-well optical bottom plate. The transgenic worms were fed with either an empty vector (L4440) or *GFP(RNAi)* and incubated for 48-hours. Animals were anesthetized and imaged employing the ArrayScan V^{TI}. The SpotDetector Bioapplication program was utilized, the mRFP channel to count the number of animals by identifying the number of mRFP positive heads (Figure 4.4 A). This assay counted the number of red-heads in each well, this confirmed that the COPAS^{TM} BIOSORT was accurately placing the correct number of animals into each well and were almost identical in all wells (Figure 4.4 B). Using the GFP channel the SpotDetector program also indentified the number, size and total fluorescence of the GFP positive accumulations within the intestinal cells of the worms (Figure 4.4 A). For our analysis I used total GFP spot area but analysis of the other parameters yielded similar trends (data not shown). The total GFP spot area was then divided by the number of animals to determine an average florescence per animal for each well (Figure 4.4 B). The SpotDetetor Bioapplication program showed a wide dynamic range between *GFP(RNAi)* and vector (RNAi) controls (Figure 4.4 A,B,C).

Figure 4.4: Validation of RNAi Screening Methods

Data analysis of transgenic animals post 48 hour exposure to L4440 (vec) or GFP RNAi. 100 worms were sorted into wells of a 96-well plate and imaged using the ArrayScan V^{TI}. A. Representative fluorescent images of one field of mRFP (red) heads and GFP intestinal accumulations. B. Comparison of total head count, total GFP spot area, total GFP spot count, and total GFP spot intensity (n=36 wells or 3,600 worms) C. Scatter plot comparing total GFP spot area per well between controls.

A.

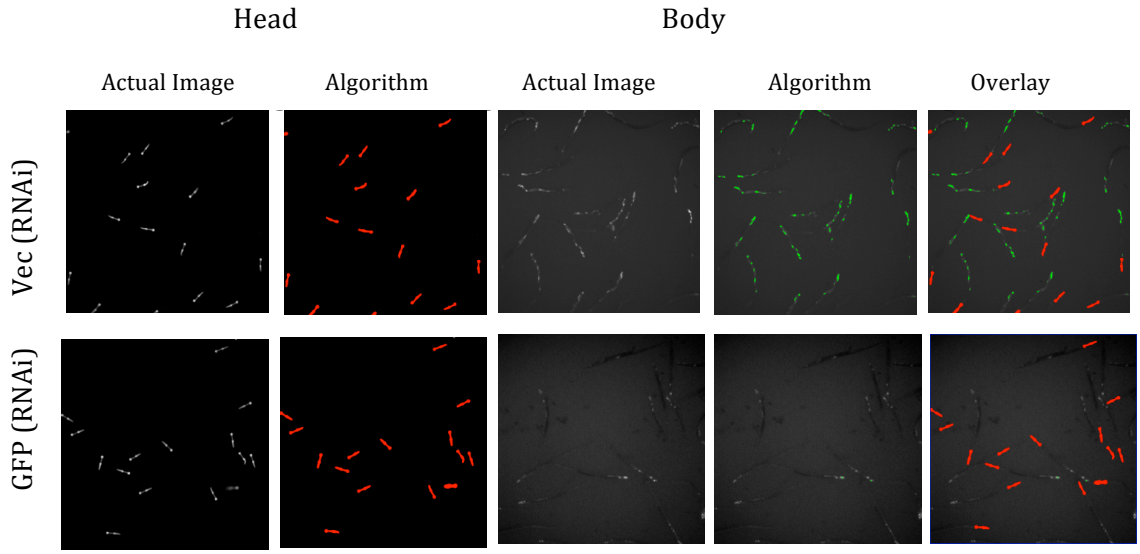
Head
Body
Actual Image
Algorithm
Actual Image
Algorithm
Overlay
Vec (RNAi)
GFP (RNAi)

B.

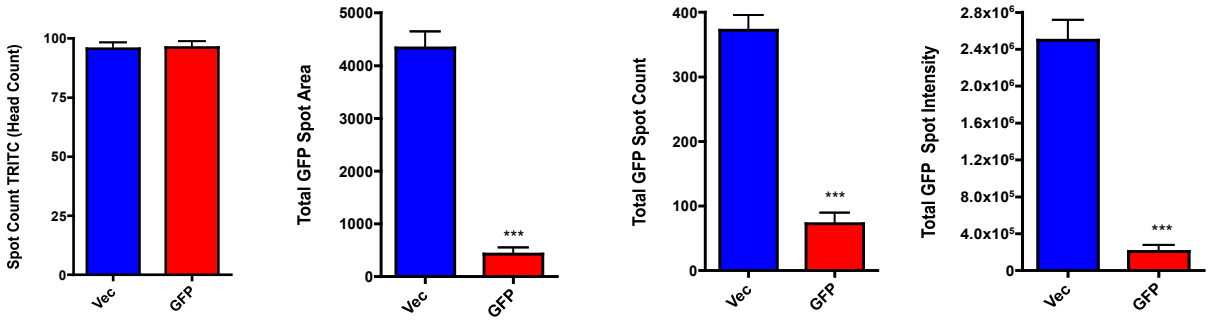
Spot Count TRITC (Head Count)
Total GFP Spot Area
Total GFP Spot Count
Total GFP Spot Intensity
Vec
GFP
***

C.

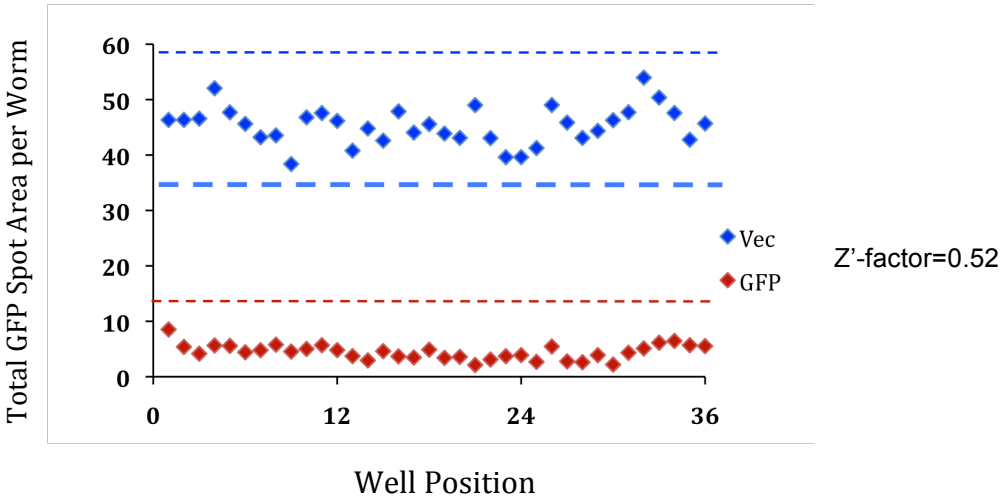
Total GFP Spot Area per Worm
Well Position
Vec
GFP
Z'-factor=0.52

This data was used to calculate the Z'-factor, a commonly used metric to assess overall assay quality [286]. Values between 0.5 and 1 are considered excellent and indicate a quality assay format. The Z'-factor for this experiment was 0.52. These findings suggest that *GFP(RNAi)* and vector(RNAi) could be used to define a robust assay with a wide dynamic range.

4.6 GENOME-WIDE RNAi SCREEN

After establishing a robust assay for HCS using the sGFP::ATZ animals, I preformed a genome-wide RNAi screen. The Arhinger feeding library contains *E. coli* strains expressing double-stranded RNAs for 16,757 genes, which covers approximately 86% of the *C. elegans* genome [276]. The RNAi library is arrayed by chromosome number and consists of 203 96-well plates. Transgenic sGFP::ATZ animals were sorted into a 96-well microtiter plate, utilizing the COPAS^{TM} BIOSORT to select a tightly gated population of animals (Figure 4.5 A). After a 48 hour RNAi exposure the worms were immobilized and imaged utilizing the ArrayScan V^{TI}. The ArrayScan V^{TI} equipped with a 5x objective and 0.63x coupler acquires 9 fields to cover the entire well of a 96-well plate (Figure 4.5 B). Imaging takes ~60 to 80 minutes per 96-well plate, therefore limiting the number of plates that can be imaged in one day. In theory, an entire genome-wide RNAi screen can be performed by one person in ~20 days. Utilizing these established conditions all ~17,000 RNAi's were examined.

Figure 4.5: Genome-Wide RNAi Library Screen

A. Sorting parameters B. Visualization of 9 fields imaged by the ArrayScan VTI C. Representative of z-score analysis from one 96-well plate from genome-wide screen. Z-score is used to compare effect of RNAi on transgene expression of GFP; X-axis represents well position and Y–axis represents z-score value. D. Distribution of Chromosome I z-scores (Chromosome I is comprised of 2,445 clones dispersed over 29, 96-well plates)

A.

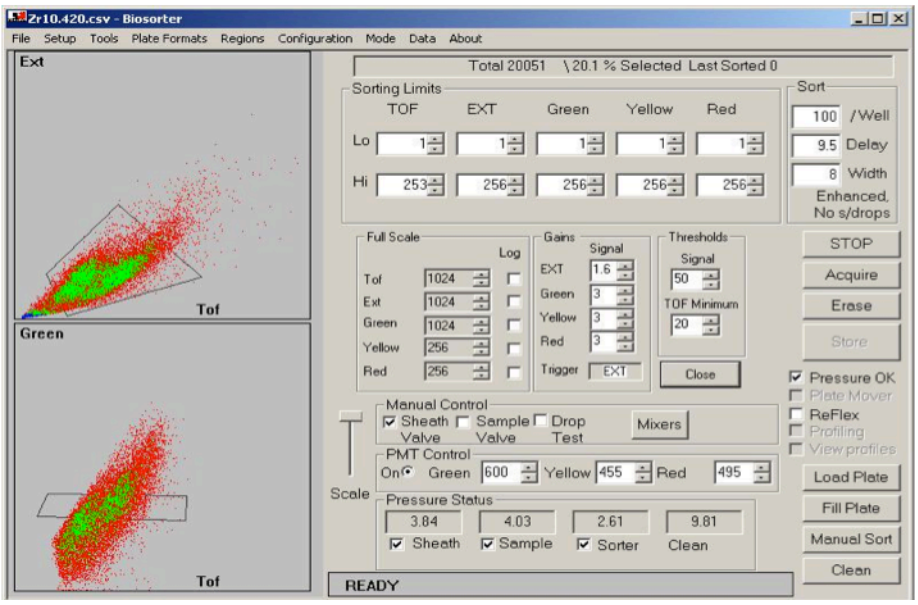
Zr10.420.csv - Biosorter
File Setup Tools Plate Formats Regions Configuration Mode Data About
Ext
Tof
Green
Tof
Total 20051 \ 20.1 % Selected Last Sorted 0
Sorting Limits
TOF EXT Green Yellow Red
Lo 1 1 1 1 1
Hi 253 256 256 256 256
Sort
100 /Well
9.5 Delay
8 Width
Enhanced, No s/drops
Full Scale
Log
Tof 1024
Ext 1024
Green 1024
Yellow 256
Red 256
Gains
Signal
EXT 1.6
Green 3
Yellow 3
Red 3
Trigger EXT
Thresholds
Signal 50
TOF Minimum 20
Close
STOP
Acquire
Erase
Store
Pressure OK
Plate Mover
ReFlex
Profiling
View profiles
Load Plate
Fill Plate
Manual Sort
Clean
Manual Control
Sheath Valve
Sample Valve
Drop Test
Mixers
Scale
PMT Control
On
Green 600
Yellow 455
Red 495
Pressure Status
3.84 4.03 2.61 9.81
Sheath Sample Sorter Clean
READY

B.

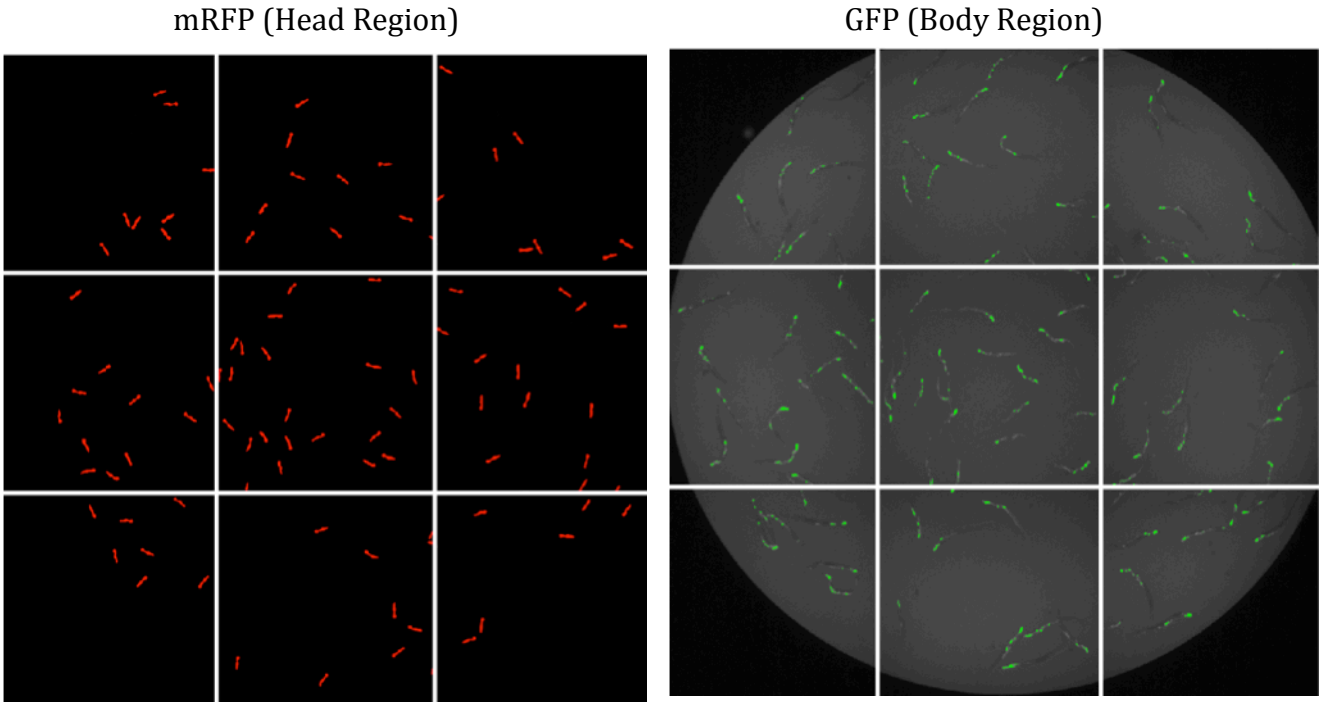
mRFP (Head Region)
GFP (Body Region)

C.

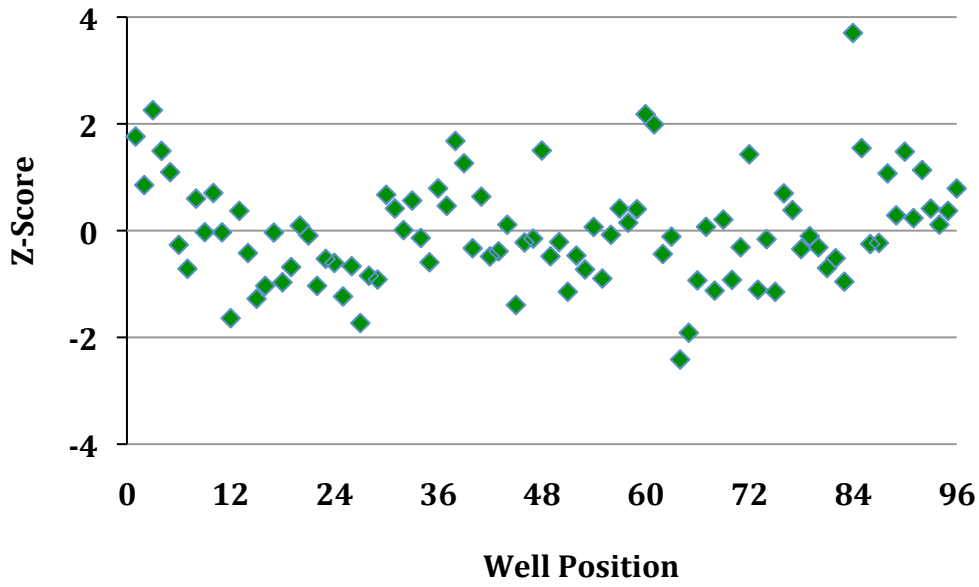
4
2
0
-2
-4
Z-Score
0
12
24
36
48
60
72
84
96
Well Position

D.

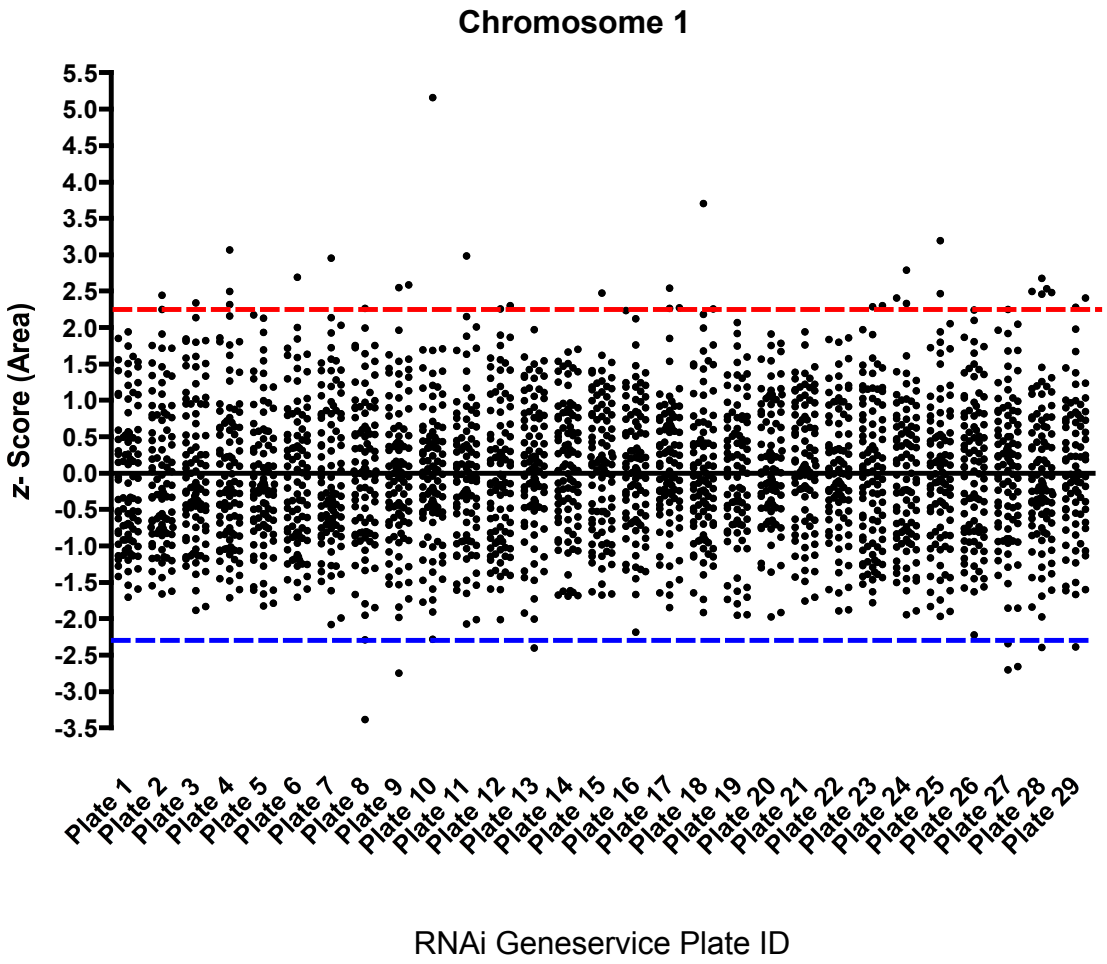
Chromosome 1
5.5
5.0
4.5
4.0
3.5
3.0
2.5
2.0
1.5
1.0
0.5
0.0
-0.5
-1.0
-1.5
-2.0
-2.5
-3.0
-3.5
z- Score (Area)
Plate 1
Plate 2
Plate 3
Plate 4
Plate 5
Plate 6
Plate 7
Plate 8
Plate 9
Plate 10
Plate 11
Plate 12
Plate 13
Plate 14
Plate 15
Plate 16
Plate 17
Plate 18
Plate 19
Plate 20
Plate 21
Plate 22
Plate 23
Plate 24
Plate 25
Plate 26
Plate 27
Plate 28
Plate 29
RNAi Geneservice Plate ID

Upon completion of imaging, a *z*-score value for each RNAi clone was calculated. A *z*-score indicates how many standard deviations an observation is above or below the mean. In this analysis, I considered any RNAi clone that had an absolute *z*-score > 2.35 as a potential hit (Figure 4.5 C,D) [287]. A second round of screening verified this list of potential gene candidates.

The secondary screening of all potential candidates was completed in liquid culture using similar methods and conditions used in the original screen, except that: 1) RNAi cultures were tested in triplicate (n=300), 2) the RNAi controls vector(RNAi) and *GFP(RNAi)* were included on each individual plate, and 3) each experiment was completed in duplicate on separate days. A two-tailed *t*-test was then used to determine if there was a significant difference in the amount of sGFP::ATZ accumulations in RNAi treated animals as compared to that of the vector(RNAi) controls between the GFP positive accumulations in sGFP::ATZ animals exposed to empty feeding vector and a potential positive RNAi (Figure 4.6 A & B).

4.7 GENOME WIDE RNAi SCREENING RESULTS

From the initial screen I identified 245 clones for the secondary screen of which 108 RNAi clones recapitulated the initial sGFP::ATZ accumulation phenotype. Of the 108 positive cloned, 104 genes that enhanced the sGFP::ATZ accumulation and the remaining 4 decreased sGFP::ATZ accumulations (Table 4.1). Based on Wormbase annotations for the genes I manually classified the list of genetic modifiers of

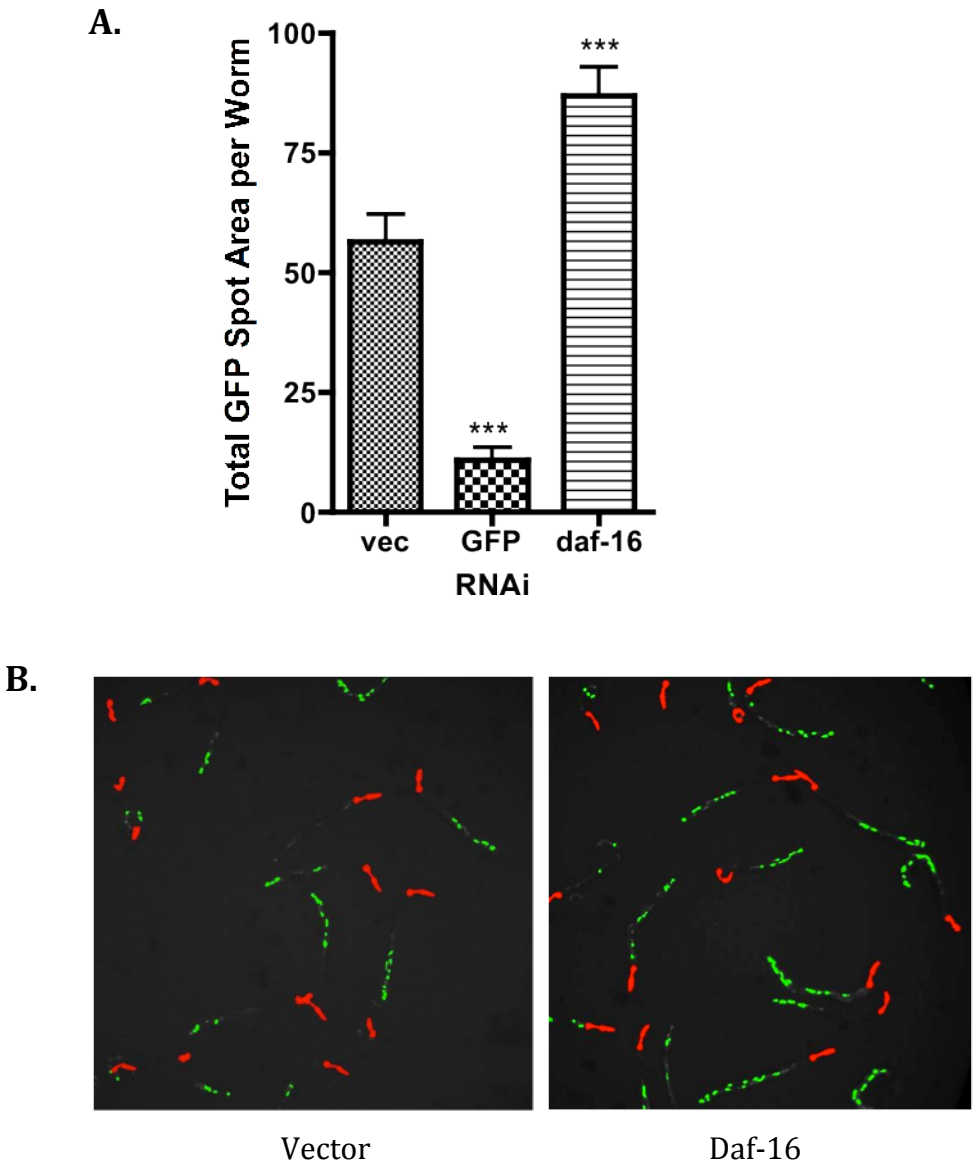

Figure 4.6: Validation of RNAi Screen Hit *Daf-16*.

A. Comparison of total GFP spot area and B. Fluorescent images from sGFP::ATZ animals fed vector or *daf-16* RNAi (mRFP= head region, GFP= ATZ Intestinal inclusions)

Table 4.1 Modifiers of sGFP::ATZ Accumulations

Sequence name	Gene name	Description	*z*-Score	Ortholog and/or Homolog	Other Screen Hit
RNA Synthesis and Processing					
F48F7.1	alg-1	Argonaute like gene 1; protein involved in the production of small temporal RNA	3.06	H,M	Nollen
F18H3.3	pab-2	Poly(A)-binding protein 2	2.89	H, Y	
Y46G5A.4	phi-10	Protein involved in embryogenesis	2.6	H, Y	Nollen
T07A9.8		Protein involved in positive regulation of growth rate	2.54	H, M, Y	
F42A6.7	hrp-1	single-stranded DNA binding protein that interacts with telomeres	2.52	H, M, Y	
C04A2.2	egl-27	Part of an ATP-dependent complex with nucleosome remodelling and histone deacetylation	2.47	H, M	
K11E4.5	nhr-71	Protein containing a nuclear hormone receptor C4-type zinc finger domain	2.35	-	
Protein Synthesis					
Y39B6A.35		Member of the queuine tRNA-ribosyltransferase family	3.85	H, M	
C14B9.7	rpl-21	Member of the ribosomal protein L21e family	2.9	H, M, Y	Nollen
F42C5.8	rps-8	Ribosomal protein small subunit 8	2.72	H, M, Y	
K02A4.1	bcat-1	reversibly transaminates branched-chain L-amino acids to control their metabolism and acts in apoptosis	2.61	H, M, Y	
W01B11.3		Protein involved in larval growth; embryogenesis; and the regulation of DNA transposition	2.45	H, M, Y	
T20B12.3		Protein involved in positive growth regulation	2.37	H, M, Y	
Protein Chaperones					
ZC395.10		moderate similarity to a region of butyrate-induced transcript 1	2.94	H,Y	
Y41E3.11		Protein involved in positive growth regulation and lipid storage	2.68	H, M	
Vesicle					
ZK180.4	sar-1	Vesicle coat complex COPII	3.71	H, M, Y	
Y113G7A.3	sec-23	Vesicle coat protein complex II (COPII)-coated vesicle component	3.56	H, M, Y	
Insulin Signaling Pathway					
R13H8.1	daf-16	forkhead family transcription factor	3.7	H, M	
par2.3	aak-1	AMPKalpha homlog 2 which is an AMP-activated protein kinase	3.21	Y	
Y62F5A.b	age-1	Aging alteration 1; protein involved in dauer larva formation	-2.36	H, M, Y	
Cell Stress Response					
C03C10.6		region of moderate similarity to a region of mouse 9030205A07Rik; which is required for drinking behavior	3.63	H, M	
C07B5.5	nuc-1	Nuclease 1; endonuclease that is involved in DNA degradation during apoptosis	3.47	H, M	
ZK1193.5	dve-1	required for the mitochondrial unfolded protein response signaling	3.34	-	
C41C4.4	ire-1	serine/threonine protein kinase and stress-activated endoribonuclease	3.32	H, M, Y	
Y75B7B.2		potential enzymatic component of a DNA damage response pathway	3.11	H, M	
ZK455.7	pgp-3	multidrug resistance protein of the ATP-binding cassette (ABC) superfamily	2.92	Y	
C34E10.1	gop-3	Gro-1 operon 3	2.62	H, M, Y	
B0496.8		Member of the PET domain containing family	2.4	H, M	
F08B1.1	vhp-1	VH1-like phosphatase 1; MAPK phosphatase	-2.38	H, M	
RNAi response					
K12B6.1	sago-1	protein that acts with other argonaute proteins sequentially to direct gene silencing	4.29	-	
Transcription					
K08A2.b	nhr-88	contains a nuclear hormone receptor C4-type zinc finger domain	3.27	H, M	
B0464.7	baf-1	required to stabilize segregated chromatin, required for proper nuclear assembly	3.25	H, M	

F53H1.4		may be involved in chromatin-mediated transcription regulation	3.22	-
Y104h12a.1	nhr-41	likely functions as a transcription factor	3.12	H, M
Y32F6A.3	pap-1	encodes a poly (A) polymerase	3.1	H, M, Y
F54F2.5	ztf-1	Protein containing a zinc finger C2H2 type repeat; which bind nucleic acids	2.82	-
C07H6.7	lin-39	transcription factor involved in cell fate determination	2.48	M, H
F13G11.1		DNA binding domain family	2.35	-
Protein Transport				
T02C12.1	hum-5	unconventional class I myosin heavy chain	3.71	M, H, Y
C43G2.2	bicd-1	Protein involved in locomotion	3.52	M, H
C38C6.2	atg-2	transporter of small neutral amino acids and some larger aromatic amino acids	3.33	M, H, Y
Y119D3_443.c	cdh-12	predicted to function in cellular adhesion	3.31	M, H
R05G6.7		Member of the eukaryotic porin family	3.14	M, H, Y
Protein Signaling				
C30F12.1		Protein involved in lipid storage and FGF receptor signal transduction	5.16	M, H
Y47D3B.2	nlp-21	Protein of unknown function	3.04	-
F49C5.6		Member of the 7-transmembrane chemoreceptor family of G protein-coupled receptors (GPCR)	2.98	-
F13A7.8		Member of the 7-transmembrane chemoreceptor family of G protein-coupled receptors (GPCR)	2.83	-
T10D4.10		Member of the 7-transmembrane chemoreceptor family of G protein-coupled receptors (GPCR)	2.6	-
ZC84.4		similarity to opiate receptor-like 1; which is a G protein-coupled receptor	2.58	-
ZK262.11		Member of the 7-transmembrane chemoreceptor family of G protein-coupled receptors (GPCR)	2.36	-
Ubiquitin				
T07E3.4		serve as a link between a target protein and a ubiquitin-conjugating enzyme	4.79	-
h06104.4	ubl-1	similar to Drosophila ubiquitin/ ribosomal protein S27a	2.94	M, H, Y
Y82E9BL.15		serve as a link between a target protein and a ubiquitin-conjugating enzyme	2.84	-
Catalytic Activity				
T03F6.3		Protein with high similarity to glucosamine-6-phosphate deaminase 2	3.53	M, H
F18H3.3	pab-2	Poly(A)-binding protein 2	2.89	H, Y
F59E12.13	fut-3	Fucosyl transferase 3 protein	2.89	H. M
B0218.5		Protein involved in lipid storage	2.84	-
C49F5.1	sams-1	S-adenosyl methionine synthetase	2.75	H, M, Y
H32C10.1		Predicted phosphatase	2.74	H, M, Y
H06I04.3		Putative SAM-dependent rRNA methyltransferase	2.7	H, M, Y
M79.1	abl-1	putative tyrosine protein kinase	2.67	H, M
T07A9.3	kgb-1	putative protein serine/threonine kinase	2.46	Y
T01C8.5		Aspartate aminotransferase/Glutamic oxaloacetic transaminase	2.44	H, M, Y
B0464.4	bre-3	encodes a protein similar to beta-glycosyltransferases	2.38	-
B0546.2		Member of the ovarian tumor (OTU)-like cysteine protease family	2.38	H, M
Embryogenesis				
Y39A1A.13		Protein involved in morphogenesis and gametogenesis	4.49	-
F39E9.2		functions in germ line mitosis; embryogenesis; and fertility	3.64	-
F14D2.2		Protein involved in embryogenesis	3.49	-
W02H5.b		Protein involved in embryogenesis	3.26	H

T22F3.3		Protein that is required for embryonic development	3.11	H, M, Y	
B0393.6		Protein involved in embryogenesis	2.95	-	
Y110A7A.d	mat-1	Metaphase to anaphase transition 1; component of the anaphase-promoting complex required for embryogenesis	2.69	H, M, Y	
W03H9.4		Protein involved in embryogenesis	2.47	H, M	
R107.6	cls-2	protein involved in embryogenesis and mitotic kinetochore assembly	2.42	H, M	
Miscellaneous Functions					
Y38E10A.d		Protein containing two C-type lectin domains	3.15	H	
C17C3.5		Protein involved in osmoregulation	2.97	-	
F09A5.4		Member of the Mob1 and phocein family	2.79	H, M, Y	
C23H4.1	cab-1	C terminus of AEX-binding protein 1; component of a neuronal transmission pathway	2.69	H, M	
Y39B6a.27		Member of the DUF895 domain of unknown function family	2.59	H, M	
Y37D8A.9	mrg-1	Mortality factor-related gene (MRG) family protein-1	2.56	H	
C50C3.8	bath-42	BTB and MATH domain containing 42; protein that interacts with RIC-3 to regulate maturation of nicotinic acetylcholine receptors	2.53	-	
Y76A2B.3		Protein with high similarity to long-chain fatty acid Coenzyme A ligase 5	2.53	H, M, Y	
C33D9.1	exc-5	Excretory canal abnormal 5; putative RhoGEF domain protein	2.53	H, M	
F21D5.3		Protein containing a multicopper oxidase	2.51	Y	
C16H3.2	lec-9	Protein with high similarity to C. elegans LEC-8; which binds to glycolipid; involved in response to bacterium	2.5	H, M	
C04A11.4	adm-2	Member of the reprolysin (M12B) zinc metalloprotease family	2.45	H, M	
F38A5.1		Protein involved in lipid storage	2.45	H, M, Y	
F10E7.11		Member of the Egl-27 and MTA1 homology 2 (ELM2) domain family	2.41	H, M	
F37C12.7		Protein involved in morphogenesis of an epithelium and locomotory behavior	2.35	H, M, Y	
F08B12.1		Member of the prominin family	-3.03	H, M	
Unknown No Described Functions					
C02D4.1	jud-4	Protein of unknown function	6.09	-	
K08D10.1		Member of the DUF1280 domain of unknown function family	5.08	-	
F28B12.1		Protein of unknown function	4.78	-	
R08C7.12		Protein of unknown function	4.01	-	
R09F10.3		Protein of unknown function	3.97	-	
Y39B6B.q		Member of the queuine tRNA-ribosyltransferase family	3.85	-	
T14G8.4		Protein of unknown function	3.83	-	
W03G1.5		Protein of unknown function	3.79	H, M	
B0464.8		Protein of unknown function	3.69	-	
F31D4.8		Protein of unknown function	3.15	-	
C33A12.3		Protein of unknown function	2.94	H, M	
T19D12.1		Protein of unknown function	2.71	Y	
R08C7.1		Protein of unknown function	2.59	-	
F25D7.2		Protein of unknown function	2.54	H, M	
K11H12.8		Protein of unknown function	2.54	H, M	
Y43F8B.12		Protein of unknown function	2.42	-	
ZK512.1		Protein of unknown function	-2.47	-	
Y82E9BR.13		Protein involved in positive growth regulation	-3.09	-	Choe

sGFP::ATZ accumulations into the following major categories: RNA synthesis and processing (7), cell stress response (9), transcription (8), Protein transport or signaling (12), catalytic activity (12), and unknown functions (18) (Table 1) [288]. Many of these genes identified have orthlogs in humans (62%), mice (55%), and yeast (33%) (Table 1) [288]. These findings suggested that modifiers of *C. elegans* ATZ accumulation could be conserved in humans.

4.7.1 Comparison of RNAi screen candidates with other RNAi screens

The RNAi clones identified in Table 4.1 may target genes that specifically protect against toxic sGFP::ATZ accumulations or possibly genes that protect against general protein accumulations. To examine if the genes identified were specific for ATZ accumulation, I compared our list of 104 genes that increase sGFP::ATZ accumulation with the published results of other protein misfolding RNAi screens including: polyglutamine repeat containing proteins (Huntington's disease) [173], α-synuclein (Parkinson's disease) [289], tau (frontotemporal dementia) [176], and SOD-G85R accumulation (Lou Gehrig's disease) [280]. Additionally, I compared our screen results to those from a genome-wide hypertonic stress sensitivity screen, because this screen has been shown to have significant overlap ($p<1.278e^{-10}$) with identified hits to the polyglutamine aggregation RNAi screen which suggests that the cellular mechanisms for dealing with hypertonic stress and misfolded proteins could be similar in *C. elegans* (Table 4.1 and Figure 4.7) [290].

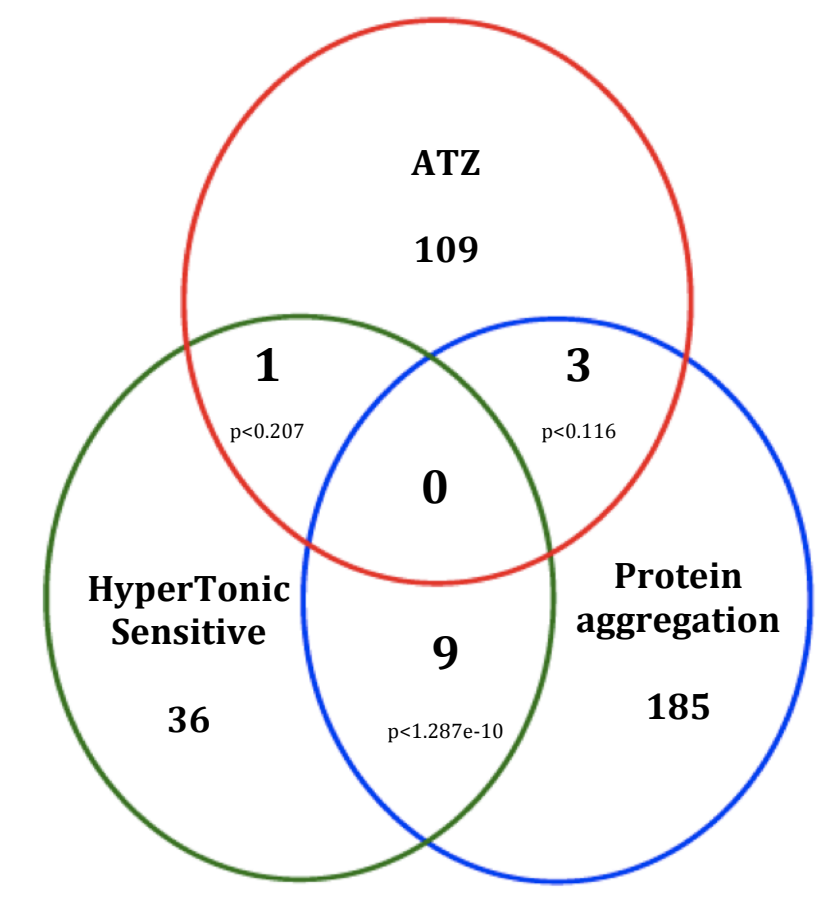

Figure 4.7 Comparison of Genome-wide RNAi screens

Venn Diagrams illustrating the distribution of common genes between the sGFP::ATZ genome wide screen and two other genome-wide screens in *C. elegans.*

To test for significant overlap in modifiers detected in other *C. elegans* models of protein aggregation disorders, I utilized a modified Fisher's exact test [288]. None of the RNAi screens, showed a significant overlap of modifier genes. In fact, there was no overlap between the genes identified in enhancing α-synuclein or tau accumulation, as compared to those that enhanced sGFP::ATZ accumulation [176, 289]. Furthermore, the hypertonic stress screen and the SOD-G85R accumulation screens each only had one gene that overlapped with sGFP::ATZ screen results: Y82E9BR.13 and alg-1, respectively [280, 290]. The greatest overlap was with polyglutamine genome-wide RNAi screen, in which three genes were identified (p value= 0.116). Overall, no significant overlap was detected between our hits and those of other published screens (Figure 4.7), suggesting that the cellular response to accumulated sGFP::ATZ is different to the cellular response mechanism to different types of aggregated protein located in different cell types (intestine vs. muscle) and subcellular locations (ER vs. cytosolic).

4.7.2 Confirmation of Hit Analysis Utilizing Genetic Mutant

Given the inherent variability associated with RNAi knock down, I confirmed modifiers effects in a genetic loss-of-function mutant background. For example, *daf-16(RNAi)* enhanced sGFP::ATZ accumulation. To determine if the similar phenotype occurs in *daf-16(m26)* loss-of-function mutants, I crossed the loss-of-function mutant *daf-16(m26)* with $P_{nhx\text{-}2}$*sGFP::ATZ* transgenic line to produce a $P_{nhx\text{-}2}$*sGFP::ATZ* ;*daf-16(m26)* transgenic line. $P_{nhx\text{-}2}$*sGFP::ATZ* ;*daf-16(m26)* display a significant increase in total GFP

fluorescence, which is consistent with the RNAi screening results These results confirmed that the RNAi screening method was successful at identifying a genetic modifier of the sGFP::ATZ accumulation.

4.8 DISCUSSION

In this study, I developed a high-throughput, semi-automatic genome-wide RNAi screening protocol that utilizes liquid culturing, large particle flow cell sorting, and automated image acquisition to quantify changes in a fluorescent reporter fusion protein. These studies demonstrate that an automated genome-wide RNAi screen can eliminate the labor intensiveness, subjective analysis and operator fatigue associated with past RNAi screens.

Several studies demonstrate the usefulness of both the COPAS^{TM} BIOSORT worm sorter and liquid culturing conditions to help accelerate and streamline genome-wide RNAi screens. However, the combination has not been used together frequently. Moreover, by adding the ArrayScan V^{TI} as an automated imaging platform, an entire genome-wide RNAi screen can be performed by one person in ~20 days. Additionally, the output from the ArrayScan V^{TI} imaging can be analyzed utilizing a variety of different parameters, including fluorescent spot count, number, or intensity. Furthermore, the images of each well are stored on a server and can be re-examined for RNAi effect and reanalyzed using different parameters.

I utilized the high throughput genome-wide RNAi screening protocol to identify genes that affect the accumulation of the aggregation prone protein ATZ, expressed in *C. elegans*. I identified 104 genes that affected the disposition of sGFP::ATZ. The genes were classified into following major categories: RNA synthesis and processing, transcription, stress response, protein transport or signaling, catalytic activity, and unknown functions (Table 4.1). Taken together this diverse collection of genes suggests that sGFP::ATZ is regulated by transcriptional, post-transcriptional and post-translational processes.

To identify genes specifically involved in the disposition of sGFP::ATZ and not in global protection against aggregation-prone proteins, I compared the list of 104 genes that increased sGFP::ATZ accumulation with those from RNAi screens targeting the accumulation of polyglutamine repeat containing proteins (Huntington's disease) [173], α-synuclein (Parkinson's disease) [289], tau (frontotemporal dementia) [176], and SOD-G85R accumulation (Lou Gehrig's disease) [280]. A genome-wide RNAi screen for modifiers of polyglutamine aggregation, identified 186 genes corresponding to five functional classes: translation, RNA metabolism, proteins synthesis, protein folding, and protein degradation [173]. The authors suggest that these genes involved in RNA processing and protein synthesis may play an important role as sensors of protein damage [173]. However, when comparing those genes to those in our study, there were only three genes in common; F48F7.1 *(alg-1),* Y46G5A.4 *(phi-10)* and C14B9.7 *(rpl-21*). The genes *alg-1* and *phi-1* are involved in RNA synthesis and processing while *rpl-21* is involved in protein synthesis. This overlap suggests that active transcription of a subset of genes can regulate aggregation proteins. In support of this notion, I identified

additional seven genes involved in RNA synthesis and processing. The knockdown of genes identified in RNA synthesis and processing may result in RNA processing defects, or an increase in the synthesis of proteins by a defective translational machinery. Both outcomes could explain the observed increase in sGFP::ATZ accumulations, especially if these genes are involved in the proteostasis pathway [291]. Additionally, a number of transcription factors were also identified from the genome-wide RNAi screen, suggesting that those factors may be involved in the transcription of genes also in this network.

The only RNAi identified in a screen for hypertonic stress induced protein aggregation and in our screen was Y82E9BR.13, which is a gene of unknown function that has no known ortholog in humans and therefore was not investigated further [290]. The lack of overlap between the different RNAi screens targeting aggregation prone proteins could be due to technical differences in experimental design. However, the difference maybe attributed to: the nature of the transgene (polyQ vs ATZ), cell type (muscle, intestine, neuronal) and the sub-cellular location (ER, cytoplasm) of protein aggregation.

Several genes in the insulin/ insulin-like growth factor signaling (IIS) pathway were identified in our genome-wide RNAi screen. In *C. elegans,* the IIS pathway is comprised of a phosphorylation cascade that ultimately modulates longevity, stress resistance, and reproductive development [260-263]. Briefly, insulin and IGF-I hormones signal through dimeric (*daf-2*) receptor tyrosine kinases to activate phosphoinositide 3-kinase (*age-1*), which in turn activates the serine/threonine kinases, AKT/PKB and PDK-1. AKT-1 phosphorylates DAF-16, which inhibits DAF-16 from

entering the nucleus. Elimination of signaling through the DAF-2 pathway results in the dephosphorylation of DAF-16 and results in translocation into the nucleus. DAF-16 is a FOXO transcription factor that promotes the expression of many genes that mediate the effect of decreased IIS such as stress resistance and increased longevity [260, 264-266]. When DAF-16 protein is eliminated via RNAi, sGFP::ATZ animals showed a significant increase in the total amount of sGFP::ATZ. Additionally, the P_{nhx-2}*sGFP::ATZ* ;*daf-16(m26)* animals displayed a significant increase in total GFP fluorescence. Since we used an *nhx-2* promoter devoid of DAF-16 binding sites and nhx-2::GFP is not affected by DAF-16 (RNAi) (data not shown) we conclude that *daf-16* is important for the elimination of sGFP::ATZ.

In *daf-2* mutants, DAF-16 is translocated into the nucleus and promotes target gene expression. If this is correct then ATZ/*daf-2* mutant animals would display a significant decrease in sGFP::ATZ accumulation consistent with activation of DAF-16. Indeed this is the case when we crossed the loss-of-function mutant *daf-2(e1370)* with sGFP::ATZ (data not shown). The Arhinger library does not contain a *daf-2 (RNAi)*, however when *age-1 (*which is located downstream of *daf-2),* is knocked down the result phenocopies the *daf-2* mutant. Consistent with this result *age-1(RNAi)* showed a significant decrease in sGFP::ATZ accumulations in our genome-wide RNAi screen.

Interestingly the COPII vesicle components, *sec-23* and *sar-1*, were both identified as potential hits from our genome-wide RNAi screen for sGFP::ATZ modifiers. COPII vesicles are involved in the anterograde transport of proteins from the ER to the Golgi membrane. *Sar-1* is a small GTPase that initiates vesicle coat assembly, while *sec-23* is a GTPase-activating protein that stimulates the GTPase activity of *sar-1*.

When the COPII components were knocked down via RNAi an increase in sGFP::ATZ was shown. In humans, ~10% of ATZ is secreted by hepatocytes, we suspect that the increase in sGFP::ATZ is due to retention of the small amount of soluble sGFP::ATZ, that is normally processed through the conventional ER to Golgi secretory pathway [3].

Several novel groups of genes were also identified in our genome-wide RNAi screen. One group contained genes encoding for G-protein coupled receptors (GPCR's). GPCR's are transmembrane receptors that activate a variety of signal transduction pathways in mammalian cells [292]. In *C. elegans*, GPCRs often act as chemosensory receptors, but many are predicted to be neuropeptide receptors as well [293, 294]. Conceivably some of the GPCRs participate in sensing accumulated proteins or cell stress and transmit to downstream signaling pathways to restore proteostasis. GPCR's are of great interest because ~40% of all prescription pharmaceuticals are targeted to G-protein coupled receptors [295].

In conclusion, I establish a semi-automated high throughput quantitative genome-wide RNAi screen technology and used this method to identify ~100 genes that modify the accumulation of ATZ. Many of these genes implicated in playing a role in the disposal of ATZ are novel and provide a source of ATZ genetic modifiers for future study.

5.0 CONCLUSIONS AND FUTURE DIRECTIONS

The goal of my dissertation was to generate a tractable genetic model that would facilitate the identification of modifiers affecting the severity of α1- antitrypsin deficiency. To accomplish this objective, I helped developed a *C. elegans* model of ATZ deficiency, and utilized this model to identify genes that modulated the accumulation of the Z mutant of α1- antitrypsin (ATZ). This analysis was accomplished through the use of phenotypic analysis and RNAi screening strategies. In summary, our studies showed that the *C. elegans* model recapitulates the ER transport defect associated with the liver disease of ATD patients, in which there is secretion of ATM and intracellular retention of ATZ. Expression of ATZ showed significant negative effects on the health of the animals. Both targeted and a global RNAi screen revealed multiple genes that effect the accumulation of ATZ and many of these genes may serve as future drug targets.

One limitation of this system is that ATZ is constitutively expressed in the animals. Although this mode of expression is similar to that *in vivo*, promoters that have constitutive expression may lead to cellular adaptation over time, which could activate a different set of modifiers than those that are known to function in the acute response to protein misfolding induced cellular stress. Thus, the genetic modifiers of protein stress pathway in this constitutive system may differ significantly from studies in transgenic mice, cell culture, or yeast systems which utilize inducible promoters that govern ATZ expression [83]. The future generation of inducible promoters in *C. elegans* should

provide an opportunity to make a direct comparison between the effects of constitutive versus acute presentation of an aggregation prone protein in this genetic model.

A second limitation of this system, is that the disposition of the accumulated proteins are more difficult to follow in *C. elegans* than in systems allowing conventional pulse-chase analysis. However, we are generating a transgenic ATZ strain utilizing a pTimer fluorescent tag. Fluorescent timers change color in a time-dependent fashion, providing the ability to monitor protein synthesis, maturation, and trafficking in real-time, *in vivo* [296]. In *C. elegans*, fluorescent timers have recently been utilized to visualize muscle development [296]. Our goal will be to utilize pTimer to monitor ATZ protein production and degradation in the animals. The development of a transgene utilizing the pTimer in place of GFP could demonstrate how ATZ is processed in the *C. elegans* intestine.

The aim of Chapter 3 was to determine if the disposal mechanism of sGFP::ATZ in *C. elegans* parallels those in mammalian systems. In general, studies show that the ERAD/ proteasomal pathway is responsible for the elimination of misfolded soluble proteins, whereas the autophagy-lysosome pathway is specialized for degradation of insoluble aggregates and higher order polymers [70, 76, 85-88]. The *C. elegans* ATZ expression strains were used to identify genes that modified the ATZ phenotype. My results confirmed a portion of the misfolded sGFP::ATZ was degraded through the autophagy pathways. Knockdown of all of the autophagy genes investigated via RNAi resulted in significant increases in sGFP::ATZ accumulation, which is consistent with studies on ATZ disposition in other systems [201-203]. Furthermore, co-injection of $P_{nhx\text{-}2}$*sGFP::ATZ* and $P_{nhx\text{-}2}$*mCherry::lgg-1* resulted in an increase in baseline expression of

lgg-1 puncta compared to $P_{nhx\text{-}2}$*sGFP::ATM* co-injected with $P_{nhx\text{-}2}$*mCherry::lgg-1* (data not shown). These results suggested that autophagy was constitutively activated in ATZ animals. The generation of a transgenic line by co-injection of the $P_{nhx\text{-}2}$*sGFP::ATZ* and $P_{nhx\text{-}2}$*mCherry::lgg-1* into the loss-of-function autophagy mutant *unc-51(e1269)* should help confirm this notion by showing a diffuse *lgg-1* expression pattern concomitant with an increase in ATZ accumulation.

I also examined the rate that different ERAD and proteasome components had on ATZ accumulation. My results suggested that only a portion of ATZ is eliminated through ERAD. Interestingly, knockdown of *cdc-48* resulted in a decrease in ATZ accumulation. Conceivably, this phenomenon might be attributed to an increase in autophagy. However, *cdc-48(RNAi)* of autophagy deficient ATZ transgenic animals ($P_{nhx\text{-}2}$*sGFP::ATZ; unc51(e369))* still resulted in a significant decrease in ATZ. This study suggested that knockdown of *cdc-48* decreased the accumulation of ATZ by a non-autophagy, non-proteasomal pathway.

CDC-48 represents 1% of total cytosolic protein and is recruited by a myriad of adaptors to provide energy and/or mechanical force for wide-ranging cellular processes. For instance, *cdc-48* has been shown to complex with the seriene/threonine phosphotase (PP2A) in the insulin/ insulin-like signaling pathway (IIS) [259]. One possibility is that *cdc-48(RNAi)* knockdown causes an increase in PP2A activity, resulting in a shut down of the insulin/ insulin-like growth factor signaling (IIS) pathway, thereby allowing DAF-16 to enter the nucleus. Thus, this result would phenocopy the effects of decreased IIS, which decreases the accumulation of other aggregation prone proteins [87], including sGFP::ATZ (data not shown). Furthermore, when the loss-of-

function mutant *daf-16(m26)* is crossed with P_{nhx-2}*sGFP::ATZ* transgenic line to produce a P_{nhx-2}*sGFP::ATZ* ;*daf-16(m26)* transgenic line animals display a significant increase in total GFP fluorescence, which is consistent with the IIS playing a role in the disposal of ATZ in *C. elegans*.

Interestingly, *rpt-5* (RNAi), which knocks down a regulatory component of the proteasome, resulted in a decrease in ATZ accumulation in *C. elegans*. This paradoxical result is at odds with the ERAD findings and suggested that the inhibition of proteasomal function may be having a complex effect on ATZ accumulation. Similarly, *rpt-5* (RNAi) reduced the accumulation of prototypical luminal ERAD substrates, NHK and PPM2. These paradoxical findings could be explained by the experiment design, as we assessed the animals 48 hours after initiation of RNAi treatment. This duration of RNAi treatment may be sufficient to decrease overall global protein synthesis. A decrease in overall protein synthesis is a known effect of proteasomal inhibition [122, 243]. Additionally, the differential half-life of the ERAD substrates could result in the difference levels of accumulation between the ERAD and UFD substrates. The utilization of a shorter time course should help resolve this discrepancy.

These disparate findings may also be specific to the inhibition of *rpt-5*. I have only investigated one other component of the proteasome, *rpn-10,* but knockdown via RNAi was ineffective. Therefore, in future experiments additional components of the 26S proteasome should be investigated. Currently, our lab has the RNAi clones for ten of the different *rpt* and *rpn* components, all of which need to be first tested utilizing the P_{nhx-2}*Ub::R::mCherry* control line. Next RNAi clones can be tested on P_{nhx-2}*sGFP::ATZ* transgenic lines in a time-dependent fashion to determine if *rpt-5* is unique in its

decrease in ATZ accumulation or if decreased accumulation occurs with inhibition of any proteasome component.

Another important aspect of this study was the assessment of the UPR response in transgenic animals expressing P_{nhx-2}*sGFP::ATZ.* Transgenic P_{nhx-2}*sGFP::ATZ;*P_{hsp-4}*::mCherry* animals showed a marked increase in *hsp-4* activation relative to P_{nhx-2}*sGFP::ATM;*P_{hsp-4}*::mCherry,* suggesting that sGFP::ATZ expression in *C. elegans* constitutively activated the UPR. Paradoxically, *ire-1* inactivation appeared to decrease ATZ accumulation in an *xbp-1* independent fashion. Recent studies show that *ire-1* activation has a function independent of its nuclease activity, of which the latter cleaves the mRNA encoding *xbp-1* resulting in activation and translation of *xbp-1* [123-125]. This independent function, Regulated Ire1-Dependent Decay (RIDD), results in the rapid turnover of mRNAs in a manner not dependent on *xbp-1* activity [297]. RIDD studies indicate that both *ire-1* activation and ER stress are required for activation of this pathway [298].

Since, expression of ATZ in *C. elegans* induced *hsp-4* activation (i.e., *ire-1* activation), and knockdown of *ire-1* would further increase ER stress, it is conceivable that the residual *ire-1* activity activated the RIDD pathway, which preferentially degrades ATZ mRNA. This hypothesis could be tested by also knocking down components of the RIDD pathway and assaying the level of ATZ mRNA by qRT-PCR compared to mRNA levels in *ire-1(RNAi)* treated ATZ animals. As an alternative hypothesis, the elimination of *ire-1* could result in the stimulation of autophagy, and activation of this pathway could be responsible for the decrease in ATZ accumulation. P_{nhx-2}*sGFP::ATZ; unc51(e369)*

animals exposed to *ire-1* RNAi should help determine whether *ire-1* knockdown activates an autophagy dependent elimination of ATZ.

The aim of Chapter 4 was to utilize an unbiased genome-wide RNAi screen to identify additional modifier genes or pathways that play a pivotal role in the disposal of sGFP::ATZ in *C. elegans.* Different RNAi screening strategies have been used to interrogate the *C. elegans* genome; including at least 15 different genome-wide RNAi screens utilizing the RNAi feeding technique [274-280]. However past screens have been limited by being labor intensive, subjective, and prone to operator fatigue. In this study, I developed a high-throughput, semi-automated genome-wide RNAi screening protocol that utilized liquid culturing, large particle flow cell sorting, and automated image acquisition to quantify changes in a fluorescent reporter fusion protein.

One technical limitation associated with this screening method is failure of the ArrayScan V^{TI} to focus correctly on the individual animals. This could result in a population being eliminated from the analysis. However the use of the “red-heads” (P_{myo-2}::mRFP co-injection marker) to auto-focus and the ability to scan archival images, although labor intensive, should help minimize this effect. Future directions of this technology include rescreening of random plates from the feeding library to establish overall reproducibly, although preliminary studies showed plate-to-plate results were highly reproducible. Additionally, we could use different algorithms to re-analyze the data in attempts to reduce false positive rates. Recent studies in RNAi screening have suggested that the use of the strictly standardized mean difference (SSMD) reduces the false positive rates [299]. Since this technique resulted in quantifiable data, we should be able to reanalyze the data utilizing the SSMD instead of *z*-score to determine which

technique is more sensitive and specific.

Utilizing this high throughput genome-wide RNAi screening protocol, I identified 108 genes that affected the disposition of sGFP::ATZ. The genes were classified into following major categories: RNA synthesis and processing, transcription, stress response, protein transport or signaling, catalytic activity, and unknown functions. Taken together, this diverse collection of genes suggests that sGFP::ATZ is regulated by transcriptional, post-transcriptional and post-translational processes.

Interestingly, several genes in the insulin/ insulin-like growth factor signaling (IIS) pathway were identified in our genome-wide RNAi screen. Elimination of signaling through the DAF-2 pathway results in the dephosphorylation of DAF-16 and results in translocation into the nucleus. DAF-16 is a FOXO transcription factor that promotes the expression of many genes that mediate the effect of decreased IIS such as stress resistance and increased longevity [260, 264-266]. When DAF-16 protein is eliminated via RNAi, sGFP::ATZ animals showed a significant increase in the total amount of sGFP::ATZ. In *daf-2* mutants, DAF-16 is translocated into the nucleus and promotes target gene expression. If this pathway affected ATZ accumulation then the ATZ;*daf-2* mutant animals should display a significant decrease in sGFP::ATZ accumulation consistent with activation of DAF-16. Although, the Arhinger library does not contain a *daf-2 (RNAi)*, when *age-1 (*which is located downstream of *daf-2),* was knocked down the results showed a decrease in ATZ accumulation. Independent investigations in our laboratory have shown that knockdown of the IIS pathway decreased the accumulation of in the disposal of ATZ. Therefore, future investigations will be directed at elucidating

the mechanism that the IIS pathway has on ATZ accumulation and possibly including potential drug targets of the IIS pathway.

Further investigations of the results from the RNAi screen include retesting all 108 potential RNAi clones utilizing the $P_{nhx\text{-}2}$*GFP* transgenic animals to test for effect of RNAi on promoter activity. Therefore, any clones shown to have a significant effect on the *nhx-2* promoter can be removed from future analysis. Furthermore, a number of loss-of-function mutants are available from the 108 potential genes. To confirm RNAi results $P_{nhx\text{-}2}$*sGFP::ATZ* will be crossed with loss-of-function mutants, and imaged for resulting ATZ accumulation confirming RNAi screen results. Moreover, due to the ease of the screening technique, we could possibly test the potential positive RNAi clones utilizing the other luminal ERAD substrate controls (NHK, Saar, PPM2) to determine if these results are specific to ATZ or can be applied to aggregation-prone proteins in general.

In conclusion, I established a *C. elegans* ATZ model that recapitulates the ER retention aspect of liver disease in ATD patients. This transgenic animal will become a useful tool for both drug discovery in addition to future studies defining the molecular mechanisms of genetic modifiers that alter the disease phenotype.

APPENDIX A

WORM STRAINS USED IN THIS STUDY

Strain	Name	Abbr.	Promoter	Fluorescent Protein	Description
Bristol	N2	N2			Wild-type worms
CB4856	Hawaiian polymorphic	HA			Wild-type worms
VK689	P_{nhx-2}*sGFP::ATM*	sGFP:: ATM	*nhx-2*	GFP	Secreted GFP expressed in pseudocoelomic space outside of intestinal cells
VK694	P_{nhx-2}*sGFP::ATZ*	sGFP:: ATZ	*nhx-2*	GFP	Accumulations in intestinal cells
VK413	P_{nhx-2}*GFP*		*nhx-2*	GFP	Intestinal expression of GFP
VK414	P_{nhx-2}*sGFP*		*nhx-2*	GFP	Secreted GFP expressed in pseudocoelomic space outside of intestinal cells
VK471	P_{nhx-2}*sATM*		*nhx-2*		Wild-type
VK472	P_{nhx-2}*sATZ*		*nhx-2*		Intracellular inclusions in intestinal cells
VK643	P_{nhx-2}*sGFP::ATZ*$_{Saar}$	Saar	*nhx-2*	GFP	Low levels expression, small accumulations in intestinal cells
VK1223	P_{nhx-2}*sGFP::AT*$_{NHK}$	NHK	*nhx-2*	GFP	Low levels diffuse expression in intestinal cells
VK1239	P_{srp-2}*sGFP::ATM*		*srp-2*	GFP	Hypodermal expression, secretion of GFP
VK1240	P_{srp-2}*sGFP::ATZ*		*srp-2*	GFP	Hypodermal expression, accumulation of GFP
VK1093	P_{nhx-2}*mCherry::lgg-1*	Lgg-1	*nhx-2*	mCherry	mCherry puncta in intestinal cells, associated with autophagosomes expression
VK737	P_{hsp-4}*::GFP*	Hsp-4	*hsp-4*	GFP	Basal expression in spermatheca, under ER stress conditions diffuse GFP throughout body
VK739	P_{hsp-4}::*mCherry*		*hsp-4*	mCherry	Basal expression diffuse intestine, under ER stress conditions diffuse mCherry throughout body
VK1267	P_{nhx-2}*CPL-1::YFP*	CPL-1	*nhx-2*	YFP	Low level diffuse YFP puncta associated with lysosomes
VK1269	P_{nhx-2}*CPL-1ppm2::YFP*	PPM2	*nhx-2*	YFP	Low level diffuse expressio with a few accumulations in

					intestinal cells
VK1261	P*nhx-2*dsRED::KDEL	KDEL	*nhx-2*	dsRED	Diffuse red fluorescence associated with ER
VK1243	P*nhx-2*Ub::R::mCherry	UB	*nhx-2*	mCherry	Low to no expression
VK1244	P*nhx-2*Ub::M::mCherry	UBGM	*nhx-2*	mCherry	Diffuse mCherry expression throughout worm
VK805	P*nhx-2*sGFP::ATZ; *daf-2(e1370)*	ATZ; daf-2	*nhx-2*		Loss of sGFP::ATZ accumulations in intestine when ATZ is expressed in the daf-2(e1360) background
VK757	P*nhx-2*sGFP::ATZ; *daf-16(m26)*	ATZ; daf-16	*nhx-2*	GFP	Increase in sGFP::ATZ accumulations in intestine when ATZ is expressed in the daf-16(m26) background
VK1377	P*nhx-2*sGFP::ATM; P*hsp-4*::mCherry	ATM; hsp-4		GFP & mCherry	Low level secreted GFP, low mCherry expression in intestinal cells
VK1378	P*nhx-2*sGFP::ATZ; P*hsp-4*::mCherry	ATZ; hsp-4		GFP & mCherry	sGFP::ATZ expressed as accumulations in intestine, Induction of *hsp-4::mCherry*
VK1751	P*nhx-2*sGFP::ATZ; *pek-1(ok278)*	ATZ; pek-1		GFP	sGFP::ATZ expression is increased
VK1757	P*nhx-2*sGFP::ATZ; *ire-1(v33)*	ATZ; ire-1		GFP	sGFP::ATZ expression is decreased

BIBLIOGRAPHY

1. Eriksson, S. and C. Larsson, *Purification and partial characterization of pas-positive inclusion bodies from the liver in alpha 1-antitrypsin deficiency.* N Engl J Med, 1975. **292**(4): p. 176-180.
2. Janus, E.D., N.T. Phillips, and R.W. Carrell, *Smoking, lung function, and alpha 1-antitrypsin deficiency.* Lancet, 1985. **1**(8421): p. 152-154.
3. Lomas, D.A., et al., *The mechanism of Z alpha 1-antitrypsin accumulation in the liver.* Nature, 1992. **357**(6379): p. 605-607.
4. DeMeo, D.L. and E.K. Silverman, *Alpha1-antitrypsin deficiency. 2: genetic aspects of alpha(1)-antitrypsin deficiency: phenotypes and genetic modifiers of emphysema risk.* Thorax, 2004. **59**(3): p. 259-264.
5. Stoller, J.K. and L.S. Aboussouan, *Alpha1-antitrypsin deficiency.* Lancet, 2005. **365**(9478): p. 2225-2236.
6. Perlmutter, D.H., *Liver injury in alpha1-antitrypsin deficiency: an aggregated protein induces mitochondrial injury.* J Clin Invest, 2002. **110**(11): p. 1579-1583.
7. Law, R.H., et al., *An overview of the serpin superfamily.* Genome Biol, 2006. **7**(5): p. 216-226.
8. Elliott, P.R., et al., *Inhibitory conformation of the reactive loop of α_1-antitrypsin.* Nature Struct. Biol., 1996. **3**(8): p. 676-681.
9. Djie, M.Z., et al., *Role of the P2 residue in determining the specificity of serpins.* Biochemistry, 1996. **35**(35): p. 11461-11469.
10. Huntington, J.A., R.J. Read, and R.W. Carrell, *Structure of a serpin-protease complex shows inhibition by deformation.* Nature, 2000. **407**(6806): p. 923-926.
11. Silverman, G.A., et al., *The serpins are an expanding superfamily of structurally similar but functionally diverse proteins: Evolution, mechanism of inhibition, novel functions, and a revised nomenclature.* J Biol Chem, 2001. **276**(36): p. 33293-33296.
12. Irving, J.A., et al., *Phylogeny of the serpin superfamily: implications of patterns of amino acid conservation for structure and function.* Genome Res, 2000. **10**(12): p. 1845-1864.
13. Ray, C.A., et al., *Viral inhibition of inflammation: cowpox virus encodes an inhibitor of the interleukin-1 beta converting enzyme.* Cell, 1992. **69**(4): p. 597-604.
14. Schick, C., et al., *Cross-class inhibition of the cysteine proteinases cathepsins K, L, and S by the serpin squamous cell carcinoma antigen 1: A kinetic analysis.* Biochemistry, 1998. **37**(15): p. 5258-5266.
15. Irving, J.A., et al., *Evidence that serpin architecture intrinsically supports papain-like cysteine protease inhibition: engineering alpha(1)-antitrypsin to inhibit cathepsin proteases.* Biochemistry, 2002. **41**(15): p. 4998-5004.
16. Nagata, K., *HSP47 as a collagen-specific molecular chaperone: function and expression in normal mouse development.* Semin Cell Dev Biol, 2003. **14**(5): p. 275-282.

17. Perry, D.J., *Antithrombin and its inherited deficiencies.* Blood Rev, 1994. **8**(1): p. 37-55.
18. Rosenberg, R.D. and P.S. Damus, *The purification and mechanism of action of human antithrombin- heparin cofactor.* J Biol Chem, 1973. **248**(18): p. 6490-505.
19. Choay, J., et al., *Structure-activity relationship in heparin: a synthetic pentasaccharide with high affinity for antithrombin III and eliciting high anti-factor Xa activity.* Biochem Biophys Res Commun, 1983. **116**(2): p. 492-9.
20. Lomas, D.A., et al., *alpha 1-Antitrypsin Mmalton (Phe52-deleted) forms loop-sheet polymers in vivo. Evidence for the C sheet mechanism of polymerization.* J Biol Chem, 1995. **270**(28): p. 16864-16870.
21. Lomas, D.A., et al., *Alpha 1-antitrypsin Siiyama (Ser53-->Phe). Further evidence for intracellular loop-sheet polymerization.* J Biol Chem, 1993. **268**(21): p. 15333-15335.
22. Lomas, D.A., et al., *Molecular mousetraps and the serpinopathies.* Biochem Soc Trans, 2005. **33**(Pt 2): p. 321-330.
23. Nzeako, U.C., E. Frigas, and W.J. Tremaine, *Hereditary angioedema: a broad review for clinicians.* Arch Intern Med, 2001. **161**(20): p. 2417-2429.
24. Zhou, A., et al., *Structural mechanism for the carriage and release of thyroxine in the blood.* Proc Natl Acad Sci U S A, 2006. **103**(36): p. 13321-13326.
25. Pike, R.N., et al., *Serpins: finely balanced conformational traps.* IUBMB Life, 2002. **54**(1): p. 1-7.
26. Bird, P.I., *Regulation of pro-apoptotic leucocyte granule serine proteinases by intracellular serpins.* Immunol Cell Biol, 1999. **77**(1): p. 47-57.
27. Bird, C.H., et al., *Selective regulation of apoptosis: the cytotoxic lymphocyte serpin proteinase inhibitor 9 protects against granzyme B-mediated apoptosis without perturbing the Fas cell death pathway.* Mol Cell Biol, 1998. **18**(11): p. 6387-6398.
28. Abraham, S., et al., *Maspin functions as tumor suppressor by increasing cell adhesion to extracellular matrix in prostate tumor cells.* J Urol, 2003. **169**(3): p. 1157-1161.
29. Al-Ayyoubi, M., P.G. Gettins, and K. Volz, *Crystal structure of human maspin, a serpin with antitumor properties: reactive center loop of maspin is exposed but constrained.* J Biol Chem, 2004. **279**(53): p. 55540-55544.
30. Bailey, C.M., et al., *Mammary serine protease inhibitor (Maspin) binds directly to interferon regulatory factor 6: identification of a novel serpin partnership.* J Biol Chem, 2005. **280**(40): p. 34210-34217.
31. Bailey, C.M., et al., *Biological functions of maspin.* J Cell Physiol, 2006. **209**(3): p. 617-624.
32. Bass, R., A.M. Fernandez, and V. Ellis, *Maspin inhibits cell migration in the absence of protease inhibitory activity.* J Biol Chem, 2002. **277**(49): p. 46845-46848.
33. Hopkins, P.C.R. and J. Whisstock, *Function of maspin.* Science, 1994. **265**: p. 1893-4.
34. Gettins, P.G., *Serpin structure, mechanism, and function.* Chem Rev, 2002. **102**(12): p. 4751-4803.

35. Fulton, K.F., et al., *The high resolution crystal structure of a native thermostable serpin reveals the complex mechanism underpinning the stressed to relaxed transition.* J Biol Chem, 2005. **280**(9): p. 8435-8442.
36. Kounnas, M.Z., et al., *Cellular internalization and degradtion of antithrombin III-thrombin, heparin cofactor II-thrombin, and α1-antitrypsin-trypsin complexes is mediated by the low density lipoprotein receptor-related protein.* J. Biol. Chem., 1996. **271**(11): p. 6523-6529.
37. Makarova, A., et al., *The low density lipoprotein receptor-related protein modulates protease activity in the brain by mediating the cellular internalization of both neuroserpin and neuroserpin-tissue-type plasminogen activator complexes.* J Biol Chem, 2003. **278**(50): p. 50250-50258.
38. Bird, P.I. and G.A. Silverman, *Ovalbumin Serpins*. Nature Encyclopedia of the Human Genome, ed. D.N. Cooper. Vol. 4. 2003, London: Nature Publishing Group. 462-468.
39. Schick, C., et al., *The reactive site loop of the serpin SCCA1 is essential for cysteine proteinase inhibition.* Proc. Natl. Acad. Sci. USA, 1998. **95**: p. 13465-13470.
40. Lomas, D.A. and R. Mahadeva, *Alpha1-antitrypsin polymerization and the serpinopathies: pathobiology and prospects for therapy.* J Clin Invest, 2002. **110**(11): p. 1585-1590.
41. Lomas, D.A. and R.W. Carrell, *Serpinopathies and the conformational dementias.* Nat Rev Genet, 2002. **3**(10): p. 759-768.
42. Belorgey, D., et al., *Protein misfolding and the serpinopathies.* Prion, 2007. **1**(1): p. 15-20.
43. Silverman, G.A. and D.A. Lomas, *Molecular and cellular aspects of the serpinopathies and disorders in serpin activity*, ed. G.A. Silverman and D.A. Lomas. 2007, Singapore: World Scientific Publishing Co. Pte. Ltd. 672.
44. Gooptu, B., U.I. Ekeowa, and D.A. Lomas, *Mechanisms of emphysema in alpha1-antitrypsin deficiency: molecular and cellular insights.* Eur Respir J, 2009. **34**(2): p. 475-488.
45. Davis, R.L., et al., *Familial encephalopathy with neuroserpin inclusion bodies.* Am J Pathol, 1999. **155**(6): p. 1901-1913.
46. Davis, R.L., et al., *Familial dementia caused by polymerization of mutant neuroserpin.* Nature, 1999. **401**(6751): p. 376-379.
47. Davis, R.L., et al., *Association between conformational mutations in neuroserpin and onset and severity of dementia.* Lancet, 2002. **359**(9325): p. 2242-2247.
48. Gooptu, B. and D.A. Lomas, *Conformational pathology of the serpins: themes, variations, and therapeutic strategies.* Annu Rev Biochem, 2009. **78**: p. 147-176.
49. Miranda, E., et al., *The intracellular accumulation of polymeric neuroserpin explains the severity of the dementia FENIB.* Hum Mol Genet, 2008. **17**(11): p. 1527-1539.
50. Miranda, E., K. Romisch, and D.A. Lomas, *Mutants of neuroserpin that cause dementia accumulate as polymers within the endoplasmic reticulum.* J Biol Chem, 2004. **279**(27): p. 28283-28291.
51. Ranes, J. and J.K. Stoller, *A review of alpha-1 antitrypsin deficiency.* Semin Respir Crit Care Med, 2005. **26**(2): p. 154-66.

52. Crystal, R.G., et al., *The alpha 1-antitrypsin gene and its mutations. Clinical consequences and strategies for therapy.* Chest, 1989. **95**(1): p. 196-208.
53. Myerowitz, R.L., Z.T. Handzel, and J.B. Robbins, *Human serum 1 -antitrypsin: isolation and demonstration of electrophoretic and immunologic heterogeneity.* Clin Chim Acta, 1972. **39**(2): p. 307-17.
54. Blanco, I., E.F. Bustillo, and M.C. Rodriguez, *Distribution of alpha1-antitrypsin PI S and PI Z frequencies in countries outside Europe: a meta-analysis.* Clin Genet, 2001. **60**(6): p. 431-41.
55. Silverman, G.A. and D.A. Lomas, *Molecular and Cellular Aspects of the Serpinopathies and Disorders in Serpin Activity*. 2007: World Scientific Publishing. 639.
56. Cox, D.W. and G.D. Billingsley, *Rare deficiency types of alpha 1-antitrypsin: electrophoretic variation and DNA haplotypes.* Am J Hum Genet, 1989. **44**(6): p. 844-854.
57. Luisetti, M. and N. Seersholm, *Alpha1-antitrypsin deficiency. 1: epidemiology of alpha1-antitrypsin deficiency.* Thorax, 2004. **59**(2): p. 164-169.
58. Sveger, T., *Liver disease in alpha1-antitrypsin deficiency detected by screening of 200,000 infants.* New England Journal of Medicine, 1976. **294**(24): p. 1316-1321.
59. Eriksson, S., *Studies in alpha 1-antitrypsin deficiency.* Acta Med Scand Suppl, 1965. **432**: p. 1-85.
60. Crystal, R.G., *Alpha 1-antitrypsin deficiency, emphysema, and liver disease. Genetic basis and strategies for therapy.* J Clin Invest, 1990. **85**(5): p. 1343-1352.
61. Perlmutter, D.H., *Liver injury in alpha1-antitrypsin deficiency: an aggregated protein induces mitochondrial injury.* J Clin Invest, 2002. **110**(11): p. 1579-83.
62. Eden, E., et al., *Atopy, asthma, and emphysema in patients with severe alpha-1-antitrypysin deficiency.* Am J Respir Crit Care Med, 1997. **156**(1): p. 68-74.
63. Fregonese, L. and J. Stolk, *Hereditary alpha-1-antitrypsin deficiency and its clinical consequences.* Orphanet J Rare Dis, 2008. **3**: p. 16.
64. Teckman, J.H. and D.H. Perlmutter, *Retention of mutant alpha(1)-antitrypsin Z in endoplasmic reticulum is associated with an autophagic response.* Am J Physiol Gastrointest Liver Physiol, 2000. **279**(5): p. G961-G974.
65. Janoff, A., *Elastases and emphysema. Current assessment of the protease-antiprotease hypothesis.* Am Rev Respir Dis, 1985. **132**(2): p. 417-33.
66. Kok, K.F., et al., *Heterozygous alpha-1 antitrypsin deficiency as a co-factor in the development of chronic liver disease: a review.* Neth J Med, 2007. **65**(5): p. 160-6.
67. Teckmann, J., D. Qu, and D. Perlmutter, *Molecular pathogenesis of liver diseases in alpha-antitrypsin deficiency.* Hepatology, 1996. **24**: p. 1504-1516.
68. Teckmann, J., et al., *The proteasome participants in degradation of mutant α 1-antitrypsin Z in the endoplasmic reticulum of hepatoma-derived hepatocytes.* J Biol Chem, 2001(48): p. 44865-44872.
69. Wu, Y., et al., *A lag in intracellular degradation of mutant α 1- antitrypsin correlates with the liver disease phenotype in homozygous PiZZ α 1- antitrypsin defficiency* Proc Natl Acad Sci U S A, 1994(91): p. 9014-9018.

70. Kamimoto, T., et al., *Intracellular inclusions containing mutant alpha1-antitrypsin Z are propagated in the absence of autophagic activity.* J Biol Chem, 2006. **281**(7): p. 4467-4476.
71. Werner, E.D., J.L. Brodsky, and A.A. McCracken, *Proteasome-dependent endoplasmic reticulum-associated protein degradation: an unconventional route to a familiar fate.* Proc Natl Acad Sci U S A, 1996. **93**(24): p. 13797-13801.
72. Qu, D., et al., *Degradation of a mutant secretory protein, alpha1-antitrypsin Z, in the endoplasmic reticulum requires proteasome activity.* J Biol Chem, 1996. **271**(37): p. 22791-22795.
73. McCracken, A.A., et al., *Construction and expression of alpha 1-proteinase inhibitor mutants and the effects of these mutations on secretion of the variant inhibitors.* J Biol Chem, 1991. **266**(12): p. 7578-82.
74. Brodsky, J.L. and A.A. McCracken, *ER protein quality control and proteasome-mediated protein degradation.* Semin Cell Dev Biol, 1999. **10**(5): p. 507-13.
75. McCracken, A.A. and K.B. Kruse, *Selective protein degradation in the yeast exocytic pathway.* Mol Biol Cell, 1993. **4**(7): p. 729-36.
76. Kruse, K.B., et al., *Mutant fibrinogen cleared from the endoplasmic reticulum via endoplasmic reticulum-associated protein degradation and autophagy: an explanation for liver disease.* Am J Pathol, 2006. **168**(4): p. 1299-1308.
77. Kruse, K.B., J.L. Brodsky, and A.A. McCracken, *Characterization of an ERAD gene as VPS30/ATG6 reveals two alternative and functionally distinct protein quality control pathways: one for soluble Z variant of human alpha-1 proteinase inhibitor (A1PiZ) and another for aggregates of A1PiZ.* Mol Biol Cell, 2006. **17**(1): p. 203-312.
78. Carlson, J.A., et al., *Accumulation of PiZ alpha 1-antitrypsin causes liver damage in transgenic mice.* J Clin Invest, 1989. **83**(4): p. 1183-11890.
79. Dycaico, M.J., et al., *Neonatal hepatitis induced by alpha 1-antitrypsin: a transgenic mouse model.* Science, 1988. **242**(4884): p. 1409-1412.
80. Dycaico, M.J., et al., *Neonatal growth delay in alpha-1-antitrypsin disease. Influence of genetic background.* Mol Biol Med, 1989. **6**(2): p. 137-141.
81. Carlson, J.A., et al., *Accumulation of PiZ alpha 1-antitrypsin causes liver damage in transgenic mice.* J Clin Invest, 1989. **83**(4): p. 1183-90.
82. Rudnick, D.A. and D.H. Perlmutter, *Alpha-1-antitrypsin deficiency: a new paradigm for hepatocellular carcinoma in genetic liver disease.* Hepatology, 2005. **42**(3): p. 514-521.
83. Hidvegi, T., et al., *Accumulation of mutant alpha1-antitrypsin Z in the endoplasmic reticulum activates caspases-4 and -12, NFkappaB, and BAP31 but not the unfolded protein response.* J Biol Chem, 2005. **280**(47): p. 39002-39015.
84. Kistner, A., et al., *Doxycycline-mediated quantitative and tissue-specific control of gene expression in transgenic mice.* Proc Natl Acad Sci U S A, 1996. **93**(20): p. 10933-8.
85. Berger, Z., et al., *Rapamycin alleviates toxicity of different aggregate-prone proteins.* Hum Mol Genet, 2006. **15**(3): p. 433-442.
86. Ravikumar, B., et al., *Inhibition of mTOR induces autophagy and reduces toxicity of polyglutamine expansions in fly and mouse models of Huntington disease.* Nat Genet, 2004. **36**(6): p. 585-595.

87. Yamamoto, A., M.L. Cremona, and J.E. Rothman, *Autophagy-mediated clearance of huntingtin aggregates triggered by the insulin-signaling pathway.* J Cell Biol, 2006. **172**(5): p. 719-731.
88. Yu, W.H., et al., *Macroautophagy--a novel Beta-amyloid peptide-generating pathway activated in Alzheimer's disease.* J Cell Biol, 2005. **171**(1): p. 87-98.
89. Luirink, J. and I. Sinning, *SRP-mediated protein targeting: structure and function revisited.* Biochim Biophys Acta, 2004. **1694**(1-3): p. 17-35.
90. Fewell, S.W., B.W. Day, and J.L. Brodsky, *Identification of an inhibitor of hsc70-mediated protein translocation and ATP hydrolysis.* J Biol Chem, 2001. **276**(2): p. 910-914.
91. Brodsky, J.L., et al., *The requirement for molecular chaperones during endoplasmic reticulum-associated protein degradation demonstrates that protein export and import are mechanistically distinct.* J Biol Chem, 1999. **274**(6): p. 3453-60.
92. Nishikawa, S., J.L. Brodsky, and K. Nakatsukasa, *Roles of molecular chaperones in endoplasmic reticulum (ER) quality control and ER-associated degradation (ERAD).* J Biochem, 2005. **137**(5): p. 551-5.
93. Barlowe, C., et al., *COPII: a membrane coat formed by Sec proteins that drive vesicle budding from the endoplasmic reticulum.* Cell, 1994. **77**(6): p. 895-907.
94. Muniz, M., P. Morsomme, and H. Riezman, *Protein sorting upon exit from the endoplasmic reticulum.* Cell, 2001. **104**(2): p. 313-20.
95. Letourneur, F., et al., *Coatomer is essential for retrieval of dilysine-tagged proteins to the endoplasmic reticulum.* Cell, 1994. **79**(7): p. 1199-207.
96. Malhotra, V., et al., *Role of an N-ethylmaleimide-sensitive transport component in promoting fusion of transport vesicles with cisternae of the Golgi stack.* Cell, 1988. **54**(2): p. 221-7.
97. Ellgaard, L. and A. Helenius, *Quality control in the endoplasmic reticulum.* Nat Rev Mol Cell Biol, 2003. **4**(3): p. 181-91.
98. Gorlach, A., P. Klappa, and T. Kietzmann, *The endoplasmic reticulum: folding, calcium homeostasis, signaling, and redox control.* Antioxid Redox Signal, 2006. **8**(9-10): p. 1391-418.
99. Ahner, A. and J.L. Brodsky, *Checkpoints in ER-associated degradation: excuse me, which way to the proteasome?* Trends Cell Biol, 2004. **14**(9): p. 474-8.
100. McCracken, A.A. and J.L. Brodsky, *Evolving questions and paradigm shifts in endoplasmic-reticulum-associated degradation (ERAD).* Bioessays, 2003. **25**(9): p. 868-77.
101. Romisch, K., *Endoplasmic reticulum-associated degradation.* Annu Rev Cell Dev Biol, 2005. **21**: p. 435-56.
102. Cabral, C.M., et al., *Organizational diversity among distinct glycoprotein endoplasmic reticulum-associated degradation programs.* Mol Biol Cell, 2002. **13**(8): p. 2639-2650.
103. Meusser, B., et al., *ERAD: the long road to destruction.* Nat Cell Biol, 2005. **7**(8): p. 766-772.
104. Sayeed, A. and D.T. Ng, *Search and destroy: ER quality control and ER-associated protein degradation.* Crit Rev Biochem Mol Biol, 2005. **40**(2): p. 75-91.

105. Schubert, U., et al., *Rapid degradation of a large fraction of newly synthesized proteins by proteasomes.* Nature, 2000. **404**(6779): p. 770-4.
106. Vembar, S.S. and J.L. Brodsky, *One step at a time: endoplasmic reticulum-associated degradation.* Nat Rev Mol Cell Biol, 2008. **9**(12): p. 944-57.
107. Kanehara, K., S. Kawaguchi, and D.T. Ng, *The EDEM and Yos9p families of lectin-like ERAD factors.* Semin Cell Dev Biol, 2007. **18**(6): p. 743-50.
108. Molinari, M., *N-glycan structure dictates extension of protein folding or onset of disposal.* Nat Chem Biol, 2007. **3**(6): p. 313-20.
109. Olivari, S. and M. Molinari, *Glycoprotein folding and the role of EDEM1, EDEM2 and EDEM3 in degradation of folding-defective glycoproteins.* FEBS Lett, 2007. **581**(19): p. 3658-64.
110. Jahn, T.R. and S.E. Radford, *The Yin and Yang of protein folding.* FEBS J, 2005. **272**(23): p. 5962-70.
111. Molinari, M., et al., *Sequential assistance of molecular chaperones and transient formation of covalent complexes during protein degradation from the ER.* J Cell Biol, 2002. **158**(2): p. 247-57.
112. Svedine, S., et al., *Carbohydrates act as sorting determinants in ER-associated degradation of tyrosinase.* J Cell Sci, 2004. **117**(Pt 14): p. 2937-49.
113. Nishikawa, S., A. Hirata, and A. Nakano, *Inhibition of endoplasmic reticulum (ER)-to-Golgi transport induces relocalization of binding protein (BiP) within the ER to form the BiP bodies.* Mol Biol Cell, 1994. **5**(10): p. 1129-43.
114. Huyer, G., et al., *A striking quality control subcompartment in Saccharomyces cerevisiae: the endoplasmic reticulum-associated compartment.* Mol Biol Cell, 2004. **15**(2): p. 908-21.
115. Huyer, G., et al., *Distinct machinery is required in Saccharomyces cerevisiae for the endoplasmic reticulum-associated degradation of a multispanning membrane protein and a soluble luminal protein.* J Biol Chem, 2004. **279**(37): p. 38369-78.
116. Kota, J., C.F. Gilstring, and P.O. Ljungdahl, *Membrane chaperone Shr3 assists in folding amino acid permeases preventing precocious ERAD.* J Cell Biol, 2007. **176**(5): p. 617-28.
117. Nakatsukasa, K. and J.L. Brodsky, *The recognition and retrotranslocation of misfolded proteins from the endoplasmic reticulum.* Traffic, 2008. **9**(6): p. 861-70.
118. Lilley, B.N. and H.L. Ploegh, *A membrane protein required for dislocation of misfolded proteins from the ER.* Nature, 2004. **429**(6994): p. 834-40.
119. Plemper, R.K., et al., *Mutant analysis links the translocon and BiP to retrograde protein transport for ER degradation.* Nature, 1997. **388**(6645): p. 891-5.
120. Wahlman, J., et al., *Real-time fluorescence detection of ERAD substrate retrotranslocation in a mammalian in vitro system.* Cell, 2007. **129**(5): p. 943-55.
121. Wiertz, E.J., et al., *Sec61-mediated transfer of a membrane protein from the endoplasmic reticulum to the proteasome for destruction.* Nature, 1996. **384**(6608): p. 432-8.
122. Jentsch, S. and S. Rumpf, *Cdc48 (p97): a "molecular gearbox" in the ubiquitin pathway?* Trends Biochem Sci, 2007. **32**(1): p. 6-11.
123. Patil, C. and P. Walter, *Intracellular signaling from the endoplasmic reticulum to the nucleus: the unfolded protein response in yeast and mammals.* Curr Opin Cell Biol, 2001. **13**(3): p. 349-55.

124. Schroder, M. and R.J. Kaufman, *The mammalian unfolded protein response.* Annu Rev Biochem, 2005. **74**: p. 739-89.
125. Schroder, M. and R.J. Kaufman, *ER stress and the unfolded protein response.* Mutat Res, 2005. **569**(1-2): p. 29-63.
126. Fulda, S., et al., *Cellular stress responses: cell survival and cell death.* Int J Cell Biol. **2010**: p. 214074.
127. Travers, K.J., et al., *Functional and genomic analyses reveal an essential coordination between the unfolded protein response and ER-associated degradation.* Cell, 2000. **101**(3): p. 249-58.
128. Bertolotti, A., et al., *Dynamic interaction of BiP and ER stress transducers in the unfolded-protein response.* Nat Cell Biol, 2000. **2**(6): p. 326-32.
129. Okamura, K., et al., *Dissociation of Kar2p/BiP from an ER sensory molecule, Ire1p, triggers the unfolded protein response in yeast.* Biochem Biophys Res Commun, 2000. **279**(2): p. 445-50.
130. Credle, J.J., et al., *On the mechanism of sensing unfolded protein in the endoplasmic reticulum.* Proc Natl Acad Sci U S A, 2005. **102**(52): p. 18773-84.
131. Aragon, T., et al., *Messenger RNA targeting to endoplasmic reticulum stress signalling sites.* Nature, 2009. **457**(7230): p. 736-40.
132. Korennykh, A.V., et al., *Structural and functional basis for RNA cleavage by Ire1.* BMC Biol. **9**(1): p. 47.
133. Lopez-Lastra, M., A. Rivas, and M.I. Barria, *Protein synthesis in eukaryotes: the growing biological relevance of cap-independent translation initiation.* Biol Res, 2005. **38**(2-3): p. 121-46.
134. Rock, K.L., et al., *Inhibitors of the proteasome block the degradation of most cell proteins and the generation of peptides presented on MHC class I molecules.* Cell, 1994. **78**(5): p. 761-71.
135. Ciechanover, A., *Proteolysis: from the lysosome to ubiquitin and the proteasome.* Nat Rev Mol Cell Biol, 2005. **6**(1): p. 79-87.
136. Ciechanover, A., *The ubiquitin-proteasome pathway: on protein death and cell life.* EMBO J, 1998. **17**(24): p. 7151-60.
137. Ciechanover, A. and A.L. Schwartz, *The ubiquitin-proteasome pathway: the complexity and myriad functions of proteins death.* Proc Natl Acad Sci U S A, 1998. **95**(6): p. 2727-30.
138. Myung, J., K.B. Kim, and C.M. Crews, *The ubiquitin-proteasome pathway and proteasome inhibitors.* Med Res Rev, 2001. **21**(4): p. 245-73.
139. Nandi, D., et al., *The ubiquitin-proteasome system.* J Biosci, 2006. **31**(1): p. 137-55.
140. Adhikari, A. and Z.J. Chen, *Diversity of polyubiquitin chains.* Dev Cell, 2009. **16**(4): p. 485-6.
141. Sullivan, J.A., K. Shirasu, and X.W. Deng, *The diverse roles of ubiquitin and the 26S proteasome in the life of plants.* Nat Rev Genet, 2003. **4**(12): p. 948-58.
142. Glickman, M.H. and A. Ciechanover, *The ubiquitin-proteasome proteolytic pathway: destruction for the sake of construction.* Physiol Rev, 2002. **82**(2): p. 373-428.
143. Baker, S.P. and P.A. Grant, *The Proteasome: Not just degrading anymore.* Cell, 2005. **10**(013): p. 361-363.

144. Voges, D., P. Zwickl, and W. Baumeister, *The 26S proteasome: a molecular machine designed for controlled proteolysis.* Annu Rev Biochem, 1999. **68**: p. 1015-68.
145. Heinemeyer, W., P.C. Ramos, and R.J. Dohmen, *The ultimate nanoscale mincer: assembly, structure and active sites of the 20S proteasome core.* Cell Mol Life Sci, 2004. **61**(13): p. 1562-78.
146. Klionsky, D.J., A.M. Cuervo, and P.O. Seglen, *Methods for monitoring autophagy from yeast to human.* Autophagy, 2007. **3**(3): p. 181-206.
147. Abeliovich, H. and D.J. Klionsky, *Autophagy in yeast: mechanistic insights and physiological function.* Microbiol Mol Biol Rev, 2001. **65**(3): p. 463-79, table of contents.
148. Huang, W.P. and D.J. Klionsky, *Autophagy in yeast: a review of the molecular machinery.* Cell Struct Funct, 2002. **27**(6): p. 409-20.
149. Cuervo, A.M., *Autophagy: many paths to the same end.* Mol Cell Biochem, 2004. **263**(1-2): p. 55-72.
150. Schmid, D. and C. Munz, *Immune surveillance of intracellular pathogens via autophagy.* Cell Death Differ, 2005. **12 Suppl 2**: p. 1519-1527.
151. Rubinsztein, D.C., et al., *Autophagy and its possible roles in nervous system diseases, damage and repair.* Autophagy, 2005. **1**(1): p. 11-22.
152. Marzella, L., J. Ahlberg, and H. Glaumann, *Autophagy, heterophagy, microautophagy and crinophagy as the means for intracellular degradation.* Virchows Arch B Cell Pathol Incl Mol Pathol, 1981. **36**(2-3): p. 219-34.
153. Mortimore, G.E., B.R. Lardeux, and C.E. Adams, *Regulation of microautophagy and basal protein turnover in rat liver. Effects of short-term starvation.* J Biol Chem, 1988. **263**(5): p. 2506-12.
154. Brenner, S., *The genetics of Caenorhabditis elegans.* Genetics, 1974. **77**(1): p. 71-94.
155. Emmons, S.W., *The Nematode Caenorhabditis elegans: The Genome*. First ed, ed. W.B. Wood. 1988, Plainview: Cold Spring Harbor Laboratory Press. 47-79.
156. Pak, S.C., et al., *Srp-2 is a cross-class inhibitor that participates in post-embryonic development of the nematode Caenorhabditis elegans: Initial characterization of the Clade L serpins.* J Biol Chem, 2004. **279**: p. 15448-15459.
157. Chalfie, M. and E. Wolinsky, *The identification and suppression of inherited neurodegeneration in Caenorhabditis elegans.* Nature, 1990. **345**(6274): p. 410-416.
158. Aboobaker, A.A. and M.L. Blaxter, *Medical significance of Caenorhabditis elegans.* Ann Med, 2000. **32**(1): p. 23-30.
159. Ahringer, J., *Turn to the worm!* Curr Opin Genet Dev, 1997. **7**(3): p. 410-415.
160. Culetto, E. and D.B. Sattelle, *A role for Caenorhabditis elegans in understanding the function and interactions of human disease genes.* Hum Mol Genet, 2000. **9**(6): p. 869-877.
161. O'Kane, C.J., *Modelling human diseases in Drosophila and Caenorhabditis.* Semin Cell Dev Biol, 2003. **14**(1): p. 3-10.
162. Sonnhammer, E.L. and R. Durbin, *Analysis of protein domain families in Caenorhabditis elegans.* Genomics, 1997. **46**(2): p. 200-216.

163. Wheelan, S.J., et al., *Human and nematode orthologs--lessons from the analysis of 1800 human genes and the proteome of Caenorhabditis elegans.* Gene, 1999. **238**(1): p. 163-70.
164. Schmidt, E.E. and C.J. Davies, *The origins of polypeptide domains.* Bioessays, 2007. **29**(3): p. 262-270.
165. Derry, W.B., A.P. Putzke, and J.H. Rothman, *Caenorhabditis elegans p53: role in apoptosis, meiosis, and stress resistance.* Science, 2001. **294**(5542): p. 591-595.
166. Mushegian, A.R., et al., *Positionally cloned human disease genes: patterns of evolutionary conservation and functional motifs.* Proc Natl Acad Sci U S A, 1997. **94**(11): p. 5831-5836.
167. Rubin, G.M., et al., *Comparative genomics of the eukaryotes.* Science, 2000. **287**(5461): p. 2204-2215.
168. Culetto, E. and D. Sattelle, *A role for Caenorhabditis elegans in understanding the function and interactions of human disease genes.* Hum Mol Genet, 2000. **9**(6): p. 869-877.
169. Singleton, A.B., et al., *alpha-Synuclein locus triplication causes Parkinson's disease.* Science, 2003. **302**(5646): p. 841.
170. Hamamichi, S., et al., *Hypothesis-based RNAi screening identifies neuroprotective genes in a Parkinson's disease model.* Proc Natl Acad Sci U S A, 2008. **105**(2): p. 728-733.
171. Ruan, Q., et al., *VPS41, a protein involved in lysosomal trafficking, is protective in Caenorhabditis elegans and mammalian cellular models of Parkinson's disease.* Neurobiol Dis. **37**(2): p. 330-8.
172. Morley, J.F., et al., *The threshold for polyglutamine-expansion protein aggregation and cellular toxicity is dynamic and influenced by aging in Caenorhabditis elegans.* Proc Natl Acad Sci U S A, 2002. **99**(16): p. 10417-10422.
173. Nollen, E.A., et al., *Genome-wide RNA interference screen identifies previously undescribed regulators of polyglutamine aggregation.* Proc Natl Acad Sci U S A, 2004. **101**(17): p. 6403-6408.
174. Sveger, T., *The natural history of liver disease in alpha 1-antitrypsin deficiency children.* Acta Paediatr Scand, 1988. **77**(6): p. 847-851.
175. Sveger, T., *The natural history of liver disease in alpha 1-antitrypsin deficient children.* Acta Paediatr Scand, 1988. **77**(6): p. 847-51.
176. Kraemer, B.C., et al., *Molecular pathways that influence human tau-induced pathology in Caenorhabditis elegans.* Hum Mol Genet, 2006. **15**(9): p. 1483-96.
177. Mello, C. and A. Fire, *DNA transformation.* Methods Cell Biol, 1995. **48**: p. 451-482.
178. Davis, M.W., et al., *Rapid single nucleotide polymorphism mapping in C. elegans.* BMC Genomics, 2005. **6**: p. 118-128.
179. Hall, D.H., *Electron microscopy and three-dimensional image reconstruction.* Methods Cell Biol, 1995. **48**: p. 395-436.
180. Nott, A., H. Le Hir, and M.J. Moore, *Splicing enhances translation in mammalian cells: an additional function of the exon junction complex.* Genes Dev, 2004. **18**(2): p. 210-22.

181. Okkema, P.G., et al., *Sequence requirements for myosin gene expression and regulation in Caenorhabditis elegans.* Genetics, 1993. **135**(2): p. 385-404.
182. Nehrke, K., *A reduction in intestinal cell pHi due to loss of the Caenorhabditis elegans Na+/H+ exchanger NHX-2 increases life span.* J Biol Chem, 2003. **278**(45): p. 44657-44566.
183. Long, O.S., et al., *Using Caenorhabditis elegans to Study Serpinopathies.* Methods Enzymol. **499**: p. 259-81.
184. Praitis, V., et al., *Creation of low-copy integrated transgenic lines in Caenorhabditis elegans.* Genetics, 2001. **157**(3): p. 1217-1226.
185. Yu, M.H., K.N. Lee, and J. Kim, *The Z type variation of human alpha 1-antitrypsin causes a protein folding defect.* Nat Struct Biol, 1995. **2**(5): p. 363-367.
186. Lieberman, J., C. Mittman, and H.W. Gordon, *Alpha 1 antitrypsinin the livers of patients with emphysema.* Science, 1972. **175**(17): p. 63-65.
187. Carrell, R.W., *alpha 1-Antitrypsin: molecular pathology, leukocytes, and tissue damage.* J Clin Invest, 1986. **78**(6): p. 1427-1431.
188. Teckman, J.H., D. Qu, and D.H. Perlmutter, *Molecular pathogenesis of liver disease in alpha1-antitrypsin deficiency.* Hepatology, 1996. **24**(6): p. 1504-1516.
189. Grenman, R., et al., *Radiosensitivity of head and neck cancer cells in vitro. A 96-well plate clonogenic cell assay for squamous cell carcinoma.* Arch Otolaryngol Head Neck Surg, 1988. **114**(4): p. 427-31.
190. Elliott, P.R., D. Bilton, and D.A. Lomas, *Lung polymers in Z alpha1-antitrypsin deficiency-related emphysema.* Am J Respir Cell Mol Biol, 1998. **18**(5): p. 670-674.
191. Lomas, D.A. and H. Parfrey, *Alpha1-antitrypsin deficiency. 4: Molecular pathophysiology.* Thorax, 2004. **59**(6): p. 529-535.
192. Perlmutter, D.H., *Alpha-1-antitrypsin deficiency: importance of proteasomal and autophagic degradative pathways in disposal of liver disease-associated protein aggregates.* Annual review of medicine, 2011. **62**: p. 333-345.
193. Carrell, R.W. and D.A. Lomas, *Alpha1-antitrypsin deficiency--a model for conformational diseases.* N Engl J Med, 2002. **346**(1): p. 45-53.
194. Parfrey, H., et al., *Targeting a surface cavity of alpha 1-antitrypsin to prevent conformational disease.* J Biol Chem, 2003. **278**(35): p. 33060-33066.
195. Perlmutter, D.H., *Pathogenesis of chronic liver injury and hepatocellular carcinoma in alpha-1-antitrypsin deficiency.* Pediatr Res, 2006. **60**(2): p. 233-238.
196. Perlmutter, D.H., *Liver disease in alpha1-antitrypsin deficiency*, in *Molecular and cellular aspects of the serpinopathies and disorders in serpin activity*, G.K. Silverman and D.A. Lomas, Editors. 2007, World Scientific Publishing Co. p. 483-508.
197. Vembar, S.S. and J.L. Brodsky, *One step at a time: endoplasmic reticulum-associated degradation.* Nat Rev Mol Cell Biol, 2008. **9**(12): p. 944-957.
198. Brodsky, J.L. and R.J. Wojcikiewicz, *Substrate-specific mediators of ER associated degradation (ERAD).* Curr Opin Cell Biol, 2009. **21**(4): p. 516-521.
199. Hirsch, C., et al., *Endoplasmic reticulum-associated protein degradation--one model fits all?* Biochim Biophys Acta, 2004. **1695**(1-3): p. 208-216.
200. Lord, J.M., et al., *Endoplasmic reticulum-associated protein degradation.* Semin Cell Dev Biol, 2000. **11**(3): p. 159-164.

201. Menzies, F.M., B. Ravikumar, and D.C. Rubinsztein, *Protective roles for induction of autophagy in multiple proteinopathies.* Autophagy, 2006. **2**(3): p. 224-225.
202. Rubinsztein, D.C., *The roles of intracellular protein-degradation pathways in neurodegeneration.* Nature, 2006. **443**(7113): p. 780-786.
203. Williams, A., et al., *Aggregate-prone proteins are cleared from the cytosol by autophagy: therapeutic implications.* Curr Top Dev Biol, 2006. **76**: p. 89-101.
204. Teckman, J.H., et al., *Mitochondrial autophagy and injury in the liver in alpha 1-antitrypsin deficiency.* Am J Physiol Gastrointest Liver Physiol, 2004. **286**(5): p. G851-G862.
205. Yamasaki, M., et al., *Crystal structure of a stable dimer reveals the molecular basis of serpin polymerization.* Nature, 2008. **455**(7217): p. 1255-1258.
206. Calfon, M., et al., *IRE1 couples endoplasmic reticulum load to secretory capacity by processing the XBP-1 mRNA.* Nature, 2002. **415**(6867): p. 92-96.
207. Mouysset, J., C. Kahler, and T. Hoppe, *A conserved role of Caenorhabditis elegans CDC-48 in ER-associated protein degradation.* J Struct Biol, 2006. **156**(1): p. 41-49.
208. Shen, X., et al., *Complementary signaling pathways regulate the unfolded protein response and are required for C. elegans development.* Cell, 2001. **107**(7): p. 893-903.
209. Shen, X., et al., *Genetic interactions due to constitutive and inducible gene regulation mediated by the unfolded protein response in C. elegans.* PLoS Genet, 2005. **1**(3): p. e37.
210. Urano, F., et al., *A survival pathway for Caenorhabditis elegans with a blocked unfolded protein response.* J Cell Biol, 2002. **158**(4): p. 639-646.
211. Melendez, A., et al., *Autophagy genes are essential for dauer development and life-span extension in C. elegans.* Science, 2003. **301**(5638): p. 1387-1391.
212. Roggo, L., et al., *Membrane transport in Caenorhabditis elegans: an essential role for VPS34 at the nuclear membrane.* Embo J, 2002. **21**(7): p. 1673-1683.
213. Takacs-Vellai, K., et al., *Inactivation of the autophagy gene bec-1 triggers apoptotic cell death in C. elegans.* Curr Biol, 2005. **15**(16): p. 1513-1517.
214. Brenner, S., *The Genetics of Caenorhabditis elegans.* Genetics, 1974(77): p. 71-94.
215. Gosai, S.J., et al., *Automated high-content live animal drug screening using C. elegans expressing the aggregation prone serpin alpha1-antitrypsin Z.* PLoS One. **5**(11): p. e15460.
216. Lehner, B., J. Tischler, and A.G. Fraser, *RNAi screens in Caenorhabditis elegans in a 96-well liquid format and their application to the systematic identification of genetic interactions.* Nat Protoc, 2006. **1**(3): p. 1617-20.
217. Kamath, R.S., et al., *Systematic functional analysis of the Caenorhabditis elegans genome using RNAi.* Nature, 2003. **421**(6920): p. 231-237.
218. Fire, A., et al., *Potent and specific genetic interference by double-stranded RNA in Caenorhabditis elegans.* Nature, 1998. **391**(6669): p. 806-811.
219. Kamath, R.S. and J. Ahringer, *Genome-wide RNAi screening in Caenorhabditis elegans.* Methods, 2003. **30**(4): p. 313-21.

220. Timmons, L. and A. Fire, *Specific interference by ingested dsRNA [letter].* Nature, 1998. **395**(6705): p. 854.
221. Kamath, R.S., et al., *Systematic functional analysis of the Caenorhabditis elegans genome using RNAi.* Nature, 2003. **421**(6920): p. 231-7.
222. Hoseki, J., R. Ushioda, and K. Nagata, *Mechanism and components of endoplasmic reticulum-associated degradation.* J Biochem, 2010. **147**(1): p. 19-25.
223. Hebert, D.N., R. Bernasconi, and M. Molinari, *ERAD substrates: which way out?* Semin Cell Dev Biol, 2010. **21**(5): p. 526-532.
224. Maattanen, P., et al., *Protein quality control in the ER: the recognition of misfolded proteins.* Semin Cell Dev Biol, 2010. **21**(5): p. 500-511.
225. Bernasconi, R. and M. Molinari, *ERAD and ERAD tuning: disposal of cargo and of ERAD regulators from the mammalian ER.* Current opinion in cell biology, 2011. **23**(2): p. 176-183.
226. Christianson, J.C., et al., *OS-9 and GRP94 deliver mutant alpha1-antitrypsin to the Hrd1-SEL1L ubiquitin ligase complex for ERAD.* Nat Cell Biol, 2008. **10**(3): p. 272-282.
227. Shen, Y., P. Ballar, and S. Fang, *Ubiquitin ligase gp78 increases solubility and facilitates degradation of the Z variant of alpha-1-antitrypsin.* Biochem Biophys Res Commun, 2006. **349**(4): p. 1285-1293.
228. Kroeger, H., et al., *Endoplasmic reticulum-associated degradation (ERAD) and autophagy cooperate to degrade polymerogenic mutant serpins.* J Biol Chem, 2009. **284**(34): p. 22793-22802.
229. Lin, L., et al., *A naturally occurring nonpolymerogenic mutant of alpha 1-antitrypsin characterized by prolonged retention in the endoplasmic reticulum.* J Biol Chem, 2001. **276**(36): p. 33893-33898.
230. Schmidt, B.Z. and D.H. Perlmutter, *Grp78, Grp94, and Grp170 interact with alpha1-antitrypsin mutants that are retained in the endoplasmic reticulum.* Am J Physiol Gastrointest Liver Physiol, 2005. **289**(3): p. G444-G455.
231. Hosokawa, N., et al., *A novel ER alpha-mannosidase-like protein accelerates ER-associated degradation.* EMBO Rep, 2001. **2**(5): p. 415-22.
232. Wu, Y., et al., *Elucidation of the molecular logic by which misfolded alpha 1-antitrypsin is preferentially selected for degradation.* Proc Natl Acad Sci U S A, 2003. **100**(14): p. 8229-34.
233. Sifers, R.N., et al., *A frameshift mutation results in a truncated alpha 1-antitrypsin that is retained within the rough endoplasmic reticulum.* J Biol Chem, 1988. **263**(15): p. 7330-7335.
234. Turk, D., et al., *Revised definition of substrate binding sites of papain-like cysteine proteases.* Biol Chem, 1998. **379**(2): p. 137-47.
235. Ishidoh, K. and E. Kominami, *Processing and activation of lysosomal proteinases.* Biol Chem, 2002. **383**(12): p. 1827-31.
236. Kreusch, S., et al., *An evolutionarily conserved tripartite tryptophan motif stabilizes the prodomains of cathepsin L-like cysteine proteases.* Eur J Biochem, 2000. **267**(10): p. 2965-2972.

237. McIntyre, G.F. and A.H. Erickson, *The lysosomal proenzyme receptor that binds procathepsin L to microsomal membranes at pH 5 is a 43-kDa integral membrane protein.* Proc Natl Acad Sci U S A, 1993. **90**(22): p. 10588-92.
238. Dantuma, N.P., et al., *Short-lived green fluorescent proteins for quantifying ubiquitin/proteasome-dependent proteolysis in living cells.* Nat Biotechnol, 2000. **18**(5): p. 538-543.
239. Bence, N.F., R.M. Sampat, and R.R. Kopito, *Impairment of the ubiquitin-proteasome system by protein aggregation.* Science, 2001. **292**(5521): p. 1552-1555.
240. Lindsten, K. and N.P. Dantuma, *Monitoring the ubiquitin/proteasome system in conformational diseases.* Ageing Res Rev, 2003. **2**(4): p. 433-49.
241. Varshavsky, A., *The N-end rule pathway of protein degradation.* Genes Cells, 1997. **2**(1): p. 13-28.
242. Bays, N.W. and R.Y. Hampton, *Cdc48-Ufd1-Npl4: stuck in the middle with Ub.* Curr Biol, 2002. **12**(10): p. R366-R371.
243. Ye, Y., H.H. Meyer, and T.A. Rapoport, *The AAA ATPase Cdc48/p97 and its partners transport proteins from the ER into the cytosol.* Nature, 2001. **414**(6864): p. 652-656.
244. Mayer, M.P. and B. Bukau, *Hsp70 chaperones: cellular functions and molecular mechanism.* Cell Mol Life Sci, 2005. **62**(6): p. 670-84.
245. Otero, J.H., B. Lizak, and L.M. Hendershot, *Life and death of a BiP substrate.* Semin Cell Dev Biol. **21**(5): p. 472-8.
246. Yang, Z. and D.J. Klionsky, *Eaten alive: a history of macroautophagy.* Nat Cell Biol, 2010. **12**(9): p. 814-822.
247. Tanida, I., et al., *Lysosomal turnover, but not a cellular level, of endogenous LC3 is a marker for autophagy.* Autophagy, 2005. **1**(2): p. 84-91.
248. Kuma, A., M. Matsui, and N. Mizushima, *LC3, an autophagosome marker, can be incorporated into protein aggregates independent of autophagy: caution in the interpretation of LC3 localization.* Autophagy, 2007. **3**(4): p. 323-328.
249. Ye, Y., et al., *A membrane protein complex mediates retro-translocation from the ER lumen into the cytosol.* Nature, 2004. **429**(6994): p. 841-847.
250. Guerrero, C., et al., *Characterization of the proteasome interaction network using a QTAX-based tag-team strategy and protein interaction network analysis.* Proc Natl Acad Sci U S A, 2008. **105**(36): p. 13333-8.
251. Hamazaki, J., et al., *Rpn10-mediated degradation of ubiquitinated proteins is essential for mouse development.* Mol Cell Biol, 2007. **27**(19): p. 6629-38.
252. Urano, F., et al., *A survival pathway for Caenorhabditis elegans with a blocked unfolded protein response.* J Cell Biol, 2002. **158**(4): p. 639-46.
253. Sasagawa, Y., K. Yamanaka, and T. Ogura, *ER E3 ubiquitin ligase HRD-1 and its specific partner chaperone BiP play important roles in ERAD and developmental growth in Caenorhabditis elegans.* Genes Cells, 2007. **12**(9): p. 1063-73.
254. Gardner, R.G., et al., *Endoplasmic reticulum degradation requires lumen to cytosol signaling. Transmembrane control of Hrd1p by Hrd3p.* J Cell Biol, 2000. **151**(1): p. 69-82.

255. Romisch, K., *Cdc48p is UBX-linked to ER ubiquitin ligases.* Trends Biochem Sci, 2006. **31**(1): p. 24-5.
256. Biunno, I., et al., *SEL1L a multifaceted protein playing a role in tumor progression.* J Cell Physiol, 2006. **208**(1): p. 23-38.
257. Christianson, J.C., et al., *OS-9 and GRP94 deliver mutant alpha1-antitrypsin to the Hrd1-SEL1L ubiquitin ligase complex for ERAD.* Nat Cell Biol, 2008. **10**(3): p. 272-82.
258. Francisco, A.B., et al., *Deficiency of suppressor enhancer Lin12 1 like (SEL1L) in mice leads to systemic endoplasmic reticulum stress and embryonic lethality.* J Biol Chem. **285**(18): p. 13694-703.
259. Ohama, T. and D.L. Brautigan, *Endotoxin conditioning induces VCP/p97-mediated and inducible nitric-oxide synthase-dependent Tyr284 nitration in protein phosphatase 2A.* J Biol Chem. **285**(12): p. 8711-8.
260. Lee, S.S., et al., *DAF-16 target genes that control C. elegans life-span and metabolism.* Science, 2003. **300**(5619): p. 644-647.
261. Morley, J.F. and R.I. Morimoto, *Regulation of longevity in Caenorhabditis elegans by heat shock factor and molecular chaperones.* Mol Biol Cell, 2004. **15**(2): p. 657-664.
262. Samuelson, A.V., C.E. Carr, and G. Ruvkun, *Gene activities that mediate increased life span of C. elegans insulin-like signaling mutants.* Genes Dev, 2007. **21**(22): p. 2976-94.
263. McColl, G., et al., *Insulin-like signaling determines survival during stress via posttranscriptional mechanisms in C. elegans.* Cell Metab, 2010. **12**(3): p. 260-272.
264. Murphy, C.T., et al., *Genes that act downstream of DAF-16 to influence the lifespan of Caenorhabditis elegans.* Nature, 2003. **424**(6946): p. 277-283.
265. Wang, Y. and H.A. Tissenbaum, *Overlapping and distinct functions for a Caenorhabditis elegans SIR2 and DAF-16/FOXO.* Mech Ageing Dev, 2006. **127**(1): p. 48-56.
266. Murphy, C.T., *The search for DAF-16/FOXO transcriptional targets: approaches and discoveries.* Experimental gerontology, 2006. **41**(10): p. 910-921.
267. Padmanabhan, S., et al., *A PP2A regulatory subunit regulates C. elegans insulin/IGF-1 signaling by modulating AKT-1 phosphorylation.* Cell, 2009. **136**(5): p. 939-51.
268. Tabara, H., A. Grishok, and C.C. Mello, *RNAi in C. elegans: soaking in the genome sequence.* Science, 1998. **282**(5388): p. 430-431.
269. Bernstein, E., et al., *Role for a bidentate ribonuclease in the initiation step of RNA interference.* Nature, 2001. **409**(6818): p. 363-6.
270. Castanotto, D. and J.J. Rossi, *The promises and pitfalls of RNA-interference-based therapeutics.* Nature, 2009. **457**(7228): p. 426-33.
271. Siomi, M.C. and S. Kuramochi-Miyagawa, *RNA silencing in germlines--exquisite collaboration of Argonaute proteins with small RNAs for germline survival.* Curr Opin Cell Biol, 2009. **21**(3): p. 426-34.
272. Zamore, P.D., et al., *RNAi: double-stranded RNA directs the ATP-dependent cleavage of mRNA at 21 to 23 nucleotide intervals.* Cell, 2000. **101**(1): p. 25-33.

273. Ahlquist, P., *RNA-dependent RNA polymerases, viruses, and RNA silencing.* Science, 2002. **296**(5571): p. 1270-3.
274. Fraser, A.G., et al., *Functional genomic analysis of C. elegans chromosome I by systematic RNA interference.* Nature, 2000. **408**(6810): p. 325-330.
275. Simmer, F., et al., *Genome-Wide RNAi of C. elegans Using the Hypersensitive rrf-3 Strain Reveals Novel Gene Functions.* PLoS Biol, 2003. **1**(1): p. 77-84.
276. Kamath, R.S. and J. Ahringer, *Genome-wide RNAi screening in Caenorhabditis elegans.* Methods, 2003. **30**(4): p. 313-321.
277. Ashrafi, K., et al., *Genome-wide RNAi analysis of Caenorhabditis elegans fat regulatory genes.* Nature, 2003. **421**(6920): p. 268-272.
278. Agaisse, H., et al., *Genome-wide RNAi screen for host factors required for intracellular bacterial infection.* Science, 2005. **309**(5738): p. 1248-1251.
279. Kuwahara, T., et al., *A systematic RNAi screen reveals involvement of endocytic pathway in neuronal dysfunction in alpha-synuclein transgenic C. elegans.* Hum Mol Genet, 2008. **17**(19): p. 2997-3009.
280. Wang, J., et al., *An ALS-linked mutant SOD1 produces a locomotor defect associated with aggregation and synaptic dysfunction when expressed in neurons of Caenorhabditis elegans.* PLoS Genet, 2009. **5**(1): p. e1000350.
281. Zipperlen, P., et al., *Roles for 147 embryonic lethal genes on C.elegans chromosome I identified by RNA interference and video microscopy.* EMBO J, 2001. **20**(15): p. 3984-92.
282. Dillin, A., D.K. Crawford, and C. Kenyon, *Timing requirements for insulin/IGF-1 signaling in C. elegans.* Science, 2002. **298**(5594): p. 830-834.
283. Lee, S.S., et al., *A systematic RNAi screen identifies a critical role for mitochondria in C. elegans longevity.* Nat Genet, 2003. **33**(1): p. 40-8.
284. Gosai, S.J., et al., *Automated high-content live animal drug screening using C. elegans expressing the aggregation prone serpin α 1-antitrypsin Z.* PLoS One 2010. **5**(11): p. e15460.
285. Ashrafi, K., et al., *Genome-wide RNAi analysis of Caenorhabditis elegans fat regulatory genes.* Nature, 2003. **421**(6920): p. 268-72.
286. Zhang, J.H., T.D. Chung, and K.R. Oldenburg, *A Simple Statistical Parameter for Use in Evaluation and Validation of High Throughput Screening Assays.* J Biomol Screen, 1999. **4**(2): p. 67-73.
287. Birmingham, A., et al., *Statistical methods for analysis of high-throughput RNA interference screens.* Nat Methods, 2009. **6**(8): p. 569-575.
288. Kao, C.Y., et al., *Global functional analyses of cellular responses to pore-forming toxins.* PLoS Pathog. **7**(3): p. e1001314.
289. van Ham, T.J., et al., *C. elegans model identifies genetic modifiers of alpha-synuclein inclusion formation during aging.* PLoS Genet, 2008. **4**(3): p. e1000027.
290. Choe, K.P. and K. Strange, *Genome-wide RNAi screen and in vivo protein aggregation reporters identify degradation of damaged proteins as an essential hypertonic stress response.* Am J Physiol Cell Physiol, 2008. **295**(6): p. C1488-98.
291. Gidalevitz, T., E.A. Kikis, and R.I. Morimoto, *A cellular perspective on conformational disease: the role of genetic background and proteostasis networks.* Curr Opin Struct Biol. **20**(1): p. 23-32.

292. Wettschureck, N. and S. Offermanns, *Mammalian G proteins and their cell type specific functions.* Physiol Rev, 2005. **85**(4): p. 1159-204.
293. Bargmann, C., *Molecular neurobiology. Making memories stick?* Nature, 1998. **391**(6666): p. 435-6.
294. Bargmann, C.I. and J.M. Kaplan, *Signal transduction in the Caenorhabditis elegans nervous system.* Annu Rev Neurosci, 1998. **21**: p. 279-308.
295. Kimple, A.J., et al., *Regulators of G-Protein Signaling and Their G{alpha} Substrates: Promises and Challenges in Their Use as Drug Discovery Targets.* Pharmacol Rev.
296. Chen, M.R., et al., *A novel fluorescent timer based on bicistronic expression strategy in Caenorhabditis elegans.* Biochem Biophys Res Commun. **395**(1): p. 82-6.
297. Hollien, J. and J.S. Weissman, *Decay of endoplasmic reticulum-localized mRNAs during the unfolded protein response.* Science, 2006. **313**(5783): p. 104-7.
298. Hollien, J., et al., *Regulated Ire1-dependent decay of messenger RNAs in mammalian cells.* J Cell Biol, 2009. **186**(3): p. 323-31.
299. Zhang, X.D., *An effective method for controlling false discovery and false nondiscovery rates in genome-scale RNAi screens.* J Biomol Screen. **15**(9): p. 1116-22.